ABSTRACT

TAMANG, APIL. A Multilevel Method for Solving Neutron Kinetics Equations Coupled with the Heat Transfer Equation. (Under the direction of Dmitriy Anistratov.)

A basic model for transient reactor analysis can be based on the solution of the neutron transport and heat transfer problems in the reactor core. The solution of the neutron transport equation gives the detailed distribution of neutrons in phase space. The solution of the heat transfer equation gives the temperature distribution in the reactor. The heat transfer equation is coupled to the neutron transport equation through an energy deposition source term. This term depends on the neutron angular flux distribution. The neutron transport problem, in the meantime, is dependent on spatial parameters that are functions of the spatial temperature distribution. As a result, we have a nonlinearly coupled system of equations that can be numerically challenging to solve. In this work, nonlinearly coupled models described by the neutron transport and heat transfer equations are solved using an approach based on the quasidiffusion (QD) method.

The main idea in this work is based on using equivalent low-order equations of the neutron transport problem to do the majority of the computational work in terms of solving coupled physics problems. The high-order (neutron transport) equation is solved to provide factors that are required to define the low-order equations. These equations have much smaller dimensionality than the high-order equation they were derived from. While the latter is defined for seven independent variables, the low-order equation based on the grey low-order quasidiffusion problem is defined only for functions of the spatial and time variables. This makes it computationally much easier to solve. One can thus, take advantage of using the low-order equation to search for the solutions to the coupled systems.

In this work, a multilevel scheme is developed to solve basic time-dependent reactor physics problems in 1-D slab geometry. This scheme is based on a coupled system of the transport, the multigroup low-order and the effective one-group (grey) low-order quasidiffusion problems. The heat transfer problem is coupled to the grey low-order QD problem. Numerical results that demonstrate performance of this multilevel scheme are presented. A method based on classical nonlinear fixed-point iterations for solving the transport and heat transfer equations is also used to solve the same set of problems. Comparative analysis are presented to demonstrate the efficiency provided by the multilevel scheme developed for this research.

A Multilevel Method for Solving Neutron Kinetics Equations Coupled with the Heat Transfer Equation

by
Apil Tamang

A thesis submitted to the Graduate Faculty of
North Carolina State University
in partial fulfillment of the
requirements for the Degree of
Master of Science

Nuclear Engineering

Raleigh, North Carolina

2013

APPROVED BY:

C. T. Kelley

Yousry Azmy

Dmitriy Anistratov
Chair of Advisory Committee

DEDICATION

To families and friends everywhere.

BIOGRAPHY

The author was born in Kathmandu, Nepal in 1986 to Mr. Surendra Bahadur and Mrs. Bijaya Laxmi Tamang. He is the older of the couple's two sons. He finished his high school from Nobel Academy in Kathmandu. Following his high school graduation, he moved to the United States to pursue his undergraduate studies in Engineering-Physics at Southern Arkansas University (SAU), AR. He graduated Summa Cum Laude from SAU in 2010 with a double major in Engineering-Physics and Mathematics. While at SAU, he was a supplement instructor for several freshmen and junior level math and physics courses. He was also briefly involved in experimental research with his physics professor and mentor, Dr. Abdel Bachri, in the area of cosmic-ray detection.

Following his undergraduate studies, the author enrolled at North Carolina State University (NCSU) to pursue graduate studies in Nuclear Engineering. At NCSU, he worked under the direction of his graduate adviser and mentor, Dr. Dmitriy Anistratov. His research efforts were directed in the area of developing advanced computational methods for reactor modeling. He has since, presented his work at scientific conferences and workshops.

ACKNOWLEDGEMENTS

I would like to thank my advisor, Dr. Dimitriy Anistratov for his invaluable help and support through the course of this research. This work could not have been possible without his continual feedback and persistence. I would also like to thank the department of nuclear engineering at NC state university for providing me with the environment to work on this project. Much indebtedness also extend to the CASL program for partially funding this work. Special thanks goes to Chintan Kanani for all his technical support here in the department. He helped resolve many critical computer related issues. And just as critically, this work could not be possible without all the emotional support of my friends here at NC state and elsewhere in the world. Friends and families somehow make all the hard work and efforts worth it in the end.

TABLE OF CONTENTS

LIST OF TABLES

LIST OF FIGURES

Chapter 1

Introduction

A nuclear reactor core is a sophisticated multiphysics system governed by complex thermo-mechanical processes within the materials present in the core. To perform a successful design and accurate evaluation of reactor core parameters in operating conditions, it is necessary to predict neutron densities in space and the energy spectrum with high fidelity inside the reactor core at each moment of the core operation. The distribution of these neutron densities is dependent on the material properties of the core, which in turn are dependent on the spatial distribution of the temperature in the core. Reversely, the spatial distribution of temperature at any instant of time is strongly dependent on the distribution of the neutron densities in space and in energy at that moment. As a result we have a system where the two parameters influence each other in quite complex ways. The goal of this project is to develop an efficient numerical method for the solution of these kinds of problems. A multilevel method is developed to solve the time-dependent neutron transport problems accounting for the effects from delayed neutrons and thermal feedback. This multilevel method is based on low-order forms of the neutron transport equation.

1.1 Brief Overview of the Methodology

The low-order form of the transport equation mentioned above is based on the quasidiffusion (QD) low-order equations introduced by Goldin in 1964 [1]. The QD method consists of multigroup low-order QD equations that are obtained by taking the zeroth and first moments of the multigroup transport equation. These equations are further averaged over the energy groups to obtain a low-order one-group problem. The solution to this one-group problem is the one-group scalar flux distribution. This problem is hereby referred to as the Grey Low-Order quasidiffusion (GLOQD) problem. In this research, the GLOQD equations are used to couple the thermal problem to the transport problem. The motivation for doing this is based on the

fact that the thermal response of the system at each spatial point is coupled to the neutron transport problem through an energy deposition term which dependes on the integral of the angular flux over the energy and angular variables. By using the GLOQD equations to couple to the heat transfer equation, the coupling of two physical processes happens in a low-dimensional space. Additionally, the low-order QD equations capture all necessary transport effects without any approximations.

The core idea in this research is to use the groups-collapsed equation to find the corresponding update of the scalar flux based on the given temperature [2, 3, 4, 5]. In doing that, much of the computational load of finding the updated neutron and thermal response is transferred to the grey problem instead of the high-order problem. The same idea is used in [6] to evaluate k-eigenvalues of 1-D reactor models. In this work, the efforts of calculating the multiplication factor is spent at the grey low-order level while the high-order transport and the multigroup QD equations are solved only to provide better approximating factors and spectrum for the grey problem. The approach in both these works is based on an efficient hierarchical multilevel scheme. Next, we note some important milestones in the development of efficient computational methods for the neutron transport problems.

1.2 Literature Review

The neutron transport problem is at the heart of mathematical modelling for each type of nuclear reactor core. Numerical algorithms for the neutron transport problem are based on stochastic (Monte Carlo) or deterministic methods for finding the solution. Stochastic methods involve individual particle tracking based on probabilities of physical events such as scattering, absorption, fission etc [7, 8]. Solutions of interests are evaluated as statistical averages of these events. Deterministic algorithms employ the algebraic solution of the transport equation in phase space. In any but the most simplest cases, analytic solutions for the continuous transport equation do not exist or are extremely difficult to find. As a result, discretization of the equation on spatial, angular, energy and time mesh is performed. This results in a system of algebraic equations that is solved through iterative or direct methods. Standard problems of reactor analysis result in large linear systems which are not amenable to direct inversion. Hence, iterative methods must be used. The quality of the iterative method is judged by how rapidly it converges.

The most widely used method for solving the discretized form of the transport equation is the source iteration (SI) scheme [7]. This method is based a form of Von Neumann's series solution [9]. It derives its name from the fact that the solution is derived through iterations on the scattering source. To see this, consider the time independent one-group transport equation in a nonmultiplying media. The equation has the form:

$$\left[\vec{\Omega}\cdot\vec{\nabla}+\sigma_t(\vec{r})\right]\psi(\vec{r},\vec{\Omega})=\int d\Omega'\sigma_s(\vec{r},\vec{\Omega}'\cdot\vec{\Omega})\psi(\vec{r},\vec{\Omega}')+q_{ext}(\vec{r},\vec{\Omega}). \tag{1.1}$$

The terms, $\left[\vec{\Omega}\cdot\vec{\nabla}+\sigma_t(\vec{r})\right]$ account for the loss in the neutron population through streaming and via neutron-material interactions. The terms in the right represent source in the form of scattering and external sources, respectively. In operator notation, this transport equation can be written as:

$$L\psi=S\psi+q, \tag{1.2}$$

where,

$$L\psi\equiv\vec{\Omega}\cdot\vec{\nabla}\psi+\sigma_t(\vec{r})\psi, \tag{1.3}$$

and

$$S\psi\equiv\int d\Omega'\sigma_s(\vec{r},\vec{\Omega}'\cdot\vec{\Omega})\psi(\vec{r},\vec{\Omega}'),\quad q\equiv q_{ext}(\vec{r},\vec{\Omega}) \tag{1.4}$$

denote the loss and scattering operators respectively. q refers to any external sources in the medium. Mathematically, the SI scheme is expressed as follows:

$$L\psi^{(l+1)}=S\psi^{(l)}+q\quad,\quad l\geq 0. \tag{1.5}$$

The SI scheme has a clear physical interpretation. If we start off with a zero initial flux distribution, i.e. $\psi^{(0)}=0$, then the $(l+1)^{th}$ iterate term, i.e. $\psi^{(l+1)}$ describes all the neutrons that made fewer than $l+1$ collisions since they were emitted by the source. Hence, when the scattering process is significant in the domain, higher numbers of source iterations are required for the solution to converge using source iterations. The solution of a large class of practical problems often results in prohibitively slow convergent source iterations. Hence, an efficient acceleration scheme must be used to solve transport problems. Acceleration methods can be placed into two broad categories: 1) linear (or synthetic) methods and 2) nonlinear methods.

1.2.1 Linear (Synthetic) Acceleration Methods

In 1963, Kopp [10] published the first work on *synthetic acceleration*. The main idea behind the *synthetic acceleration* scheme is the use of a low-order operator to correct for the angular flux before the next SI iteration is performed. Define $\psi^{(l+1/2)}$ as the result of a single source iteration. Then,

$$L\psi^{(l+1/2)}=S\psi^{(l)}+q,\qquad l\geq 0. \tag{1.6}$$

The goal is for $\psi^{(l+1)}$ to be closer to ψ than is $\psi^{(l+1/2)}$. To accomplish this by the synthetic method, subtract Eq. (1.6) from Eq. (1.2) to get

$$L(\psi - \psi^{(l+1/2)}) = S(\psi - \psi^{(l)}) = S(\psi - \psi^{(l+1/2)}) + S(\psi^{(l+1/2)} - \psi^{(l)}). \tag{1.7}$$

This yields the following exact equation for the *iterative error*: $\psi - \psi^{(l+1/2)}$,

$$(L - S)\left(\psi - \psi^{(l+1/2)}\right) = S\left(\psi^{(l+1/2)} - \psi^{(l)}\right), \tag{1.8}$$

which implies

$$\psi = \psi^{(l+1/2)} + (L - S)^{-1} S\left(\psi^{(l+1/2)} - \psi^{(l)}\right). \tag{1.9}$$

Eq. (1.9) expresses the solution (ψ) in terms of the previous iterate, $\psi^{(l+1/2)}$ and the correction, $\Delta\psi^{(l)} = \psi^{(l+1/2)} - \psi^{(l)}$. The idea of synthetic acceleration [10] is to replace the operator $(L - S)^{-1}$ in Eq. (1.9) by an operator that is an approximation. It is desired that this operator be computationally less expensive to evaluate than $(L-S)^{-1}$. Let M be the approximate operator used in place of $(L - S)^{-1}$. Then Eq. (1.9) becomes:

$$\psi^{(l+1)} = \psi^{(l+1/2)} + MS\Delta\psi^{(l)}. \tag{1.10}$$

The SI scheme Eq. (1.5) presented above is equivalent to the Richardson Iteration scheme for solving linear systems [11, 12, 13]. The usage of linear acceleration methods is analogous to the preconditioned Richardson's iteration [14, 15, 11]. Different choices in M yield different *synthetic* schemes of acceleration. In his work, Kopp used the diffusion equation as the low-order operator. However, this approach led to divergent behaviors when coarse meshes were used [16, 17, 18, 19]. In 1976, Alcouffe proposed a synthetic method based on the discrete diffusion approximation [20, 21] and it was called the *Diffusion Synthetic Acceleration* (DSA). It consisted of the discrete diffusion operator which was consistently derived from the high-order diamond-differenced S_N transport operator. It exhibited rapid convergence for all spatial mesh thicknesses, and spawned much theoretical and experimental work in the following years. Overview of succeeding work is summarized in [14].

Eq. (1.5) can also be recasted in the canonical form as represented by Eq. (1.11). This sets the stage for the application of Krylov based subspace methods for particle transport problems.

$$\left(I - L^{-1}S\right)\psi = L^{-1}q, \tag{1.11}$$

which can be seen from the linear algebra viewpoint as equivalent to the problem,

$$\tilde{A}\psi = b. \tag{1.12}$$

Eq. (1.12) is amenable to solution by Krylov methods from linear algebra. Their benefits are

multifold and their presence become increasingly significant [22, 23, 24]. Among others, the benefit is in that much of the analysis and tools developed from theoretical linear algebra become directly applicable. Additionally, it is observed that Kyrlov based methods show much improved efficiency by even the usage of simple preconditioners [12]. Next, we present the development of nonlinear acceleration methods for the transport problem upon which the methodology in this research is based on.

1.2.2 Nonlinear Acceleration Methods

Like linear acceleration methods, nonlinear acceleration schemes for the transport problem also utilize a two-step approach. The first step involves the evaluation of the high-order (transport) problem. The second step involves the evaluation of the low-order transport model. The low-order models are closed with the help of nonlinear factors that depend weakly on the solutions of the transport problem. The form of the nonlinear closures adopted makes each method unique. Nonlinear acceleration methods also result in rapid convergence of the high-order problem, and they have the distinct advantage of not requiring to be consitently discretized with the high-order problem for stability [25, 26].

The quasidiffusion (QD) method was proposed by Gol'din in 1964 [1]. This method involves the solution of low-order diffusion like equations which are obtained by taking angular moments of the original transport problem. The coefficients of the Low-Order Quasidiffusion (LOQD) equations are nonlinear QD factors that depend weakly on the transport solution. If the QD factors are exact, then the solution of the LOQD exactly reproduces the transport scalar flux and current. The QD factor is equal to one-third if the angular flux is a linearly anisotropic function. In this case, LOQD equations reduce to the diffusion equation. The iterative process for QD method is illustrated using a simple example in 1-D slab geometry.

- Perform a transport sweep:

$$L\psi^{(l+1/2)} = \frac{\sigma_s}{2}\phi^{(l)} + \frac{q}{2}, \qquad L \equiv \mu\frac{\partial}{\partial x} + \sigma_t. \tag{1.13}$$

- Evaluate the QD factors:

$$E^{(l+1/2)}(x) = \frac{\int_{-1}^{1} \mu^2\psi^{(l+1/2)}(x,\mu)d\mu}{\int_{-1}^{1} \psi^{(l+1/2)}(x,\mu)d\mu}. \tag{1.14}$$

- Solve the LOQD problem:

$$\frac{dJ^{(l+1)}}{dx} + (\sigma_t - \sigma_s)\phi^{(l+1)} = q, \tag{1.15}$$

$$\frac{d\left(E^{(l+1/2)}\phi^{(l+1)}\right)}{dx} + \sigma_t J^{(l+1)} = 0, \tag{1.16}$$

where $\phi(x) = \int_{-1}^{1} \psi(x,\mu)d\mu$ and $J(x) = \int_{-1}^{1} \mu\psi(x,\mu)d\mu$ are the scalar flux and current, respectively. The scalar flux obtained from the low-order quasidiffusion problem is then used to find the new estimate of ψ from Eq. (1.13).

The QD method is a member of a broader class of methods called the nonlinear projective-iteration (NPI) methods [25]. They are also known as projected discrete ordinates (PDO) methods [27]. One advantage offered by these nonlinear methods is the freedom of using independent discretization schemes for the low-order equations. For multidimensional problems, it maybe algebraically too complex to derive consistent discretizations of the low-order problems. In this research, the high-order (transport) and low-order (QD) equations are discretized with independent schemes.

Independent discretization can also be used advantageously to improve the accuracy of the transport solution. By using a more accurate discretiztion of the low-order problem, the transport problem can be evaluated to give more accurate high-order fluxes. This effect is demonstrated in works [25, 26] etc.

Variants of the NPI (PDO) methods have been developed and used to solve different classes of problems. In particular, QD method has been used to solve problems in radiation hydrodynamics and neutron transport. The QD method is an efficient iterative method that results in rapid convergence of the high-order problem. Additionally, the QD moment equations enable one to couple the transport equation to multiphysics equations. Infact, QD based methods have been used to couple multiphysics equations to the transport problem previously. In 1972, Gol'din and his colleagues solved radiative transfer problems coupled to the energy balance equation using a frequency-averaged transfer problem [28] . This averaging procedure was based on the LOQD equations. In 1992, Anistratov and Gol'din applied this approach to solve the neutron transport equation coupled to burnup equations for reactor analysis [29]. Following in the footsteps of these works, we use the LOQD equations as a key component in the developement of a method for coupling the neutron transport equations to the equations for delayed precursors and heat transfer.

1.3 Organization of Thesis

In Chapter 2 of this thesis, we show the specific set of equations that are solved in this work. The multiphysics models are identified and the appropriate equations are listed, followed by the presentation of the details of the multilevel scheme. In chapter 3, the details of the discretizations of the equations are presented. In chapter 4, the computational results obtained by means of this method are presented. This is followed by the analysis of the results for each test. In chapter 5, we present concluding remarks and offer some suggestions for future work. A list of appendixes and bibliographic references are available at the end for further references.

Chapter 2

Multiphysics Models and Multilevel Methods

2.1 Multiphysics Model

The interaction of particles and matter in a nuclear reactor is described by a model that is based on the particle transport, fluid flow and heat transfer equations [30, 31, 32]. Let us consider physical processes characterized by a time scale such that the burnup of nuclides can be neglected. A basic model for simulating transients can be described by the following relations:

- *the multigroup neutron transport equation (detailed neutron conservation law)*

$$\begin{aligned}\frac{1}{v_g}\frac{\partial\psi_g(\vec{r},\vec{\Omega},t)}{\partial t}+\vec{\Omega}\cdot\vec{\nabla}\psi_g(\vec{r},\vec{\Omega},t)+\Sigma_{t,g}(\vec{r},t)\psi_g(\vec{r},\vec{\Omega},t)=\\ \sum_{g'=1}^{G}\int_{4\pi}\Sigma_{s,g'\to g}(\vec{r},\vec{\Omega}\cdot\vec{\Omega}',t)\psi_{g'}(\vec{r},\vec{\Omega}',t)d\Omega'\\ +\frac{\chi_g^p(\vec{r},t)}{4\pi}\sum_{g'=1}^{G}\big(1-\beta_{g'}(\vec{r},t)\big)\nu_{f,g'}(\vec{r},t)\Sigma_{f,g'}(\vec{r},t)\int_{4\pi}\psi_{g'}(\vec{r},\vec{\Omega}',t)d\Omega'\\ +\frac{1}{4\pi}\sum_{d=1}^{6}\lambda_d\chi_{d,g}^{del}(\vec{r},t)C_d(\vec{r},t)\,,\quad g=1,...,G\,,\end{aligned}\tag{2.1}$$

where g is the index of the energy group, v_g is the group neutron velocity, $\vec{\Omega}$ is the direction of neutron propagation, ψ_g is the group angular flux, χ_g^p is the fission spectrum of prompt neutrons, β_g is the delayed neutron fraction for the energy group g, C_d is the precursor concentration for the precursor group d, $\chi_{d,g}^{del}$ is the fission spectrum of delayed neutrons for the delayed

group d, λ_d is the decay constant, $\nu_{f,g}$ is the number of neutrons released per fission, $\Sigma_{x,g}$ is the macroscopic cross section of type-x which depends on nuclide density N^l (l is the nuclide index) and microscopic cross sections $\sigma_x^{l,g}$ as

$$\Sigma_{x,g} = \sum_l N^l \sigma^l_{x,g}(T)\,, \tag{2.2}$$

• *the precursor concentration balance (PCB) equations*

$$\frac{\partial C_d(\vec{r},t)}{\partial t} = -\lambda_d C_d(\vec{r},t) + \sum_{g'=1}^{G} \tilde{\beta}_{d,g'}(\vec{r},t)\nu_{f,g'}(\vec{r},t)\Sigma_{f,g'}(\vec{r},t)\int_{4\pi}\psi_{g'}(\vec{r},\Omega',t)d\Omega'\,, \tag{2.3}$$

$$d = 1, ..., 6\,,$$

where $\tilde{\beta}_{d,g}$ is the delayed neutron fraction for group d and

$$\beta_g = \sum_{d=1}^{6} \tilde{\beta}_{d,g}\,, \tag{2.4}$$

• *the heat transfer (HT) equation for material temperature*

$$\frac{\partial}{\partial t}(\rho c_p T(x,t)) - \frac{\partial}{\partial x}\left(\kappa(T)\frac{\partial T(x,t)}{\partial x}\right) = w_f \sum_{g=1}^{G}\Sigma_{f,g}(x,t)\int_{-1}^{+1}\psi_g(x,\mu',t)d\mu'\,, \tag{2.5}$$

where ρ, c_p, *and* κ refer to the material density, specific heat capacity, and the heat conductivity of the material, respectively.

Let us consider that all neutrons are prompt ($\beta_g = 0$). Then the above equations result in a system of equations for ψ^g and T which can be presented in the following operator form:
• the multigroup particle transport equation for $\Psi = \{\psi^1(\vec{r},\vec{\Omega},t), ..., \psi^g(\vec{r},\vec{\Omega},t), ..., \psi^G(\vec{r},\vec{\Omega},t)\}$

$$\frac{\partial \Psi}{\partial t} + \mathcal{L}[T]\Psi = \mathcal{S}[T]\Psi\,, \tag{2.6}$$

• the heat transfer equation for the material temperature $T = T(\vec{r},t)$

$$\frac{\partial T}{\partial t} = \mathcal{C}T + \mathcal{Q}[\Psi, T]\,. \tag{2.7}$$

The operator $\mathcal{L}$ in Eq. (2.6) describes particle streaming and collision. $\mathcal{S}$ accounts for scattering and fission processes. $\mathcal{C}$ in Eq. (2.7) is the heat transfer operator. $\mathcal{Q}$ is the energy deposition term.

We notice that the important features of this model are the following:

1. The multiphysics equations are nonlinearly coupled with each other.
2. The dimensionality of the problem is dominated by the particle transport model.
3. The particle transport equation has high dimensionality. The angular flux $\psi^g(\vec{r}, \Omega, t) = \psi^g(x, y, z, \gamma, \theta, t)$ is a function of 7 independent variables, where γ and θ are angular variables that determine the direction of particle motion. The dependence on energy is represented by the energy group index.
4. The multiphysical model is characterized by multiple time and length scales.

All these details make this physical phenomenon a challenging computational problem. The high dimensionality of the problem has the most significant effect in this regard.

We now discuss possible approaches for solving the coupled equations (2.6) and (2.7). These equations are approximated with respect to time over the interval $t^{j-1} \leq t \leq t^j$ to get

$$\mathcal{A}_1 \Psi^j + \mathcal{L}[T^j]\Psi^j = \mathcal{S}[T^j]\Psi^j + \mathcal{A}_2^{j-1}\Psi^{j-1}\,, \tag{2.8}$$

$$\mathcal{B}_1 T^j = \mathcal{C}T^j + \mathcal{Q}[\Psi^j, T^j] + \mathcal{B}_2^{j-1}T^{j-1}\,, \tag{2.9}$$

where j is the index of the current time step, and discrete operators $\mathcal{A}_1$, $\mathcal{A}_2$, $\mathcal{B}_1$, $\mathcal{B}_2$ define some time-discretization scheme. Equations (2.8) and (2.9) can be represented in the following compact form:

$$x^{j+1} = \mathcal{K}[x^j] + \mathcal{Z}[x^{j-1}] \tag{2.10}$$

where $x^j = [\psi_1^j, ...\psi_N^j, T_1^j, ...T_N^j]$ represents the vector of solution arising from the spatial discretization of the system of equations on the problem domain.

Richardson Iteration.

One way to solve the nonlinear algebraic system of equations defined by Eq.(2.10) is to apply the nonlinear Richardson iteration method, also known as the fixed-point iteration or Picard's iteration method [13, 33]. Assume that an estimation of the temperature ($T^{(n)}$) and angular flux (ψ^n) is known from the previous iteration where n is the iteration index for the Picard iteration. Then the Picard iteration is defined by

$$x^{n+1,j} = \mathcal{K}[x^{n,j}] + \mathcal{Z}[x^{j-1}], \tag{2.11}$$

where $\mathcal{Z}[x^{j-1}]$ is available from the solution of the previous time-step. The operation embodied by $\mathcal{K}$ involve the following composite operations:

1. Solve the high-order transport problem to calculate $\Psi^{(n+1)}$

$$\mathcal{A}_1 \Psi^{(n+1)} + \mathcal{L}[T^{(n)}]\Psi^{(n+1)} = \mathcal{S}[T^{(n)}]\Psi^{(n+1)} + \mathcal{A}_2^{j-1}\Psi^{j-1}\,. \tag{2.12}$$

2. Solve the heat transfer problem $T^{(n+1)}$ that corresponds to the updated $\Psi^{(n+1)}$

$$\mathcal{B}_1 T^{(n+1)} = \mathcal{C} T^{(n+1)} + \mathcal{Q}[\Psi^{(n+1)}, T^{(n+1)}] + \mathcal{B}_2^{j-1} T^{j-1} \,. \tag{2.13}$$

This iteration process can converge very slowly in case of tightly coupled multiphysics phenomena. We also notice that in this method the high-order transport problem is solved on every iteration. This step itself involves iterations of the transport problem for evaluating ψ. As a result, this approach can be computationally quite inefficient.

Newton's Method.

Another way to solve this system of equations is to linearize the problem (2.8) and (2.9) and apply Newton's method [13] to compute T and Ψ. In operator notations,

$$x^{(n+1),j} = x^{(n),j} - \frac{\mathcal{K}[x^{(n),j}]}{\mathcal{J}_{(\mathcal{K})}[x^{(n),j}]} + \mathcal{Z}[x^{j-1}] \tag{2.14}$$

where $\mathcal{J}_{(\mathcal{K})}[x^{(n),j}]$ is the Jacobian of the discrete operator $\mathcal{K}$. The Newton's method requires much smaller numbers of iterations as it converges quadratically to the solution.

However, either method will need to solve the high-order transport problem on every Picard or Newton iteration. The dimension of the space where one searches for the solution to the nonlinear system of equations (2.10) is still defined by the dimensionality of the multigroup particle transport equation (see Eqs. (2.1), (2.6)). Next, we present a way where the dimensionality of the nonlinear system of equations can be reduced.

2.2 The Effective Low-Order Transport Problem

We now present the main idea of this project. To reduce the dimensionality of the problem, we reformulate the system of equations (2.6) and (2.7) by means of a special effective low-order transport (ELOT) problem for the total scalar flux: $\phi(\vec{r}, t) = \sum_{g=1}^{G} \int_{4\pi} \psi^g d\Omega$ as follows,

$$\frac{\partial \phi}{\partial t} + \tilde{\mathcal{L}}[T, \Psi]\phi = \tilde{\mathcal{S}}[T, \Psi]\phi \tag{2.15}$$

and define the heat transfer equation with the modified energy deposition term which explicitly uses ϕ,

$$\frac{\partial T}{\partial t} = \mathcal{C} T + \tilde{\mathcal{Q}}[\psi, T]\phi \,. \tag{2.16}$$

Note that the operators $\tilde{\mathcal{L}}$ and $\tilde{\mathcal{S}}$ in the ELOT problem (2.15) depend on the high-order transport solution Ψ. The ELOT problem can be formulated by means of a projection operator in a way that Eq. (2.15) is equivalent to the original transport problem (2.6). As a result, the heat transfer equation in the form (2.16) is coupled directly to the ELOT problem (2.15) that has the same dimensionality as Eq. (2.16). The important requirement for the definition of the

ELOT problem is to be equivalent to the original transport problem and hence reproduce the transport effects accurately.

The high-order transport solution that is used to define the low-order operators of the ELOT equation (2.15) is determined from the modified high-order transport equation that is formed by means of a prolongation operator $\tilde{\mathcal{S}}$

$$\frac{\partial \Psi}{\partial t} + \mathcal{L}[T]\Psi = \tilde{\mathcal{S}}[T, \Psi]\phi \tag{2.17}$$

where ϕ is explicitly used in the scattering and fission terms.

In this example, we formulated a two-level system of equations (2.15) and (2.17) for the particle transport problem. The complete methodology developed in this research is based on a multilevel method that uses multigroup low-order fluxes in addition to the total scalar flux, i.e. $\phi_g(\vec{r}) = \int_{4\pi} \psi_g(\vec{r}, \Omega) d\Omega$. Note that the ELOT problem presented above is a one-group problem.

The proposed coupled equations (2.15)-(2.17) can be solved by means of the following iteration process on the given time step. Assume that the estimation of $\Psi^{(s)}$ is known from the previous s-th iteration. We use it to form operators $\tilde{\mathcal{S}}$, $\tilde{\mathcal{L}}$ and $\tilde{\mathcal{Q}}$ and solve the heat transfer equation directly coupled with the ELOT problem

$$\mathcal{M}_1 \phi^{(s+1)} + \tilde{\mathcal{L}}\left[T^{(s+1)}, \Psi^{(s)}\right] \phi^{(s+1)} = \tilde{\mathcal{S}}\left[T^{(s+1)}, \Psi^{(s)}\right] \phi^{(s+1)} + \mathcal{M}_2^{j-1} \phi^{j-1}\,, \tag{2.18}$$

$$\mathcal{B}_1 T^{(s+1)} = \mathcal{C} T^{(s+1)} + \tilde{\mathcal{Q}}\left[\phi^{(s+1)}, T^{(s+1)}\right] + \mathcal{B}_2^{j-1} T^{j-1} \tag{2.19}$$

to get a new estimation of the temperature $T^{(s+1)}$ and the total scalar flux $\phi^{(s+1)}$. Then we update the high-order transport solution from

$$\mathcal{A}_1 \Psi^{(s+1)} + \mathcal{L}[T^{(s+1)}]\Psi^{(s+1)} = \tilde{\mathcal{S}}[T^{(s+1)}, \Psi^{(s)}]\phi^{(s+1)} + \mathcal{A}_2^{j-1} \Psi^{j-1} \tag{2.20}$$

to obtain $\Psi^{(s+1)}$ for the given $T^{(s+1)}$ and $\phi^{(s+1)}$. Now the next iteration begins.

2.3 Mutlilevel Method

We now present the multilevel method used for solving time-dependent multigroup neutron transport equation coupled with the equations of delayed neutrons precursors and heat transfer equation. We consider 1-D slab geometry and the case of isotropic scattering.

2.3.1 The High-Order Problem

The time-dependent transport equation with a transformed right-hand side (RHS) is defined as

$$\frac{1}{v_g}\frac{\partial \psi_g}{\partial t} + \mu\frac{\partial \psi_g}{\partial x} + \Sigma_{t,g}\psi_g = \frac{1}{2}\left(\overline{\Sigma}_{s,g,0} + \chi_g^p\overline{(1-\beta)\nu\Sigma_f}\right)\phi + \frac{1}{2}\left(q_{del,g}^{\chi} + q_{ext,g}\right), \quad (2.21)$$

$$g = 1, ..., G\,,$$

with vacuum or reflective boundary conditions

$$\psi_g(0,\mu,t)\big|_{\mu>0} = \begin{cases} 0 & \text{if BC is vaccum,} \\ \psi_g(0,-\mu,t) & \text{if BC is reflective,} \end{cases} \quad (2.22)$$

$$\psi_g(X,\mu,t)\big|_{\mu<0} = \begin{cases} 0 & \text{if BC is vaccum,} \\ \psi_g(X,-\mu,t) & \text{if BC is reflective,} \end{cases} \quad (2.23)$$

where

$$\overline{(1-\beta)\nu\Sigma_f} = \frac{\sum_{g=1}^{G}(1-\beta_g)\nu_{f,g}\Sigma_{f,g}\phi_g}{\sum_{g=1}^{G}\phi_g}\,, \quad (2.24)$$

$$\overline{\Sigma}_{s,g,0} = \frac{\sum\limits_{g'=1}^{G}\Sigma_{s,g'\to g,0}\phi_{g'}}{\sum\limits_{g'=1}^{G}\phi_{g'}}\,, \quad (2.25)$$

and

$$q_{del,g}^{\chi} = \sum_{d=1}^{6}\chi_{d,g}^{del}\lambda_d C_d\,. \quad (2.26)$$

Here $q_{del,g}^{\chi}$ is the delayed neutron source in group g, and $q_{ext,g}$ is the group external source. Note that the right-hand side (RHS) of the transport problem is replaced by spectrum-averaged scattering and fission cross-sections. These cross-sections are multiplied by the total scalar flux to determine neutron production due to scattering and fission.

2.3.2 The Low-Order Problem

2.3.2.1 The Multigroup Low-Order Quasidiffusion Equations

The multigroup quasidiffusion (MLOQD) equations are obtained by taking the zeroth and first order angular moments of the high-order transport equation. In slab geometry, this translates to integrating Eq. (2.21) in μ with weights 1 and μ independently. We get the following set of

equations as a result:

$$\frac{1}{v_g}\frac{\partial \phi_g}{\partial t} + \frac{\partial J_g}{\partial x} + \left(\Sigma_{t,g} - \Sigma_{s,g\to g,0}\right)\phi_g = \sum_{g'=1}^{g-1} \Sigma_{s,g'\to g,0}\phi_{g'} + \left(Q_{s,g,0} + \chi_g^p \overline{(1-\beta)\nu\Sigma_f}\right)\phi + q_{del,g}^{\chi} + q_{ext,g}\,, \quad (2.27)$$

$$\frac{1}{v_g}\frac{\partial J_g}{\partial t} + \frac{\partial \left(E_g \phi_g\right)}{\partial x} + \Sigma_{t,g} J_g = 0\,, \quad (2.28)$$

with vacuum or reflective boundary conditions

$$J_g(0,t) = \begin{cases} C_{L,g}(t)\phi_g(0,t) & \text{if BC is vacuum,} \\ 0 & \text{if BC is reflective,} \end{cases} \quad (2.29)$$

$$J_g(X,t) = \begin{cases} C_{R,g}(t)\phi_g(X,t) & \text{if BC is vacuum,} \\ 0 & \text{if BC is reflective,} \end{cases} \quad (2.30)$$

where

$$E_g(x,t) = \frac{\int_{-1}^{1} \mu^2 \psi_g(x,\mu,t)d\mu}{\int_{-1}^{1} \psi_g(x,\mu,t)d\mu}\,, \quad (2.31)$$

$$C_{L,g}(t) = \frac{\int_{0}^{1} \mu \psi_g(0,\mu,t)d\mu}{\int_{0}^{1} \psi_g(0,\mu,t)d\mu}\,, \quad (2.32)$$

$$C_{R,g}(t) = \frac{\int_{-1}^{0} \mu \psi_g(X,\mu,t)d\mu}{\int_{-1}^{0} \psi_g(X,\mu,t)d\mu}\,, \quad (2.33)$$

and

$$Q_{s,g,0} = \frac{\sum_{g'=g+1}^{G} \Sigma_{s,g'\to g,0}\phi_{g'}}{\sum_{g=1}^{G} \phi_g}\,. \quad (2.34)$$

2.3.2.2 The Grey Low-Order Quasidiffusion Equations

The effective low-order transport problem discussed in section (2.2) is based on *the grey (one-group) low-order quasidiffusion (GLOQD) equations* for the total scalar flux and current. They are defined as follows:

$$\frac{\partial}{\partial t}\left(\frac{\phi}{\bar{v}}\right) + \frac{\partial J}{\partial x} + \left(\overline{\Sigma}_a - \overline{(1-\beta)\nu\Sigma_f}\right)\phi = q_{del} + q_{ext}\,, \quad (2.35)$$

$$\frac{\partial}{\partial t}\left(\frac{J}{\tilde{v}}\right)+\frac{\partial\left(\overline{E}\phi\right)}{\partial x}+\overline{\Sigma}_t J+\overline{\zeta}\phi=0\,, \tag{2.36}$$
$$0\leq x\leq X\,,$$

with vacuum or reflective boundary conditions

$$J(0)=\begin{cases}\bar{C}_L\phi(0) & \text{if BC is vacuum,}\\ 0 & \text{if BC is reflective,}\end{cases} \tag{2.37}$$

$$J(X)=\begin{cases}\bar{C}_R\phi(X) & \text{if BC is vacuum,}\\ 0 & \text{if BC is reflective,}\end{cases} \tag{2.38}$$

where

$$q_{del}=\sum_{d=1}^{6}\lambda_d C_d \tag{2.39}$$

is the delayed neutron source,

$$q_{ext}=\sum_{g=1}^{G}q_{ext,g}\,, \tag{2.40}$$

is the external source,

$$\bar{v}=\frac{\sum_{g=1}^{G}\phi_g}{\sum_{g=1}^{G}\frac{\phi_g}{v_g}}\,, \tag{2.41}$$

$$\tilde{v}=\frac{\sum_{g=1}^{G}|J_g|}{\sum_{g=1}^{G}\frac{|J_g|}{v_g}}\,, \tag{2.42}$$

are the averaged velocities,

$$\overline{\Sigma}_a=\frac{\sum_{g=1}^{G}\Sigma_{a,g}\phi_g}{\sum_{g=1}^{G}\phi_g}\,, \tag{2.43}$$

$$\overline{(1-\beta)\nu\Sigma_f}=\frac{\sum_{g=1}^{G}(1-\beta_g)\nu_{f,g}\Sigma_{f,g}\phi_g}{\sum_{g=1}^{G}\phi_g}\,, \tag{2.44}$$

$$\overline{\Sigma}_t=\frac{\sum_{g=1}^{G}\Sigma_{t,g}|J_g|}{\sum_{g=1}^{G}|J_g|}\,, \tag{2.45}$$

$$\overline{E}=\frac{\sum_{g=1}^{G}E_g\phi_g}{\sum_{g=1}^{G}\phi_g}\,, \tag{2.46}$$

$$\bar{C}_L=\frac{\sum_{g=1}^{G}C_{L,g}\phi_g(0)}{\sum_{g=1}^{G}\phi_g(0)}\,, \tag{2.47}$$

$$\bar{C}_R = \frac{\sum_{g=1}^{G} C_{R,g}\phi_g(X)}{\sum_{g=1}^{G} \phi_g(X)}\,, \tag{2.48}$$

and

$$\overline{\zeta} = \frac{\sum\limits_{g=1}^{G} (\Sigma_{t,g} - \overline{\Sigma_t}) J_g}{\sum\limits_{g=1}^{G} \phi_g}\,. \tag{2.49}$$

The spectrum-averaged cross sections and factors (2.41)-(2.49) are calculated by means of the solution of the multigroup LOQD equations. The energy-averaging technique that produces these equivalent one-group QD equations was presented by Gol'din and his colleagues [28, 34, 35, 36]. If J_g is an alternating function in the energy groups, simple averaging without taking the absolute values of the group currents can lead to zero in the denominator in Eq. (2.45). The expressions for $\overline{\Sigma}_t$ in Eq. (2.45) and $\overline{\zeta}$ in Eq. (2.49) are formulated in a way such as to avoid this problem, as well as obtain exact LOQD equations summed over the energy groups. To see the latter, substitute Eq. (2.49) in Eq. (2.36). One gets

$$\overline{\Sigma}_t J + \overline{\zeta}\phi = \overline{\Sigma}_t J + \sum_{g=1}^{G} \left(\Sigma_{t,g} - \overline{\Sigma}_t\right) J_g \tag{2.50}$$

$$= \sum_{g=1}^{G} \Sigma_t J_g \tag{2.51}$$

Also note that in the event that J_g=0 in every groups, Eq. (2.45) is evaluated as follows:

$$\overline{\Sigma}_t = \frac{\sum_{g=1}^{G} \Sigma_{t,g}|J_g + \epsilon|}{\sum_{g=1}^{G} |J_g + \epsilon|}\,, \tag{2.52}$$

for an extremely small parameter, for instance, $\epsilon = 10^{-25}$.

2.3.2.3 The Equations for Precursor Concentrations and Heat Transfer

To couple the equations for precursor concentrations (2.3), and heat conduction (2.5) with the GLOQD equations (2.35) and (2.36), we transform equivalently some terms in these equations by means of the total scalar flux and corresponding spectrum-averaged cross-sections. As a result, *the transformed PCB equations* are given by

$$\frac{\partial C_d}{\partial t} = -\lambda_d C_d + \overline{\tilde{\beta}\nu\Sigma_f}_d \phi\,, \quad d = 1, ..., 6\,, \tag{2.53}$$

where

$$\overline{\tilde{\beta}\nu\Sigma_f}_d = \frac{\sum_{g=1}^{G} \tilde{\beta}_{d,g}\nu_{f,g}\Sigma_{f,g}\phi_g}{\sum_{g=1}^{G}\phi_g}\,, \tag{2.54}$$

and *the transformed HT equation* are given by

$$\frac{\partial}{\partial t}(\rho c_p T) + \frac{\partial W}{\partial x} = w_f \overline{\Sigma}_f \phi\,, \quad 0 \le x \le X\,, \tag{2.55}$$

$$W = -\varkappa \frac{\partial T}{\partial x}\,, \tag{2.56}$$

with Dirichlet boundary conditions

$$T|_{x=0} = T_L\,, \quad T|_{x=X} = T_R\,, \tag{2.57}$$

where

$$\overline{\Sigma}_f = \frac{\sum_{g=1}^{G}\Sigma_{f,g}\phi_g}{\sum_{g=1}^{G}\phi_g}\,. \tag{2.58}$$

2.4 Algorithms of the Multilevel Methods

The multilevel equations presented in the previous section is solved by a nested iterative scheme. We refer to this as the Multilevel Projection (MP) method as it is based on series of projections of the high-order transport problem on lower-dimensional spaces. Figure 2.1 illustrates the flow of information and the order of solving the multilevel equations in this iterative scheme. Algorithm **1** lists the detailed steps that are followed when problems are solved using this method. On each time step (t^j), this method consists of three iteration cycles.

- On the outer cycle, we solve the multigroup transport equation (2.21).
- On the first inner cycle, we solve the MLOQD equations ((2.27) - (2.28)).
- In the innermost cycle, we solve the GLOQD equations coupled with the PCB and HT equations ((2.35)-(2.36), (2.53), & (2.55)).

If the neutronics boundary condition is reflective, the incoming angular fluxes are set using the following relation:

$$\psi_g^{j(s)}(x^*, -\mu_m) = \begin{cases} \frac{\phi_g^{j(0)}(x^*)}{\phi_g^{j-1}(x^*)}\psi_g^{j-1}(x^*, -\mu_m) & \text{if } s = 1, \\ \psi_g^{j-1(s-1)}(x^*, -\mu_m) & \text{if } s > 1, \end{cases} \tag{2.59}$$

for $x^* = 0,\ \mu_m > 0$ and $x^* = X,\ \mu_m < 0$.

Algorithm 1: The Iteration Algorithm for the Multilevel Projection (MP) method.

$j = 0$

while $t^j \leq t^{end}$ **do**

  $j = j + 1$, $t^j = t^{j-1} + \Delta t^j$

  $s = -1$

  Set $\phi_g^{j,(s)}\Big|_{s=0} = \phi_g^{(j-1)}$ and $\phi^{j,(s)}\big|_{s=0} = \phi^{(j-1)}$

  while $\{||1 - \phi^{j,(s)}/\phi^{j,(s-1)}||_\infty > \varepsilon_{\phi,1}$ *or* $||1 - T^{j,(s)}/T^{j,(s-1)}||_\infty > \varepsilon_{T,1}$ $\}$ **do**

    $s = s + 1$

    if $s > 0$ **then for** $g = 1, ..., G$ **do**

      In case of α-approximation, calculate $\alpha_{g,i}^{j(s-1)} = \ln(\phi_{g,i}^{j,(s-1)}/\phi_{g,i}^{j-1})/\Delta t^j$

      Calculate $\Sigma_{\cdot,g}(T^{j,(s-1)})$, $\overline{\Sigma}_{s,g,0}^{j,(s-1)}$, $\overline{(1-\beta)\nu\Sigma_f}^{j,(s-1)}$, $q_{del,g}^{\chi}(C_d^{j,(s-1)})$ etc

      Use Eq. (2.59) to set $\psi_g^j(0)$ and $\psi_g^j(X)$

      Solve the transport equation to calculate $\psi_g^{j,(s-1/2)}$

      Calculate $E_g^{j,(s-1/2)}$ etc

    $l = 0$

    while $\{||1 - \phi^{j,(s,l)}/\phi^{j,(s,l-1)}||_\infty > \varepsilon_{\phi,2}$ *or* $||1 - T^{j,(s,l)}/T^{j,(s,l-1)}||_\infty > \varepsilon_{T,2}\}$ **do**

      $l = l + 1$

      for $g = 1, ..., G$ **do**

        Calculate $\Sigma_{\cdot,g}^{j,(s,l-1)} = \Sigma_{\cdot,g}(T^{j,(s,l-1)})$, $q_{del,g}^{\chi}(C_d^{j,(s,l-1)})$

        Calculate $Q_{s,g,0}^{j,(s,l-1)}$

      for $g = 1, ..., G$ **do**

        Solve the MLOQD equations to calculate $\phi_g^{j,(s,l)}$ and $J_g^{j,(s,l)}$

      Calculate spectrum-averaged factors, $\overline{E}^{j,(s,l)}$, $\overline{\Sigma}_a^{j,(s,l)}$, $\overline{(1-\beta)\nu\Sigma_f}^{j,(s,l)}$, $\overline{\nu\Sigma_f}^{j,(s,l)}$, $\overline{\Sigma}_{tr}^{j,(s,l)}$, $\bar{\zeta}^{j(s,l)}$ etc

      $n = 0$

      while $\{||\phi^{j,(s,l,n-1)} - \phi^{j,(s,l,n)}||_\infty > (1 + \varepsilon_{\phi,3})||\phi^{j,(s,l,n)}||_\infty$ *or* $||T^{j,(s,l,n-1)} - T^{j,(s,l,n)}||_\infty > (1 + \varepsilon_{T,3})||T^{j,(s,l,n)}||_\infty\}$ **do**

        $n = n + 1$

        Solve the GLOQD equations coupled with reactor kinetics and heat equations to calculate $T^{j,(s,l,n)}$ and $\phi^{j,(s,l,n)}$ using Newton's method

      Calculate $J^{j,(s,l,n)}$

      for $d = 1, ..., 6$ **do**

        Calculate $C_d^{j,(s,l)}$

      $\phi^{j,(s,l)} = \phi^{j,(s,l,n)}$ and $T^{j,(s,l)} = T^{j,(s,l,n)}$

    $\phi_g^{j,(s)} = \phi_g^{j,(s,l)}$, $\phi^{j,(s)} = \phi^{j,(s,l)}$ and $T^{j,(s)} = T^{j,(s,l)}$

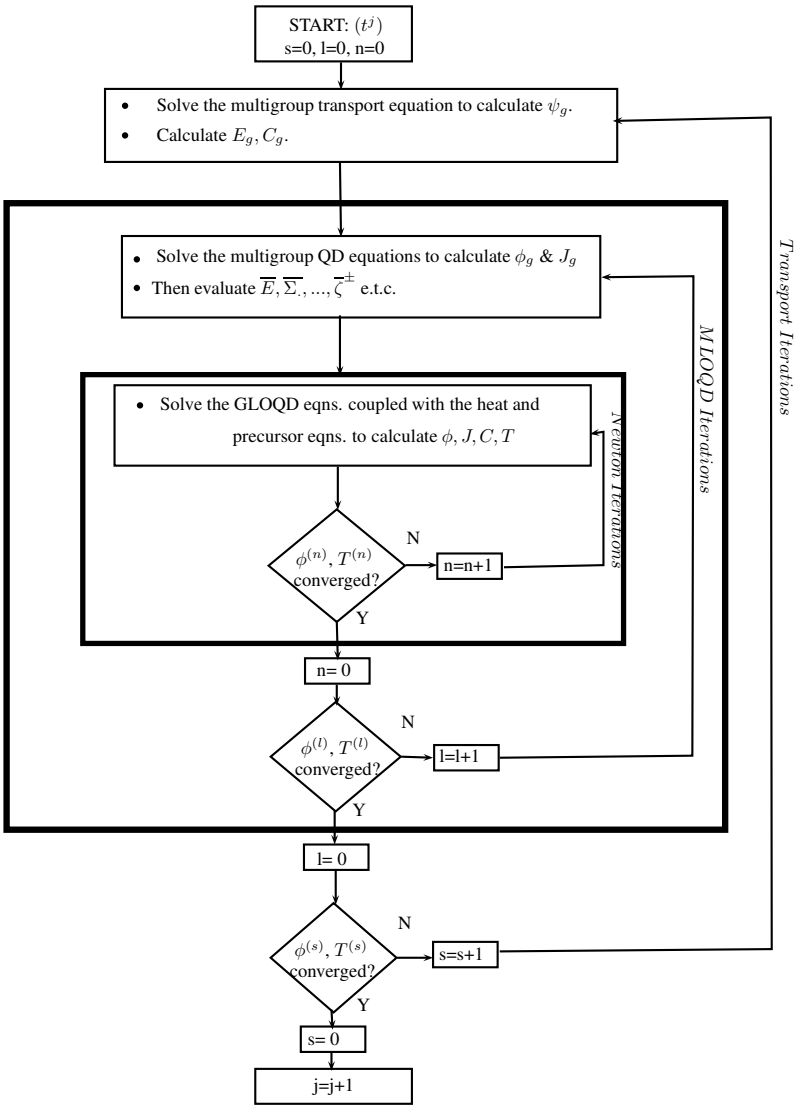

Figure 2.1: Algorithm flowchart for the MP method.

The Fixed Point Iteration (FPI) scheme discussed in section 2.1 is also used to solve the test problems. Figure 2.2 illustrates the main components of this method in a flowchart. Algorithm **2** lists the detailed steps that are followed while solving problems using this method. On each time step (t^j), this method consists of two main stages:

- For the available temperature $(T^{j,(m)})$, the coupled system of multigroup transport and PCB equation is solved by means of the multilevel QD method to obtain the transport solutions: $\psi_g^{j,(m+1)}$ and $\phi_g^{j,(m+1)}$
- The transport solution is used to update the energy deposition term, and the HT equation

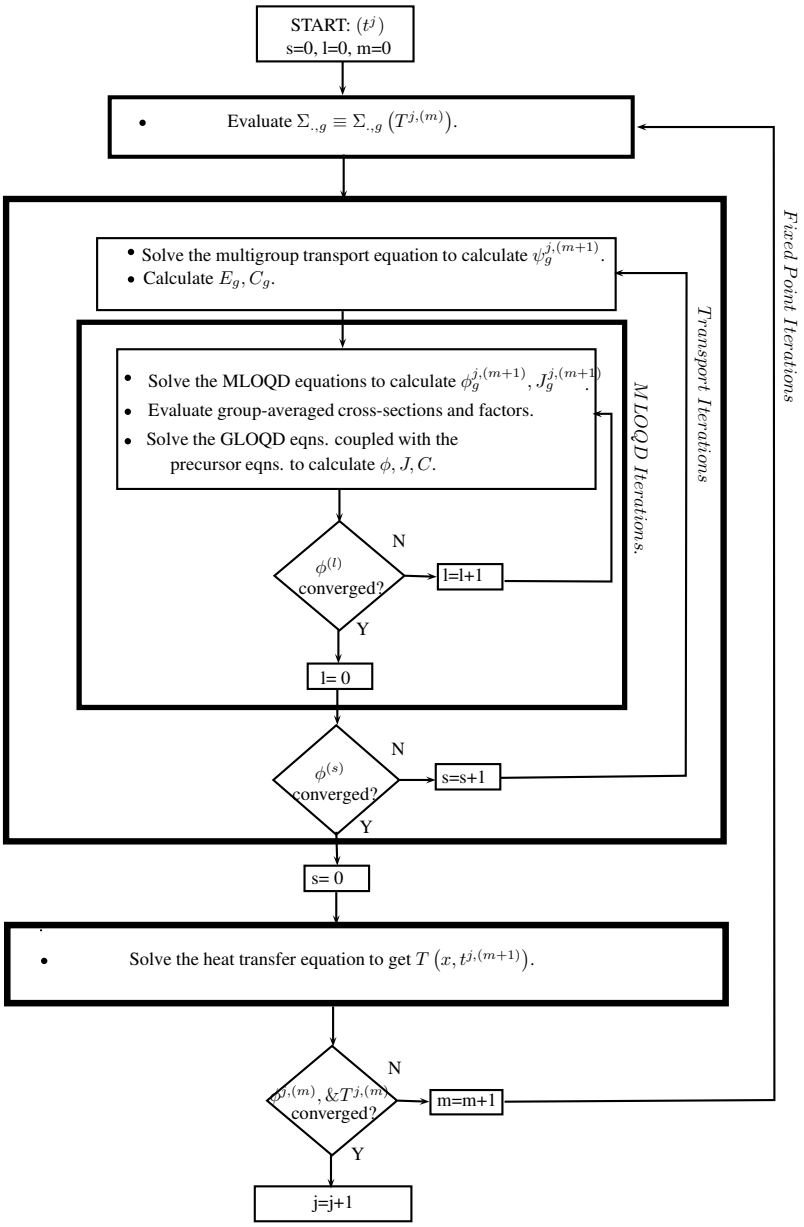

Figure 2.2: Algorithm flowchart for the FPI method.

is solved to calculate a new estimate of the temperature distribution, i.e. $(T^{j,m+1})$.

Algorithm 2: The Iteration Algorithm for the Fixed-Point Iteration (FPI) method.

$j = 0$

while $t^j \leq t^{end}$ **do**

  $j = j + 1$, $t^j = t^{j-1} + \Delta t^j$

  $m = -1$

  Set $\phi_g^{j,(m,s)}\Big|_{m=0,s=0} = \phi_g^{(j-1)}$, $\phi^{j,(m,s)}\big|_{m=0,s=0} = \phi^{(j-1)}$

  Set $C^{j,(m,s)}\big|_{m=0,s=0} = C^{(j-1)}$, $T^{j,(m,s)}\big|_{m=0} = T^{(j-1)}$

  $\Sigma_{\cdot,g}(T^{j,(s-1)})$,

  while $\{||1 - \phi^{j,(m)}/\phi^{j,(m-1)}||_\infty > \varepsilon_{\phi,1}$ *or* $||1 - T^{j,(m)}/T^{j,(m-1)}||_\infty > \varepsilon_{T,1}\}$ **do**

    m=m+1

    for *g=1,....G* **do**

      Calculate $\Sigma_{\cdot,g}\left(T^{j,(m-1)}\right)$

    s=-1

    while $\{||1 - \phi^{j,(m,s)}/\phi^{j,(m,s-1)}||_\infty > \varepsilon_{\phi,2}\}$ **do**

      $s = s + 1$

      if $s > 0$ **then for** $g = 1, ..., G$ **do**

        In case of α-approximation, calculate $\alpha_{g,i}^{j(m,s-1)} = \ln(\phi_{g,i}^{j,(m,s-1)}/\phi_{g,i}^{j-1})/\Delta t^j$

        Calculate $\overline{\Sigma}_{s,g,0}^{j,(m,s-1)}$, $\overline{(1-\beta)\nu\Sigma_f}^{j,(m,s-1)}$, $q_{del,g}^{\chi}(C_d^{j,(m,s-1)})$ etc

        Use Eq. (2.59) to set $\psi_g^{j,(m,s-1/2)}(0)$ and $\psi_g^{j,(m,s-1)}(X)$

        Solve the transport equation to calculate $\psi_g^{j,(m,s-1/2)}$

        Calculate $E_g^{j,(m,s-1/2)}$ etc

      $l = 0$

      while $\{||1 - \phi^{j,(m,s,l)}/\phi^{j,(m,s,l-1)}||_\infty > \varepsilon_{\phi,3}$ **do**

        $l = l + 1$

        for $g = 1, ..., G$ **do**

          Calculate $q_{del,g}^{\chi}(C_d^{j,(m,s,l-1)})$, $Q_{s,g,0}^{j,(m,s,l-1)}$

        for $g = 1, ..., G$ **do**

          Solve the MLOQD equations to calculate $\phi_g^{j,(m,s,l)}$ and $J_g^{j,(m,s,l)}$

        Calculate spectrum-averaged factors, $\overline{E}^{j,(m,s,l)}$, $\overline{\Sigma}_a^{j,(m,s,l)}$, $\overline{(1-\beta)\nu\Sigma_f}^{j,(m,s,l)}$, $\overline{\nu\Sigma_f}^{j,(m,s,l)}$, $\overline{\Sigma}_{tr}^{j,(m,s,l)}$, $\bar{\zeta}^{j(m,s,l)}$ etc

        Solve the GLOQD equations coupled with precursor equations to calculate $J^{j,(m,s,l)}$ and $\phi^{j,(m,s,l)}$.

        for $d = 1, ..., 6$ **do**

          Calculate $C_d^{j,(m,s,l)}$

      $\phi^{j,(m,s)} = \phi^{j,(m,s)}$

    $\phi_g^{j,(m)} = \phi_g^{j,(m,s)}$, $\phi^{j,(m)} = \phi^{j,(m,s)}$

    Solve the heat transfer equation to calculate $T^{j,(m)}$.

Chapter 3

Discretization and Linearization

3.1 The High-Order Problem

The transport problem is discretized in angle using the method of discrete-ordinates [7, 8]. Under this discretization, the transport problem is solved for a set of discrete directions defined by an angular quadrature set. The discrete-ordinates multigroup transport equation in 1D slab geometry with isotropic scattering is given by

$$\frac{1}{v_g}\frac{\partial \psi_{g,m}}{\partial t} + \mu_m \frac{\partial \psi_{g,m}}{\partial x} + \Sigma_{t,g}\psi_g = Q_g, \tag{3.1}$$

$$m = 1, ..., M,$$

where

$$Q_g = \frac{1}{2}\left(\overline{\Sigma}_{s,g,0} + \chi_g^p \overline{(1-\beta)\nu\Sigma_f}\right)\phi + \frac{1}{2}\left(q_{del,g}^{\chi} + q_{ext,g}\right), \tag{3.2}$$

$$\psi_{g,m} \equiv \psi_g(x, \mu_m, t), \tag{3.3}$$

$$\overline{(1-\beta)\nu\Sigma_f} = \frac{\sum_{g=1}^{G}(1-\beta_g)\nu_{f,g}\Sigma_{f,g}\phi_g}{\sum_{g=1}^{G}\phi_g}, \tag{3.4}$$

$$\overline{\Sigma}_{s,g,0} = \frac{\sum\limits_{g'=1}^{G}\Sigma_{s,g'\to g,0}\phi_{g'}}{\sum\limits_{g=1}^{G}\phi_g}, \tag{3.5}$$

and,

$$q^{\chi}_{del,g} = \sum_{d=1}^{6} \chi^{del}_{d,g} \lambda_d C_d \,. \tag{3.6}$$

3.1.1 Method of Short Characteristics

The method of short characteristics (MSC) [37, 38, 39, 40, 41, 42] is used to discretize the transport equation in space and time. This scheme solves the transport equation along particle tracks. It belongs to a broad class of methods called the method of characteristics [43]. This class of methods is used to solve hyperbolic partial differential equations. In this method, the solutions of the partial differential equations are sought in specific directions along which the partial derivatives are reduced to total differentials [44]. These directions are also called the characteristics of the equation. The detailed derivation of the MSC method for one-dimensional neutron transport equation is given below.

Consider the time-dependent discrete-ordinates neutron transport equation in 1D slab geometry for direction μ_m

$$\frac{1}{v_g}\frac{\partial \psi_{g,m}}{\partial t} + \mu_m \frac{\partial \psi_{m,g}}{\partial x} + \Sigma_{t,g}\psi_{g,m} = Q_g. \tag{3.7}$$

Let s be the distance along a characteristics that represent a particle track. The equations of characteristics are then defined by

$$ds = v_g dt, \tag{3.8}$$

$$ds = \frac{dx}{\mu_m}. \tag{3.9}$$

The partial differential equation (3.7) is reduced to an ordinary differential one along the characteristic. The derivative along the characteristic is given by

$$\frac{d\psi_{g,m}(s)}{ds} = \frac{\partial \psi_{g,m}(x,t)}{\partial t}\frac{dt}{ds} + \frac{\partial \psi_{g,m}(x,t)}{\partial x}\frac{dx}{ds}. \tag{3.10}$$

Using relations (3.7)-(3.10), we get the transport problem in the characteristic form:

$$\frac{d\psi_{m,g}}{ds} + \Sigma_{t,g}\psi_{g,m} = Q_g. \tag{3.11}$$

In our problem, the domain is defined on a discrete mesh in space and time (see Figure 3.1). The solution involves sweeping the spatial domain for all angular directions for one time-step. The sweep along the domain is performed one cell at a time in the short-characteristic method. After the solutions are obtained for the current time-step, we march up in the space-time grid

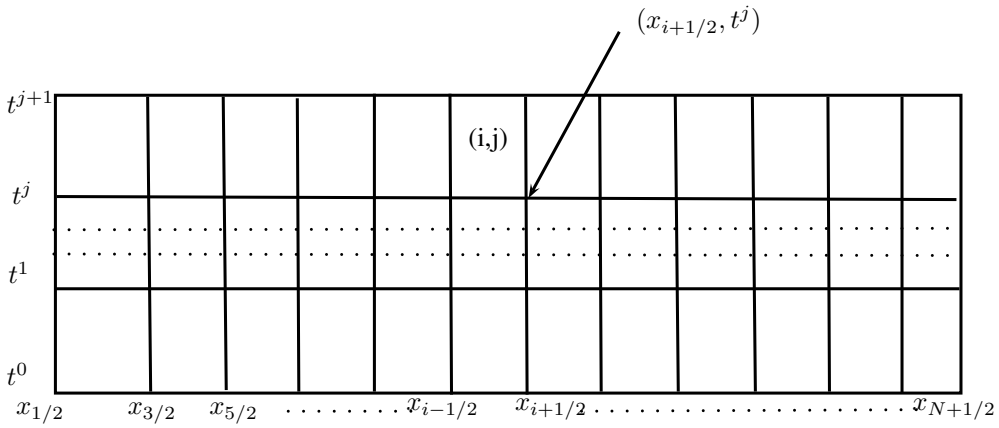

Figure 3.1: Grid in space and time for time-dependent problems in 1D slab geometry.

to evaluate the solutions for the next moment of time. The entire vector of the angular flux is needed to be stored in order to evaluate the vector of solution for the next time step using the MSC scheme.

This constrasts with the long characteristics method, where each characteristic spans the entire problem domain in the X-Y domain [8]. The method of long characteristics is also often simply called the method of characteristics in literature. The problem domain consists of non-uniform material subdomains. The usage was first reported by Askew in 1972 [45]. Major production softwares such as CASMO-5 [46] rely on this method to solve reactor-physics problems today.

Consider the solution of the transport problem using the MSC scheme in (i,j)-th cell of the grid. The value of the angular flux is known at three of the vertices. The solution of the angular flux at the fourth vertex involves tracing the particular characteristic which pass through this vertex and performing an interpolation of the upstream angular flux to evaluate the solution at the position of intersection of this characteristic with the cell face. For $\Delta x_i = \left(x_{i+1/2} - x_{i-1/2}\right)$ and $\Delta t^j = t^{j+1} - t^j$, the following cases are possible (group index g dropped for brevity),

- Case 1

$$\begin{aligned} \mu_m &> 0, \\ \frac{\Delta x_i}{\Delta t^j} &\geq v_g \mu_m. \end{aligned}$$

In Figure 3.2, $\mathcal{C}$ represents the characteristic that passes through the vertex $(x_{i+1/2}, t^j)$.

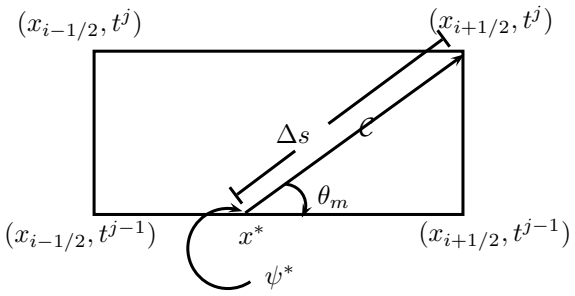

Figure 3.2: Case 1: Track originates at bottom face, $\mu_m > 0$.

The length of the segment, denoted by Δs, is oriented at an angle $\theta = cos^{-1}(\mu_m)$. The characteristic enters the cell (i,j) at point x^*, the value of which is given by

$$x^* = x_{i+1/2} - \mu_m v_g \Delta t^j. \tag{3.12}$$

The source and cross-section over the track are approximated by the averages of their respective values, i.e.

$$\Sigma_{t,i}^{j-1/2} = \frac{1}{2}\left(\Sigma_{t,i}^{j} + \Sigma_{t,i}^{j-1}\right). \tag{3.13}$$

$$Q_i^{j-1/2} = \frac{1}{2}\left(Q_i^{j} + Q_i^{j-1}\right). \tag{3.14}$$

The value of the incoming angular flux, ψ^* at point x^* is determined by means of the linear interpolation of the values of the angular fluxes at the bottom vertexes of the cell, i.e.

$$\psi^* = \frac{1}{\Delta x_i}\left[\left(x^* - x_{i-1/2}\right)\psi_{i+1/2}^{j-1} + \left(x_{i+1/2} - x^*\right)\psi_{i-1/2}^{j-1}\right]. \tag{3.15}$$

where $\psi_{i\pm1/2}^{j-1}$ are available from the results of the previous time step. The value of the angular flux at vertex $(x_{i+1/2}, t^j)$ is then evaluated as follows:

$$\psi_{i+1/2}^{j} = \psi^* e^{-\Sigma_{t,i}^{j-1/2}\Delta s} + \frac{Q_i^{j-1/2}}{\Sigma_{t,i}^{j-1/2}}\left(1 - e^{-\Sigma_{t,i}^{j-1/2}\Delta s}\right), \tag{3.16}$$

where

$$\Delta s = v\Delta t. \tag{3.17}$$

- Case 2

$$\mu_m < 0, \tag{3.18}$$
$$\frac{\Delta x_i}{\Delta t^j} \geq v_g|\mu_m|. \tag{3.19}$$

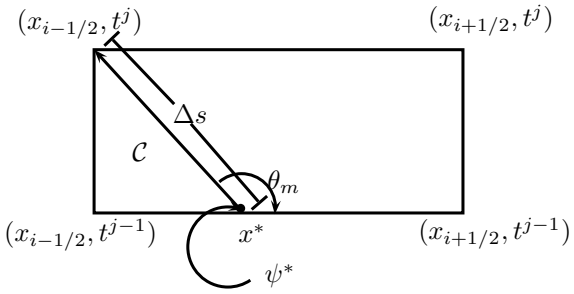

Figure 3.3: Case 2: Track originates at bottom face, $\mu_m < 0$.

The value of the entrant angular flux at x^* is approximated in the same manner as in Case 1. The angular flux is to be evaluated for the vertex $(x_{i-1/2}, t^j)$. It is given by the expression

$$\psi^j_{i-1/2} = \psi^* e^{-\Sigma^{j-1/2}_{t,i}\Delta s} + \frac{Q^{j-1/2}_i}{\Sigma^{j-1/2}_{t,i}}\left(1 - e^{-\Sigma^{j-1/2}_{t,i}\Delta s}\right), \tag{3.20}$$

where

$$\Delta s = v\Delta t.$$

- Case 3

$$\mu_m > 0, \tag{3.21}$$
$$\frac{\Delta x_i}{\Delta t^j} < v_g\mu_m. \tag{3.22}$$

The angular flux is to be determined at $(x_{i+1/2}, t^j)$. This case corresponds to a situation where the characteristic line enters the cell from the left face. The point of entry is denoted by t^* and the value of the entrant angular flux is linearly interpolated using the values in the vertexes: $(x_{i-1/2}, t^{j-1})$ and $(x_{i-1/2}, t^j)$. The angular flux at vertex $(x_{i+1/2}, t^j)$ is then

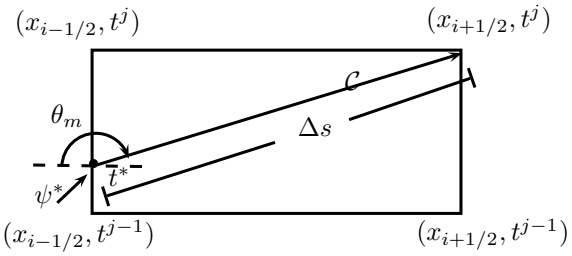

Figure 3.4: Case 3: Track originates from left face, $\mu_m > 0$.

evaluated as follows:

$$\psi^j_{i+1/2} = \psi^* e^{-\Sigma^{j-1/2}_{t,i}\Delta s} + \frac{Q^{j-1/2}_i}{\Sigma^{j-1/2}_{t,i}} \left(1 - e^{-\Sigma^{j-1/2}_{t,i}\Delta s}\right). \tag{3.23}$$

where

$$\psi^* = \frac{1}{\Delta t^j}\left[\left(t^* - t^{j-1}\right)\psi^j_{i-1/2} + \left(t^j - t^*\right)\psi^j_{i-1/2}\right], \tag{3.24}$$

$$t^* = t^j - \frac{\Delta s}{v_g}, \tag{3.25}$$

$$\Delta s = \frac{\Delta x_i}{\mu_m}. \tag{3.26}$$

- Case 4

$$\begin{aligned} \mu_m &< 0, \\ \frac{\Delta x_i}{\Delta t^j} &< v_g|\mu_m|. \end{aligned}$$

In this case, the angular flux is to be determined for the top-left vertex at $(x_{i-1/2}, t^j)$. Given the values of the angular flux at the two vertexes of the incoming face, the following relation is used to evaluate the unknown in this case

$$\psi^j_{i-1/2} = \psi^* e^{-\Sigma^{j-1/2}_{t,i}\Delta s} + \frac{Q^{j-1/2}_i}{\Sigma^{j-1/2}_{t,i}} \left(1 - e^{-\Sigma^{j-1/2}_{t,i}\Delta s}\right), \tag{3.27}$$

where

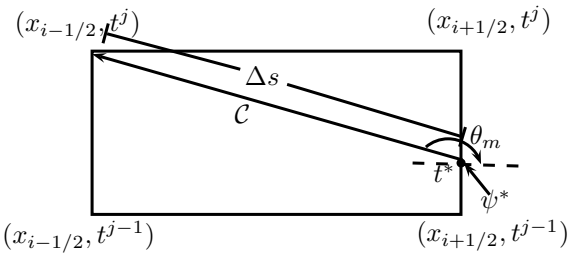

Figure 3.5: Case 4: Track orginates from right face, $\mu_m < 0$.

$$\psi^* = \frac{1}{\Delta t^j}\left[\left(t^* - t^{j-1}\right)\psi^j_{i+1/2} + \left(t^j - t^*\right)\psi^{j-1}_{i+1/2}\right], \tag{3.28}$$

$$t^* = \frac{1}{v_g\mu_m}\Delta x_i + t^j, \tag{3.29}$$

$$\Delta s = \frac{\Delta x_i}{|\mu_m|}. \tag{3.30}$$

The MSC method results in the determination of the groupwise cell-edge angular fluxes $\left(\psi^j_{g,m,i+1/2}\right)$ for a given moment of time (t^j). To proceed with solving the MLOQD equations, it is necessary to determine the cell-averaged QD factors (E_g) for each cell in the spatial domain. This is done by first evaluating the cell-average angular flux as follows:

$$\psi^j_{m,g,i} = \omega^j_{m,i}\psi^j_{m,g,i-1/2} + (1-\omega^j_{m,g,i})\psi^j_{m,g,i+1/2}\,, \tag{3.31}$$
$$m = 1, ..., M,$$

where

$$\omega^j_{m,g,i} = \frac{1}{\tau^j_{m,g,i}} - \frac{1}{e^{\tau^j_{m,g,i}} - 1}, \tag{3.32}$$
$$i = 1, ..., N, \quad \mu_m > 0,$$

$$\omega^j_{m,g,i} = \frac{1}{\tau^j_{m,g,i}} - \frac{e^{-\tau^j_{m,g,i}}}{1 - e^{\tau^j_{m,g,i}}}, \tag{3.33}$$
$$i = 1, ..., N, \quad \mu_m < 0,$$

and

$$\tau^j_{m,g,i} = \frac{\Sigma^{j-1/2}_{t,g,i}\Delta x_i}{|\mu_m|}. \tag{3.34}$$

The cell-averaged QD factors are then evaluated as

$$E^j_{g,i} = \frac{\sum_{m=1}^{M} \mu_m^2 \psi^j_{m,g,i} w_m}{\sum_{m=1}^{M} \psi^j_{m,g,i} w_m} \tag{3.35}$$

3.1.2 α -Approximation for Time-Dependent Transport

The $\alpha-$ approximation for the time-dependent transport equation [5, 47, 48] is based on the assumption that the angular flux depends on time as follows:

$$\psi(x, \mu, t) = \tilde{\psi}(x, \mu) e^{\alpha t} \,. \tag{3.36}$$

This leads to the following approximation of the derivative term for $t^{j-1} < t < t^j$:

$$\frac{\partial \psi_{m,g,i}}{\partial t} \approx \alpha^j_{g,i} \psi^j_{m,g,i} \,. \tag{3.37}$$

The rate of change in time, $\alpha_{g,i}$, is estimated by the corresponding rate of change of the group scalar flux in the given spatial cell:

$$\alpha_{g,i} = \frac{1}{\phi_{g,i}} \frac{d\phi_{g,i}}{dt} = \frac{d \ln(\phi_{g,i})}{dt} \,, \tag{3.38}$$

where $\phi_{g,i}$ is obtained from the solution of the MLOQD problem. Eq. (3.38) is evaluated for a given time-step as follows,

$$\alpha^j_{g,i} = \frac{\ln\left(\frac{\phi^j_{g,i}}{\phi^{j-1}_{g,i}}\right)}{\Delta t^j} \,. \tag{3.39}$$

Using Eqs. (3.36) and (3.39) to approximate the time-derivative term in Eq. (3.1) and integrating the continuous transport problem over the i-th spatial cell, we get the following detailed balance equation for the cell:

$$\frac{\Delta x_i}{v_g} \alpha^j_{g,i} \psi^j_{m,g,i} + \mu_m (\psi^j_{m,g,i+1/2} - \psi^j_{m,g,i-1/2}) + \Sigma^j_{t,g,i} \psi^j_{m,g,i} \Delta x_i = \mathcal{Q}^j_{m,g,i} \Delta x_i \,, \tag{3.40}$$

where $\psi^j_{m,g,i\pm1/2}$ denotes the cell-edge fluxes, and $\psi^j_{m,g,i}$ denotes the cell-average angular flux in the i-th cell. The cell-average angular flux for the i-th cell is defined as

$$\psi^j_{m,g,i} = \frac{1}{\Delta x_i} \int_{x_{i-1/2}}^{i+1/2} \psi_{m,g}(x, t^j) dx \,. \tag{3.41}$$

Rearranging Eq. (3.40), we get

$$\mu_m(\psi^j_{m,g,i+1/2} - \psi^j_{m,g,i-1/2}) + (\Sigma^j_{t,g,i} + \frac{\alpha^j_{g,i}}{v_g})\psi^j_{m,g,i}\Delta x_i = \mathcal{Q}^j_{m,g,i}\Delta x_i \,. \tag{3.42}$$

Thus, on each time step (t^j), one needs to solve the high-order transport equation of the form

$$\mu_m(\psi^j_{m,g,i+1/2} - \psi^j_{m,g,i-1/2}) + \tilde{\Sigma}^j_{t,g,i}\psi^j_{m,g,i}\Delta x_i = \mathcal{Q}^j_{m,g,i}\Delta x_i \,, \tag{3.43}$$

$$\tilde{\Sigma}^j_{t,g,i} = \begin{cases} \Sigma^j_{t,g,i} + \frac{\alpha^j_{g,i}}{v_g} \,, & \text{if} \quad \Sigma^j_{t,g,i} + \frac{\alpha^j_{g,i}}{v_g} > \delta_\alpha \,, \\ \delta_\alpha \,, & \text{if} \quad \Sigma^j_{t,g,i} + \frac{\alpha^j_{g,i}}{v_g} \leq \delta_\alpha \,, \end{cases} \tag{3.44}$$

where δ_α is a given parameter (for example, δ_α=10^{-4}).

The system of equations, Eq. (3.42) is solved using the method of step-characteristics (SC) [49]. This method is second order accurate in slab geometry and yields positive cell-average and cell-edges fluxes for positive source and boundary terms. Using the SC scheme, the expression for the flux exiting the i-th cell is evaluated as follows. For $\mu_m \gtrless 0$,

$$\psi_{m,g,i\pm1/2} = \psi_{m,g,i\mp1/2}e^{\mp\tilde{\Sigma}_{t,g,i}\Delta x_i/|\mu_m|} + \left(1 - e^{\mp\tilde{\Sigma}_{t,g}\Delta x_i/|\mu_m|}\right)\frac{Q_{g,i}}{\tilde{\Sigma}_{t,g,i}}. \tag{3.45}$$

and the cell-average flux is evaluated as

$$\psi_{m,g,i} = \omega_{m,g,i}\psi_{m,g,i-1/2} + (1 - \omega_{m,g,i})\psi_{m,g,i+1/2} \,, \tag{3.46}$$

where

$$\omega_{m,g,i} = \frac{1}{\tau_{m,g,i}} - \frac{1}{e^{\tau_{m,g,i}} - 1} \,, \tag{3.47}$$
$$i = 1, ..., N \,, \;\; g = 1, ..., G \,, \;\; \mu_m > 0 \,,$$

$$\omega^j_{m,g,i} = \frac{1}{\tau_{m,g,i}} - \frac{e^{-\tau_{m,g,i}}}{1 - e^{-\tau_{m,g,i}}} \,, \tag{3.48}$$
$$i = 1, ..., N \,, \;\; g = 1, ..., G \,, \;\; \mu_m < 0 \,,$$

$$\tau_{m,g,i} = \frac{\tilde{\Sigma}_{t,g,i}\Delta x_i}{\mu_m} \,. \tag{3.49}$$

Note that the storage of the vector of angular flux is not required in this scheme. The vector of scalar flux from the previous time step is used to evaluate the solution of the transport problem for the current time step.

3.2 The Low-Order Equations

3.2.1 The Multigroup Low-Order QD Equations

The low-order quasidiffusion equations are discretized in space using a finite volume (FV) scheme [6, 25]. The balance equation given by Eq. (2.27) is integrated over the i-th spatial interval, i.e. $x_{i-1/2} \leq x \leq x_{i+1/2}$. The first-moment equation given by Eq. (2.28) is integrated around the node $x_{i+1/2}$ over $x_i \leq x \leq x_{i+1}$, where x_i and x_{i+1} are midpoints of cells adjacent to $x_{i+1/2}$. This results in the following,

$$\begin{aligned}
&\frac{\Delta x_i}{v_g}\frac{d\phi_{g,i}}{dt} + J_{g,i+1/2} - J_{g,i-1/2} + (\Sigma_{t,g,i} - \Sigma_{s,g\to g,0,i})\phi_{g,i}\Delta x_i = \\
&\Delta x_i \sum_{g'=1}^{g-1} \Sigma_{s,g'\to g,0,i}\phi_{g',i} + \left(Q_{s,g,0,i} + \chi_{g,i}\overline{(1-\beta)\nu\Sigma}_{f,i}\right)\phi_i\Delta x_i + \left(q^{\chi}_{del,g,i} + q_{ext,g,i}\right)\Delta x_i\,, \quad (3.50)
\end{aligned}$$

$$i = 1, ..., N\,,$$

$$\frac{\Delta x_{i+1/2}}{v_g}\frac{dJ_{g,i+1/2}}{dt} + E_{g,i+1}\phi_{g,i+1} - E_{g,i}\phi_{g,i} + \Sigma_{t,g,i+1/2}\Delta x_{i+1/2}J_{g,i+1/2} = 0\,, \quad (3.51)$$

$$i = 0, ..., N\,,$$

where

$$\Delta x_{i+1/2} = \frac{1}{2}\left(\Delta x_i + \Delta x_{i+1}\right)\,, \quad (3.52)$$

$$\Delta x_0 = 0, \quad \Delta x_{N+1/2} = 0\,, \quad (3.53)$$

$$\phi_{g,i} = \sum_{m=1}^{M}\psi_{g,m,i}w_m, \quad J_{g,i+1/2} = \sum_{m=1}^{M}\mu_m\psi_{g,m,i+1/2}w_m\,, \quad (3.54)$$

$$E_{g,i} = \frac{\sum_{m=1}^{M}\mu_m^2\psi_{g,m,i}w_m}{\sum_{m=1}^{M}\psi_{g,m,i}w_m}, \quad Q_{s,g,0,i} = \frac{\sum_{g'=g+1}^{G}\Sigma_{s,g'\to g}\phi_{g',i}}{\sum_{g'=1}^{G}\phi_{g',i}}\,, \quad (3.55)$$

$$\overline{(1-\beta)\nu\Sigma}_{f,i} = \frac{\sum\limits_{g=1}^{G}(1-\beta_g)\,\nu_{f,g,i}\Sigma_{f,g,i}\phi_{g,i}}{\sum\limits_{g=1}^{G}\phi_{g,i}}\,, \tag{3.56}$$

$$\Sigma_{t,g,i+1/2} = \frac{\Sigma_{t,g,i}\Delta x_i + \Sigma_{t,g,i+1}\Delta x_{i+1}}{\Delta x_i + \Delta x_{i+1}}. \tag{3.57}$$

The equations (3.50) and (3.51) are discretized in time by means of the fully implicit scheme. This gives us

$$\frac{\Delta x_i}{v_g}\left[\frac{\phi^j_{g,i}-\phi^{j-1}_{g,i}}{\Delta t^j}\right] + J^j_{g,i+1/2} - J^j_{g,i-1/2} + (\Sigma^j_{t,g,i} - \Sigma^j_{s,g\to g,0,i})\Delta x_i\phi^j_{g,i} =$$
$$\Delta x_i\sum_{g'=1}^{g-1}\Sigma^j_{s,g'\to g,0,i}\phi^j_{g',i} + \Delta x_i\big(Q^j_{s,g,0,i} + \chi^j_{g,i}\overline{(1-\beta)\nu\Sigma_f}^{\,j}_i\big)\phi^j_i + \big(q^{\chi,j}_{del,g,i} + q^j_{ext,g,i}\big)\Delta x_i\,, \tag{3.58}$$

$$\frac{\Delta x_{i+1/2}}{v_g}\left[\frac{J^j_{g,i+1/2}-J^{j-1}_{g,i+1/2}}{\Delta t^j}\right] +$$
$$E^j_{g,i+1}\phi^j_{g,i+1} - E^j_{g,i}\phi^j_{g,i} + \Sigma^j_{t,g,i+1/2}\Delta x_{i+1/2}J^j_{g,i+1/2} = 0\,. \tag{3.59}$$

Rearrangement gives

$$J^j_{g,i+1/2} - J^j_{g,i-1/2} + \Big(\Sigma^j_{t,g,i} - \Sigma^j_{s,g\to g,0,i} + \frac{1}{\Delta t^j v^g}\Big)\Delta x_i\phi^j_{g,i} =$$
$$\Delta x_i\sum_{g'=1}^{g-1}\Sigma^j_{s,g'\to g,0,i}\phi^j_{g',i} + \Delta x_i\big(Q^j_{s,g,0,i} + \chi^j_{g,i}\overline{(1-\beta)\nu\Sigma_f}^{\,j}_i\big)\phi^j_i + \big(\hat{q}^{\chi,j}_{del,g,i} + q^j_{ext,g,i}\big)\Delta x_i$$
$$+ \frac{\phi^{j-1}_{g,i}\Delta x_i}{v_g\Delta t^j}, \tag{3.60}$$

$$E^j_{g,i+1}\phi^j_{g,i+1} - E^j_{g,i}\phi^j_{g,i} + \Big(\Sigma^j_{t,g,i+1/2} + \frac{1}{v_g\Delta t^j}\Big)\Delta x_{i+1/2}J^j_{g,i+1/2} = \frac{J^{j-1}_{g,i+1/2}\Delta x_{i+1/2}}{v_g\Delta t^j}. \tag{3.61}$$

Thus, on each time step (t^j) the discretized multigroup LOQD equations are defined by

$$J^j_{g,i+1/2} - J^j_{g,i-1/2} + \Big(\Sigma^j_{t,g,i} - \Sigma^j_{s,g\to g,0,i} + \frac{1}{v_g \Delta t^j}\Big)\Delta x_i \phi^j_{g,i} = \Delta x_i \sum_{g'=1}^{g-1} \Sigma^j_{s,g'\to g,0,i}\phi^j_{g',i}$$
$$+ \Delta x_i \big(Q^j_{s,g,0,i} + \chi^j_{g,i}\overline{(1-\beta)\nu\Sigma_f}_i^{\,j}\big)\phi^j_i + \big(q^{\chi,j}_{del,g,i} + q^j_{ext,g,i}\big)\Delta x_i + \mathcal{B}^{j-1}_{g,i}\,, \quad (3.62)$$

$$i = 1, ..., N_i\,,$$

$$E^j_{g,i+1}\phi^j_{g,i+1} - E^j_{g,i}\phi^j_{g,i} + \Big(\Sigma^j_{t,g,i+1/2} + \frac{1}{v_g\Delta t^j}\Big)\Delta x_{i+1/2} J^j_{g,i+1/2} = \mathcal{G}^{j-1}_{g,i+1/2}\,, \quad (3.63)$$

$$i = 0, ..., N_i\,,$$

$$J^j_{g,1/2} = B^j_{L,g}\phi^j_{g,0}\,, \quad (3.64)$$

$$J^j_{g,N_i+1/2} = B^j_{R,g}\phi^j_{g,N_i+1}\,, \quad (3.65)$$

where,

$$\mathcal{B}^{j-1}_{g,i} = \frac{\phi^{j-1}_{g,i}\Delta x_i}{v_g\Delta t^j}, \quad (3.66)$$

$$\mathcal{G}^{j-1}_{g,i+1/2} = \frac{J^{j-1}_{g,i+1/2}\Delta x_{i+1/2}}{v_g\Delta t^j}. \quad (3.67)$$

3.2.2 The Grey Low-order QD equation

To derive the discretized form of the grey balance equation (2.35), we sum Eq. (3.62) over the groups and introduce various averaged cross sections to get

$$J^j_{i+1/2} - J^j_{i-1/2} + \left(\overline{\Sigma}^j_{a,i} - \overline{(1-\beta)\nu\Sigma_{f,i}}^{\,j} + \frac{1}{\Delta t^j \overline{v}^j_i}\right)\phi^j_i \Delta x_i = \Big(q^j_{del,i} + q^j_{ext,i}\Big)\Delta x_i + \overline{\mathcal{B}}^{j-1}_i, \quad (3.68)$$

$$i = 1, ..., N_i,$$

where

$$\overline{\mathcal{B}}_i^{j-1} = \sum_{g=1}^{G} \mathcal{B}_{g,i}^{j-1}, \;\; \overline{v}_i^j = \frac{\sum\limits_{g=1}^{G} \phi_{g,i}}{\sum\limits_{g=1}^{G} \frac{\phi_{g,i}}{v_g}}, \tag{3.69}$$

$$\overline{\Sigma}_{a,i}^j = \frac{\sum\limits_{g=1}^{G} \left(\Sigma_{t,g,i}^j - \Sigma_{s,g,i}^j\right) \phi_{g,i}^j}{\sum\limits_{g=1}^{G} \phi_{g,i}^j}. \tag{3.70}$$

The discretization of the grey first moment equation (2.36) is obtained by summing Eq. (3.63) over the groups. This gives us

$$\overline{E}_{i+1}^j \phi_{i+1}^j - \overline{E}_i^j \phi_i^j + \Delta x_{i+1/2} \sum_{g=1}^{G} \left(\Sigma_{t,g,i+1/2}^j + \frac{1}{v_g \Delta t^j}\right) J_{g,i+1/2}^j = \sum_{g=1}^{G} \mathcal{G}_{g,i+1/2}^{j-1}. \tag{3.71}$$

We define

$$\tilde{v}_{i+1/2}^j = \frac{\sum_{g=1}^{G} |J_{g,i+1/2}^j|}{\sum_{g=1}^{G} \frac{|J_{g,i+1/2}^j|}{v_g}} \tag{3.72}$$

and averaged total cross-section

$$\overline{\Sigma}_{t,i+1/2}^j = \frac{\sum_{g=1}^{G} \Sigma_{t,g,i+1/2}^j |J_{g,i+1/2}^j|}{\sum_{g=1}^{G} |J_{g,i+1/2}^j|} \tag{3.73}$$

to obtain

$$\begin{aligned} &\overline{E}_{i+1}^j \phi_{i+1}^j - \overline{E}_i^j \phi_i^j + \left(\overline{\Sigma}_{t,i+1/2}^j + \frac{1}{\tilde{v}_{i+1/2}^j \Delta t^j}\right) J_{i+1/2}^j \Delta x_{i+1/2} \\ &\quad + \Delta x_{i+1/2} \sum_{g=1}^{G} \left(\Sigma_{t,g,i+1/2}^j - \overline{\Sigma}_{t,i+1/2}^j + \frac{1}{\Delta t^j}\left[\frac{1}{v_g} - \frac{1}{\tilde{v}_{i+1/2}^j}\right]\right) J_{g,i+1/2}^j = \bar{\mathcal{G}}_{i+1/2}^{j-1}, \end{aligned} \tag{3.74}$$

where

$$\bar{\mathcal{G}}_{i+1/2}^{j-1} = \sum_{g=1}^{G} \mathcal{G}_{g,i+1/2}^{j-1}. \tag{3.75}$$

We now define

$$\bar{\zeta}^{+,j}_{i+1/2} = \begin{cases} \frac{\gamma^j_{i+1/2}}{\sum_{g=1}^G \phi^j_{g,i+1}}\,, & \text{if } \gamma^j_{i+1/2} > 0 \\ 0\,, & \text{if } \gamma_{i+1/2} \le 0 \end{cases}, \quad \bar{\zeta}^{-,j}_{i+1/2} = \begin{cases} 0\,, & \text{if } \gamma_{i+1/2} > 0 \\ \frac{|\gamma^j_{i+1/2}|}{\sum_{g=1}^G \phi^j_{g,i}}\,, & \text{if } \gamma^j_{i+1/2} \le 0 \end{cases}, \tag{3.76}$$

$$\gamma^j_{i+1/2} = \sum_{g=1}^{G} \left(\Sigma^j_{t,g,i+1/2} - \overline{\Sigma}^j_{t,i+1/2} + \frac{1}{\Delta t^j} \left[\frac{1}{v_g} - \frac{1}{\tilde{v}^j_{i+1/2}} \right] \right) J^j_{g,i+1/2}\,, \tag{3.77}$$

and have

$$\begin{aligned} \left(\overline{E}^j_{i+1} + \bar{\zeta}^{+,j}_{i+1/2}\Delta x_{i+1/2}\right)\phi^j_{i+1} - \left(\overline{E}^j_{i} + \bar{\zeta}^{-.j}_{i+1/2}\Delta x_{i+1/2}\right)\phi^j_{i} \\ + \left(\overline{\Sigma}^j_{t,i+1/2} + \frac{1}{\tilde{v}^j_{i+1/2}\Delta t^j}\right) J^j_{i+1/2}\Delta x_{i+1/2} = \bar{\mathcal{G}}^{j-1}_{i+1/2}\,. \end{aligned} \tag{3.78}$$

Note that the discrete equations (3.68) and (3.78) are algebraically consistent with the discretized multigroup LOQD equations. As a result, on each time step one needs to solve the following set of the discretized GLOQD equations:

$$J^j_{i+1/2} - J^j_{i-1/2} + \left(\overline{\Sigma}^j_{a,i} - \overline{(1-\beta)\nu\Sigma_f}^{\,j}_i + \frac{1}{\Delta t^j \bar{v}^j_i} \right) \phi^j_i \Delta x_i = (q^j_{del,i} + q^j_{ext,i})\Delta x_i + \bar{\mathcal{B}}^{j-1}_i\,, \tag{3.79}$$

$$i = 1, ..., N_i\,,$$

$$\begin{aligned} \left(\overline{E}^j_{i+1} + \bar{\zeta}^{+,j}_{i+1/2}\Delta x_{i+1/2}\right)\phi^j_{i+1} - \left(\overline{E}^j_{i} + \bar{\zeta}^{-.j}_{i+1/2}\Delta x_{i+1/2}\right)\phi^j_{i} \\ + \widetilde{\Sigma}^j_{J,i+1/2} J^j_{i+1/2}\Delta x_{i+1/2} = \bar{\mathcal{G}}^{j-1}_{i+1/2}\,, \end{aligned} \tag{3.80}$$

$$i = 0, ..., N_i\,,$$

$$J^j_{1/2} = \bar{C}^j_L \phi^j_0\,, \tag{3.81}$$

$$J^j_{N_i+1/2} = \bar{C}^j_R \phi^j_{N_i+1}\,, \tag{3.82}$$

where

$$\widetilde{\Sigma}^j_{J,i+1/2} = \overline{\Sigma}^j_{t,i+1/2} + \frac{1}{\tilde{v}^j_{i+1/2}\Delta t^j}\,. \tag{3.83}$$

We now use (3.80) to eliminate currents in Eqs. (3.79) to obtain

$$
\begin{aligned}
&-\left[\frac{\overline{E}^j_{i-1}+\bar{\zeta}^{-,j}_{i-1/2}\Delta x_{i-1/2}}{\widetilde{\Sigma}^j_{J,i-1/2}\Delta x_{i-1/2}}\right]\phi^j_{i-1}\\
&\quad+\left[\frac{\overline{E}^j_{i}+\bar{\zeta}^{+,j}_{i-1/2}\Delta x_{i-1/2}}{\widetilde{\Sigma}^j_{J,i-1/2}\Delta x_{i-1/2}}+\frac{\overline{E}^j_{i}+\bar{\zeta}^{-,j}_{i+1/2}\Delta x_{i+1/2}}{\widetilde{\Sigma}^j_{J,i+1/2}\Delta x_{i+1/2}}+\Big(\overline{\Sigma}^j_{a,i}-\overline{(1-\beta)\nu\Sigma_f}^j_i+\frac{1}{\Delta t^j\bar{v}^j_i}\Big)\Delta x_i\right]\phi^j_i\\
&-\left[\frac{\overline{E}^j_{i+1}+\bar{\zeta}^{+,j}_{i+1/2}\Delta x_{i+1/2}}{\widetilde{\Sigma}^j_{J,i+1/2}\Delta x_{i+1/2}}\right]\phi^j_{i+1}=(q^j_{del,i}+q^j_{ext,i})\Delta x_i+\bar{\mathcal{B}}^{j-1}_i+\frac{\bar{\mathcal{G}}^{j-1}_{i-1/2}}{\widetilde{\Sigma}^j_{J,i-1/2}\Delta x_{i-1/2}}-\frac{\bar{\mathcal{G}}^{j-1}_{i+1/2}}{\widetilde{\Sigma}^j_{J,i+1/2}\Delta x_{i+1/2}},\\
&\qquad\qquad i=1,...,N_i\,, \quad (3.84)
\end{aligned}
$$

$$
\left[\frac{\overline{E}^j_{0}+\bar{\zeta}^{-,j}_{1/2}\Delta x_{1/2}}{\widetilde{\Sigma}^j_{J,1/2}\Delta x_{1/2}}-\bar{B}^j_L\right]\phi^j_0-\left[\frac{\overline{E}^j_{1}+\bar{\zeta}^{+,j}_{1/2}\Delta x_{1/2}}{\widetilde{\Sigma}^j_{J,1/2}\Delta x_{1/2}}\right]\phi^j_1=-\frac{\bar{\mathcal{G}}^{j-1}_{1/2}}{\widetilde{\Sigma}^j_{J,1/2}\Delta x_{1/2}}\,, \quad (3.85)
$$

$$
\begin{aligned}
&-\left[\frac{\overline{E}^j_{N_i}+\bar{\zeta}^{-,j}_{N_i+1/2}\Delta x_{N_i+1/2}}{\widetilde{\Sigma}^j_{J,N_i+1/2}\Delta x_{N_i+1/2}}\right]\phi^j_{N_i}+\left[\frac{\overline{E}^j_{N_i+1}+\bar{\zeta}^{+,j}_{N_i+1/2}\Delta x_{N_i+1/2}}{\widetilde{\Sigma}^j_{J,N_i+1/2}\Delta x_{N_i+1/2}}+\bar{B}^j_R\right]\phi^j_{N_i+1}=\\
&\qquad\qquad\qquad\qquad\qquad\qquad\qquad\qquad\qquad\qquad\frac{\bar{\mathcal{G}}^{j-1}_{N_i+1/2}}{\widetilde{\Sigma}^j_{J,N_i+1/2}\Delta x_{N_i+1/2}}\,. \quad (3.86)
\end{aligned}
$$

3.2.3 Equations for Precursor Concentrations

We approximate the equations for precursor concentration balance (PCB) by means of the fully implicit time-discretization scheme to obtain

$$
\frac{1}{\Delta t^j}\left(C^j_{d,i}-C^{j-1}_{d,i}\right)=\left(-\lambda_d C^j_{d,i}+\overline{\tilde{\beta}\nu\Sigma_f}^j_{d,i}\phi^j_i\right), \quad (3.87)
$$

As a result we have

$$
C^j_{d,i}=\left[1+\lambda_d\Delta t^j\right]^{-1}C^{j-1}_{d,i}+\Delta t^j\overline{\tilde{\beta}\nu\Sigma_f}^j_{d,i}\phi^j_i. \quad (3.88)
$$

The delayed neutron source term in Eq. (3.79) is expressed using Eq. (3.88) to get the following:

$$
q^j_{del,i}=\sum_{d=1}^{6}\lambda_d C^j_{d,i}=\Delta t^j\left[\left\langle\tilde{\beta}\nu\Sigma_f\right\rangle^j_i\phi^j_i\right]+\bar{\mathcal{C}}^{j-1}_i\,, \quad (3.89)
$$

where

$$
\left\langle\tilde{\beta}\nu\Sigma_f\right\rangle^j_i=\sum_{d=1}^{6}\frac{\lambda_d\overline{\tilde{\beta}\nu\Sigma_f}^j_{d,i}}{1+\lambda_d\Delta t^j}\,, \quad (3.90)
$$

$$\bar{\mathcal{C}}_i^{j-1} = \sum_{d=1}^{6} \frac{\lambda_d}{1+\lambda_d \Delta t^j} C_{d,i}^{j-1} \,. \tag{3.91}$$

Note that

$$\left\langle \tilde{\beta}\nu\Sigma_f \right\rangle_i^j = \sum_{d=1}^{6} \frac{\lambda_d}{1+\lambda_d \Delta t^j} \left[\frac{\sum_{g=1}^{G} \tilde{\beta}_{d,g,i}^j \nu_{f,g,i}^j \Sigma_{f,g,i}^j \phi_{g,i}^j}{\sum_{g=1}^{G} \phi_{g,i}^j} \right] = \frac{\sum_{g=1}^{G} \hat{\beta}_{g,i}^j \nu_{f,g,i}^j \Sigma_{f,g,i}^j \phi_{g,i}^j}{\sum_{g=1}^{G} \phi_{g,i}^j} \,, \tag{3.92}$$

where

$$\hat{\beta}_{g,i}^j = \sum_{d=1}^{6} \frac{\lambda_d \tilde{\beta}_{d,g,i}^j}{1+\lambda_d \Delta t^j} \,. \tag{3.93}$$

We now substitute Eq. (3.89) into Eq. (3.79) and have

$$J_{i+1/2}^j - J_{i-1/2}^j + \left(\overline{\Sigma}_{a,i}^j - \overline{(1-\beta)\nu\Sigma_f}_i^j + \frac{1}{\Delta t^j \bar{v}_i^j} \right) \phi_i^j \Delta x_i = \left(\left\langle \tilde{\beta}\nu\Sigma_f \right\rangle_i^j \Delta t^j \phi_i^j + \bar{\mathcal{C}}_i^{j-1} + q_{ext,i}^j \right) \Delta x_i + \bar{\mathcal{B}}_i^{j-1} \,. \tag{3.94}$$

This leads to

$$J_{i+1/2}^j - J_{i-1/2}^j + \left(\overline{\Sigma}_{a,i}^j - \overline{(1-\beta)\nu\Sigma_f}_i^j - \Delta t^j \left\langle \tilde{\beta}\nu\Sigma_f \right\rangle_i^j + \frac{1}{\Delta t^j \bar{v}_i^j} \right) \phi_i^j \Delta x_i = q_{ext,i}^j \Delta x_i + \hat{\mathcal{B}}_i^{j-1} \,, \tag{3.95}$$

where

$$\hat{\mathcal{B}}^{j-1} = \bar{\mathcal{B}}_i^{j-1} + \left(\bar{\mathcal{C}}_i^{j-1} \right) \Delta x_i \,, \tag{3.96}$$

and as a result we have the following equations for the total scalar fluxes:

$$\begin{aligned} &- \left[\frac{\overline{E}_{i-1}^j + \bar{\zeta}_{i-1/2}^{-,j} \Delta x_{i-1/2}}{\widetilde{\Sigma}_{J,i-1/2}^j \Delta x_{i-1/2}} \right] \phi_{i-1}^j + \left[\frac{\overline{E}_i^j + \bar{\zeta}_{i-1/2}^{+,j} \Delta x_{i-1/2}}{\widetilde{\Sigma}_{J,i-1/2}^j \Delta x_{i-1/2}} + \frac{\overline{E}_i^j + \bar{\zeta}_{i+1/2}^{-,j} \Delta x_{i+1/2}}{\widetilde{\Sigma}_{J,i+1/2}^j \Delta x_{i+1/2}} \right. \\ &\qquad \left. + \left(\overline{\Sigma}_{a,i}^j - \overline{(1-\beta)\nu\Sigma_f}_i^j - \Delta t^j \left\langle \tilde{\beta}\nu\Sigma_f \right\rangle_i^j + \frac{1}{\Delta t^j \bar{v}_i^j} \right) \Delta x_i \right] \phi_i^j \\ &- \left[\frac{\overline{E}_{i+1}^j + \bar{\zeta}_{i+1/2}^{+,j} \Delta x_{i+1/2}}{\widetilde{\Sigma}_{J,i+1/2}^j \Delta x_{i+1/2}} \right] \phi_{i+1}^j = q_{ext,i}^j \Delta x_i + \hat{\mathcal{B}}_i^{j-1} + \frac{\bar{\mathcal{G}}_{i-1/2}^{j-1}}{\widetilde{\Sigma}_{J,i-1/2}^j \Delta x_{i-1/2}} - \frac{\bar{\mathcal{G}}_{i+1/2}^{j-1}}{\widetilde{\Sigma}_{J,i+1/2}^j \Delta x_{i+1/2}} \,, \\ &\qquad\qquad i = 1, ..., N_i \,, \end{aligned} \tag{3.97}$$

$$\left[\frac{\overline{E}_0^j+\bar{\zeta}_{1/2}^{-,j}\Delta x_{1/2}}{\widetilde{\Sigma}_{J,1/2}^j\Delta x_{1/2}}-\bar{B}_L^j\right]\phi_0^j-\left[\frac{\overline{E}_1^j+\bar{\zeta}_{1/2}^{+,j}\Delta x_{1/2}}{\widetilde{\Sigma}_{J,1/2}^j\Delta x_{1/2}}\right]\phi_1^j=-\frac{\bar{\mathcal{G}}_{1/2}^{j-1}}{\widetilde{\Sigma}_{J,1/2}^j\Delta x_{1/2}}\,, \tag{3.98}$$

$$-\left[\frac{\overline{E}_{N_i}^j+\bar{\zeta}_{N_i+1/2}^{-,j}\Delta x_{N_i+1/2}}{\widetilde{\Sigma}_{J,N_i+1/2}^j\Delta x_{N_i+1/2}}\right]\phi_{N_i}^j+\left[\frac{\overline{E}_{N_i+1}^j+\bar{\zeta}_{N_i+1/2}^{+,j}\Delta x_{N_i+1/2}}{\widetilde{\Sigma}_{J,N_i+1/2}^j\Delta x_{N_i+1/2}}+\bar{B}_R^j\right]\phi_{N_i+1}^j=\frac{\bar{\mathcal{G}}_{N_i+1/2}^{j-1}}{\widetilde{\Sigma}_{J,N_i+1/2}^j\Delta x_{N_i+1/2}}\,. \tag{3.99}$$

3.2.4 The Heat Transfer Equation

We use a finite-volume discretization to approximate the HT equations (2.55)-(2.57). As a result, we get

$$\Delta x_i\rho_i\frac{d(c_{p,i}T_i)}{dt}+W_{i+1/2}-W_{i-1/2}=w_{f,i}\overline{\Sigma}_{f,i}\phi_i\Delta x_i\,,\quad i=1,...,N_i\,, \tag{3.100}$$

$$W_{i-1/2}\frac{\Delta x_i}{2}=-\varkappa_i(T_i-T_{i-1/2})\,, \tag{3.101}$$

$$W_{i+1/2}\frac{\Delta x_i}{2}=-\varkappa_i(T_{i+1/2}-T_i)\,, \tag{3.102}$$

$$i=1,...,N_i\,,$$

$$T_{1/2}=T_L\,,\quad T_{N_i+1/2}=T_R\,. \tag{3.103}$$

We discretize Eq. (3.100) in time using the fully implicit scheme to get

$$\frac{\Delta x_i\rho_i}{\Delta t^j}\left(c_{p,i}^jT_i^j-c_{p,i}^{j-1}T_i^{j-1}\right)+\left(W_{i+1/2}^j-W_{i-1/2}^j\right)=w_{f,i}^j\overline{\Sigma}_{f,i}^j\phi_i^j\Delta x_i, \tag{3.104}$$

$$i=1,...,N_i\,.$$

The equation (3.104) is reduced to the form:

$$\frac{\Delta x_i\rho_i}{\Delta t^j}c_{p,i}^jT_i^j+W_{i+1/2}^j-W_{i-1/2}^j=w_{f,i}^j\overline{\Sigma}_{f,i}^j\phi_i^j\Delta x_i+\bar{\mathcal{F}}_i^{j-1}\,, \tag{3.105}$$

where

$$\bar{\mathcal{F}}^{j-1}=\frac{\Delta x_i\rho_i}{\Delta t^j}c_{p,i}^{j-1}T_i^{j-1}\,. \tag{3.106}$$

From Eq. (3.101) and Eq. (3.102), we derive the equations for the cell-edge heat fluxes in terms of cell-averaged temperatures to get

$$W^j_{i+1/2} = -\frac{\widehat{\varkappa}^j_{i+1/2}}{\Delta x_{i+1/2}}(T^j_{i+1} - T^j_i)\,, \tag{3.107}$$

where

$$\widehat{\varkappa}^j_{i+1/2} = \frac{\varkappa^j_i \varkappa^j_{i+1}(\Delta x_i + \Delta x_{i+1})}{\varkappa^j_i \Delta x_{i+1} + \varkappa^j_{i+1}\Delta x_i}\,, \tag{3.108}$$
$$i = 0, ..., N_i\,,$$

and,

$$\Delta x_0 = 0, \quad \Delta x_{N_i+1} = 0, \tag{3.109}$$
$$T_0 = T_{1/2}, \quad T_{N_i+1} = T_{N_i+1/2}, \tag{3.110}$$
$$\varkappa_0 = \varkappa_1, \quad \varkappa_{N_i+1} = \varkappa_{N_i}\,. \tag{3.111}$$

Eliminating heat fluxes from Eq. (3.105) by means of Eq. (3.107), we get the following system of equations for T^j_i:

$$-\left[\frac{\widehat{\varkappa}^j_{i-1/2}}{\Delta x_{i-1/2}}\right]T^j_{i-1} + \left[\frac{\widehat{\varkappa}^j_{i+1/2}}{\Delta x_{i+1/2}} + \frac{\widehat{\varkappa}^j_{i-1/2}}{\Delta x_{i-1/2}} + \frac{\Delta x_i \rho_i}{\Delta t^j} c^j_{p,i}\right]T^j_i$$
$$-\left[\frac{\widehat{\varkappa}^j_{i+1/2}}{\Delta x_{i+1/2}}\right]T^j_{i+1} = w^j_{f,i}\overline{\Sigma}^j_{f,i}\phi^j_i \Delta x_i + \bar{\mathcal{F}}^{j-1}_i\,, \tag{3.112}$$
$$i = 1, ...N_i\,.$$

The boundary conditions (3.103) give extra two equations

$$T^j_0 = T^j_L\,, \quad T^j_{N_i+1} = T^j_R\,. \tag{3.113}$$

3.2.5 Newton's Method for Solving Nonlinear Equations

We reduced the system of discretized equations for GLOQD, and HT to a system of nonlinear equations for the cell-average total scalar fluxes and cell-average temperatures. The nonlinear

system is given by

$$-\left[\frac{\widehat{\varkappa}^j_{i-1/2}}{\Delta x_{i-1/2}}\right]T^j_{i-1}+\left[\frac{\widehat{\varkappa}^j_{i+1/2}}{\Delta x_{i+1/2}}+\frac{\widehat{\varkappa}^j_{i-1/2}}{\Delta x_{i-1/2}}+\frac{\Delta x_i\rho_i}{\Delta t^j}c^j_{p,i}\right]T^j_i$$
$$-\left[\frac{\widehat{\varkappa}^j_{i+1/2}}{\Delta x_{i+1/2}}\right]T^j_{i+1}=w^j_{f,i}\overline{\Sigma}^j_{f,i}\phi^j_i\Delta x_i+\bar{\mathcal{F}}^{j-1}_i\,,\ i=1,...,N_i\,, \quad (3.114)$$

$$T^j_0=T^j_L\,,\quad T^j_{N_i+1}=T^j_R\,, \quad (3.115)$$

$$-a^j_{i-1/2}\phi^j_{i-1}+\left(b^j_{i-1/2}+a^j_{i+1/2}+z^j_i\right)\phi^j_i-b^j_{i+1/2}\phi^j_{i+1}=d^j_i+q^j_{ext,i}\Delta x_i+\hat{\mathcal{B}}^{j-1}_i\,, \quad (3.116)$$
$$i=0,...,N_i+1\,,$$

where

$$a^j_{i+1/2}=\frac{\overline{E}^j_i+\bar{\zeta}^{-,j}_{i+1/2}\Delta x_{i+1/2}}{\overline{\Sigma}^j_{t,i+1/2}\Delta x_{i+1/2}}\,,\quad i=0,...,N_i\,, \quad (3.117)$$

$$a^j_{-1/2}=0\,, \quad (3.118)$$

$$b^j_{i+1/2}=\frac{\overline{E}^j_{i+1}+\bar{\zeta}^{+,j}_{i+1/2}\Delta x_{i+1/2}}{\overline{\Sigma}^j_{t,i+1/2}\Delta x_{i+1/2}}\,,\quad i=0,...,N_i\,, \quad (3.119)$$

$$b^j_{N_i+3/2}=0\,, \quad (3.120)$$

$$z^j_i=\left(\overline{\Sigma}^j_{a,i}-\overline{(1-\beta)\nu\Sigma_f}^j_i-\Delta t^j\left\langle\tilde{\beta}\nu\Sigma_f\right\rangle^j_i+\frac{1}{\Delta t^j\bar{v}^j_i}\right)\Delta x_i\,,\quad i=1,...,N_i\,, \quad (3.121)$$

$$z^j_0=-\bar{B}^j_L\,,\quad z^j_{N_i+1}=\bar{B}^j_R\,, \quad (3.122)$$

$$d^j_i=\frac{\bar{\mathcal{G}}^{j-1}_{i-1/2}}{\widetilde{\Sigma}^j_{J,i-1/2}\Delta x_{i-1/2}}-\frac{\bar{\mathcal{G}}^{j-1}_{i+1/2}}{\widetilde{\Sigma}^j_{J,i+1/2}\Delta x_{i+1/2}}\,,\quad i=1,...,N_i\,, \quad (3.123)$$

$$d^j_0=-\frac{\bar{\mathcal{G}}^{j-1}_{1/2}}{\widetilde{\Sigma}^j_{J,1/2}\Delta x_{1/2}}\,,\quad d^j_{N_i+1}=\frac{\bar{\mathcal{G}}^{j-1}_{N_i+1/2}}{\widetilde{\Sigma}^j_{J,N_i+1/2}\Delta x_{N_i+1/2}}\,, \quad (3.124)$$

$$q^j_{ext,0}=q^j_{ext,N_i+1}=0\,,\quad \hat{\mathcal{B}}^{j-1}_0=\hat{\mathcal{B}}^{j-1}_{N_i+1}=0\,. \quad (3.125)$$

Note that

$$\overline{\Sigma}^j_{a,i}=\frac{\sum_{g=1}^G\Sigma^j_{a,g,i}\phi^j_{g,i}}{\sum_{g=1}^G\phi^j_{g,i}}\,, \quad (3.126)$$

$$\overline{(1-\beta)\nu\Sigma_f}_i^j = \frac{\sum_{g=1}^G (1-\beta_g^j)\nu_{f,g,i}^j \Sigma_{f,g,i}^j \phi_{g,i}^j}{\sum_{g=1}^G \phi_{g,i}^j}\,, \tag{3.127}$$

$$\overline{\Sigma}_{f,i}^j = \frac{\sum_{g=1}^G \Sigma_{f,g,i}^j \phi_{g,i}^j}{\sum_{g=1}^G \phi_{g,i}^j}\,, \tag{3.128}$$

$$\left\langle \tilde{\beta}\nu\Sigma_f \right\rangle_i^j = \frac{\sum_{g=1}^G \hat{\beta}_{\cdot,g,i}^j \nu_{f,g,i}^j \Sigma_{f,g,i}^j \phi_{g,i}^j}{\sum_{g=1}^G \phi_{g,i}^j}\,, \tag{3.129}$$

$$\overline{\Sigma}_{t,i+1/2}^j = \frac{\sum_{g=1}^G \Sigma_{t,g,i+1/2}^j |J_{g,i+1/2}^j|}{\sum_{g=1}^G |J_{g,i+1/2}^j|}\,, \tag{3.130}$$

$$\bar{v}_i = \frac{\sum_{g=1}^G \phi_{g,i}}{\sum_{g=1}^G \frac{\phi_{g,i}}{v_g}}\,, \tag{3.131}$$

$$\tilde{v}_{i+1/2}^j = \frac{\sum_{g=1}^G |J_{g,i+1/2}^j|}{\sum_{g=1}^G \frac{|J_{g,i+1/2}^j|}{v_g}}\,, \tag{3.132}$$

$$\Sigma_{\cdot,g,i}^j = \sum_l \sigma_{\cdot,g}(T_i^j)\mathcal{N}_i^l\,, \tag{3.133}$$

$$\overline{E}_i^j = \frac{\sum_{g=1}^G E_{g,i}^j \phi_{g,i}^j}{\sum_{g=1}^G \phi_{g,i}^j}\,, \tag{3.134}$$

$$\widehat{\varkappa}_{i+1/2}^j = \widehat{\varkappa}\big(\varkappa(T_i^j), \varkappa(T_{i+1}^j)\big)\,, \tag{3.135}$$

$$c_{p,i}^j = c_p(T_i^j)\,. \tag{3.136}$$

The resulting system of nonlinear algebraic equations (3.114) and (3.116) for primary unknowns is expressed in matrix notation as

$$\mathcal{A}(u) = q_A\,, \quad u = (\phi_h, T_h)\,, \tag{3.137}$$

where

$$\phi_h = (\phi_0^j, \phi_1^j, ..., \phi_{N_i+1}^j)^T\,, \qquad T_h = (T_0^j, T_1^j, ..., T_{N_i+1}^j)^T\,, \tag{3.138}$$

$$\mathcal{A}(u) = \begin{pmatrix} \mathcal{A}_1(T_h)T_h - \mathcal{A}_2(T_h)\phi_h \\ \mathcal{A}_3(T_h)\phi_h \end{pmatrix} \tag{3.139}$$

The equation (3.139) is now solved by means of the Newton's method [13].

$$\mathcal{J}(u^{(n-1)})\delta u^{(n-1)} = -\mathcal{A}(u^{(n-1)}) + q_A\,, \quad u^{(n-1)} = (\phi_h^{(n-1)}, T_h^{(n-1)})\,, \tag{3.140}$$

$$u^{(n)} = u^{(n-1)} + \delta u^{(n-1)}\,, \tag{3.141}$$

where $\mathcal{J}$ is the Jacobian of $\mathcal{A}$. Next, we derive an approximation to the Jacobian for the nonlinear system (3.114)-(3.116).

The superscript j indicating the current time step is omitted for the brevity of notations. Assume that $u^{(n)} = (\phi_h^{(n)}, T_h^{(n)})$ (Eq. (3.138)) is an estimation of the solution $u = (\phi_h, T_h)$ of the nonlinear equations (3.114)-(3.116). Eqs. (3.114)-(3.116) are linearized about this approximate solution $u^{(n)}$. Let

$$T_i^{(n+1)} = T_i^{(n)} + \Delta T_i^{(n)}\,, \tag{3.142}$$

$$\phi_i^{(n+1)} = \phi_i^{(n)} + \Delta \phi_i^{(n)}\,, \tag{3.143}$$

where $\Delta T_i^{(n)}$ and $\Delta \phi_i^{(n)}$ are small. We remind that

$$\widehat{\varkappa}_{i+1/2} = \widehat{\varkappa}\big(\varkappa_i, \varkappa_{i+1}\big) = \frac{\varkappa_i \varkappa_{i+1}(\Delta x_i + \Delta x_{i+1})}{\varkappa_i \Delta x_{i+1} + \varkappa_{i+1}\Delta x_i}\,, \tag{3.144}$$

where

$$\varkappa_i = \varkappa(T_i)\,, \tag{3.145}$$

and introduce the following notation:

$$\widehat{\varkappa}_{i+1/2}^{(n+1)} \stackrel{\text{def}}{=} \widehat{\varkappa}_{i+1/2}(T^{(n+1)})\,. \tag{3.146}$$

Using Eq. (3.142), we have

$$\widehat{\varkappa}_{i+1/2}^{(n+1)} = \widehat{\varkappa}_{i+1/2}\big(T^{(n)} + \Delta T^{(n)}\big) = \widehat{\varkappa}_{i+1/2}^{(n)} + \delta \widehat{\varkappa}_{i+1/2}^{(n)}\,, \tag{3.147}$$

where is $\delta \widehat{\varkappa}_{i+1/2}^{(n)}$ is the resulting variation of $\widehat{\varkappa}_{i+1/2}$. Taking into account Eq. (3.144), we notice that

$$\delta \widehat{\varkappa}_{i+1/2}^{(n)} \approx \frac{\partial(\widehat{\varkappa}_{i+1/2})}{\partial(\varkappa_i)} \left(\frac{d\varkappa}{dT}\right)_i^{(n)} \Delta T_i^{(n)} + \frac{\partial(\widehat{\varkappa}_{i+1/2})}{\partial(\varkappa_{i+1})} \left(\frac{d\varkappa}{dT}\right)_{i+1}^{(n)} \Delta T_{i+1}^{(n)}\,, \tag{3.148}$$

where

$$\left(\frac{d\varkappa}{dT}\right)_i^{(n)} = \left.\frac{d\varkappa}{dT}\right|_{T=T_i^{(n)}}\,. \tag{3.149}$$

We now introduce the following notations

$$\left(\frac{d\widehat{\varkappa}}{dT}\right)_{i+1/2}^{-(n)} = \frac{\partial(\widehat{\varkappa}_{i+1/2})}{\partial(\varkappa_i)} \left(\frac{d\varkappa}{dT}\right)_i^{(n)}\,, \qquad \left(\frac{d\widehat{\varkappa}}{dT}\right)_{i+1/2}^{+(n)} = \frac{\partial(\widehat{\varkappa}_{i+1/2})}{\partial(\varkappa_{i+1})} \left(\frac{d\varkappa}{dT}\right)_{i+1}^{(s)}\,, \tag{3.150}$$

and have

$$\delta\widehat{\varkappa}_{i+1/2}^{(n)} = \left(\frac{d\widehat{\varkappa}}{dT}\right)_{i+1/2}^{-(n)} \Delta T_i^{(n)} + \left(\frac{d\widehat{\varkappa}}{dT}\right)_{i+1/2}^{+(n)} \Delta T_{i+1}^{(n)} . \tag{3.151}$$

We perform necessary differentiation and obtain

$$\left(\frac{d\widehat{\varkappa}}{dT}\right)_{i+1/2}^{-(n)} = \frac{\left(\widehat{\varkappa}_{i+1/2}^{(n)}\right)^2 \Delta x_i}{\left(\varkappa_i^{(n)}\right)^2 (\Delta x_i + \Delta x_{i+1})} \left(\frac{d\varkappa}{dT}\right)_i^{(n)} , \tag{3.152}$$

$$\left(\frac{d\widehat{\varkappa}}{dT}\right)_{i+1/2}^{+(n)} = \frac{\left(\widehat{\varkappa}_{i+1/2}^{(n)}\right)^2 \Delta x_{i+1}}{\left(\varkappa_{i+1}^{(n)}\right)^2 (\Delta x_i + \Delta x_{i+1})} \left(\frac{d\varkappa}{dT}\right)_{i+1}^{(n)} . \tag{3.153}$$

We now expand other quantities as well keeping only first-order terms

$$c_{p,i}^{(n+1)} = c_{p,i}^{(n)} + \left(\frac{dc_p}{dT}\right)_i^{(n)} \Delta T_i^{(n)} + o(\Delta T^{(n)}) , \tag{3.154}$$

$$\overline{\Sigma}_{f,i}^{(n+1)} = \overline{\Sigma}_{f,i}^{(n)} + \left(\frac{d\overline{\Sigma}_f}{dT}\right)_i^{(n)} \Delta T_i^{(n)} + o(\Delta T^{(n)}) . \tag{3.155}$$

Inserting Eqs. (3.142), (3.143), (3.151), (3.154), and (3.155) into (3.114) yeilds

$$\begin{aligned}
&- \frac{1}{\Delta x_{i-1/2}} \left(\widehat{\varkappa}_{i-1/2}^{(n)} + \delta\widehat{\varkappa}_{i-1/2}^{(n)}\right)\left(T_{i-1}^{(n)} + \Delta T_{i-1}^{(n)}\right) \\
&\qquad + \left[\frac{1}{\Delta x_{i+1/2}} \left(\widehat{\varkappa}_{i+1/2}^{(n)} + \delta\widehat{\varkappa}_{i+1/2}^{(n)}\right) + \frac{1}{\Delta x_{i-1/2}} \left(\widehat{\varkappa}_{i-1/2}^{(n)} + \delta\widehat{\varkappa}_{i-1/2}^{(n)}\right)\right. \\
&\qquad\quad \left. + \frac{\Delta x_i \rho_i}{\Delta t^j} \left(c_{p,i}^{(n)} + \left(\frac{dc_p}{dT}\right)_i^{(n)} \Delta T_i^{(n)}\right)\right] \left(T_i^{(n)} + \Delta T_i^{(n)}\right) \\
&\qquad\quad - \frac{1}{\Delta x_{i+1/2}} \left(\widehat{\varkappa}_{i+1/2}^{(n)} + \delta\widehat{\varkappa}_{i+1/2}^{(n)}\right)\left(T_{i+1}^{(n)} + \Delta T_{i+1}^{(n)}\right) = \\
&\qquad\qquad w_{f,i}^j \left(\overline{\Sigma}_{f,i}^{(n)} + \left(\frac{d\overline{\Sigma}_f}{dT}\right)_i^{(n)} \Delta T_i^{(n)}\right)\left(\phi_i^{(n)} + \Delta\phi_i^{(n)}\right)\Delta x_i + \bar{\mathcal{F}}^{j-1} .
\end{aligned} \tag{3.156}$$

The boundary conditions (3.115) lead to

$$T_0^{(n)} + \Delta T_0^{(n)} = T_L^j , \quad T_{N_i+1}^{(n)} + \Delta T_{N_i+1}^{(n)} = T_R^j . \tag{3.157}$$

Assuming that the iteration errors $\Delta T_i^{(n)}$ and $\Delta\phi_i^{(n)}$ are small and neglecting their products,

one obtains the following linearized equations:

$$
\begin{aligned}
&-\frac{1}{\Delta x_{i-1/2}}\left[\widehat{\varkappa}^{(n)}_{i-1/2}+\left(T^{(n)}_{i-1}-T^{(n)}_{i}\right)\left(\frac{d\widehat{\varkappa}}{dT}\right)^{-(n)}_{i-1/2}\right]\Delta T^{(n)}_{i-1}\\
&+\left[\frac{1}{\Delta x_{i-1/2}}\left\{\widehat{\varkappa}^{(n)}_{i-1/2}+\left(T^{(n)}_{i}-T^{(n)}_{i-1}\right)\left(\frac{d\widehat{\varkappa}}{dT}\right)^{+(n)}_{i-1/2}\right\}+\frac{1}{\Delta x_{i+1/2}}\left\{\widehat{\varkappa}^{(n)}_{i+1/2}+\left(T^{(n)}_{i}-T^{(n)}_{i+1}\right)\left(\frac{d\widehat{\varkappa}}{dT}\right)^{-(n)}_{i+1/2}\right\}\right.\\
&\qquad\left.+\frac{\Delta x_i\rho_i}{\Delta t^j}\left(c^{(n)}_{p,i}+T^{(n)}_{i}\left(\frac{dc_p}{dT}\right)^{(n)}_{i}\right)-w_{f,i}\left(\frac{d\overline{\Sigma}_f}{dT}\right)^{(n)}_{i}\phi^{(n)}_i\Delta x_i\right]\Delta T^{(n)}_{i}\\
&\qquad-\frac{1}{\Delta x_{i+1/2}}\left[\widehat{\varkappa}^{(n)}_{i+1/2}+\left(T^{(n)}_{i+1}-T^{(n)}_{i}\right)\left(\frac{d\widehat{\varkappa}}{dT}\right)^{+(n)}_{i+1/2}\right]\Delta T^{(n)}_{i+1}-w_{f,i}\overline{\Sigma}^{(n)}_{f,i}\Delta x_i\Delta\phi^{(n)}_i=\mathcal{R}^{(n)}_{heat,i}\,,
\end{aligned}
\tag{3.158}
$$

where

$$
\begin{aligned}
\mathcal{R}^{(n)}_{heat,i}=\frac{\widehat{\varkappa}^{(n)}_{i-1/2}}{\Delta x_{i-1/2}}T^{(n)}_{i-1}-\left[\frac{\widehat{\varkappa}^{(n)}_{i+1/2}}{\Delta x_{i+1/2}}+\frac{\widehat{\varkappa}^{(n)}_{i-1/2}}{\Delta x_{i-1/2}}+\frac{\Delta x_i\rho_i}{\Delta t^j}c^{(n)}_{p,i}\right]T^{(n)}_{i}+\frac{\widehat{\varkappa}^{(n)}_{i+1/2}}{\Delta x_{i+1/2}}T^{(n)}_{i+1}\\
+w_{f,i}\overline{\Sigma}^{(n)}_{f,i}\phi^{(n)}_i\Delta x_i+\bar{\mathcal{F}}^{j-1}\,.
\end{aligned}
\tag{3.159}
$$

The equations at the boundaries are the following:

$$
\Delta T^{(n)}_0=0\,,\quad \Delta T^{(n)}_{N_i+1}=0\,. \tag{3.160}
$$

The next step is to linearize the equations (3.116). We define

$$
a^{(n+1)}_{i-1/2}=a^{(n)}_{i-1/2}+\delta a^{(n)}_{i-1/2}\,, \tag{3.161}
$$

$$
b^{(n+1)}_{i-1/2}=b^{(n)}_{i-1/2}+\delta b^{(n)}_{i-1/2}\,, \tag{3.162}
$$

$$
d^{(n+1)}_{i}=d^{(n)}_{i}+\delta d^{(n)}_{i}\,, \tag{3.163}
$$

$$
z^{(n+1)}_{i}=z^{(n)}_{i}+\delta z^{(n)}_{i}\,. \tag{3.164}
$$

The equations (3.116) lead to

$$
\begin{aligned}
&-\left(a_{i-1/2}^{(n)}+\delta a_{i-1/2}^{(n)}\right)\left(\phi_{i-1}^{(n)}+\Delta\phi_{i-1}^{(n)}\right)\\
&\qquad+\left(b_{i-1/2}^{(n)}+\delta b_{i-1/2}^{(n)}+a_{i+1/2}^{(n)}+\delta a_{i+1/2}^{(n)}+z_i^{(n)}+\delta z_i^{(n)}\right)\left(\phi_i^{(n)}+\Delta\phi_i^{(n)}\right)\\
&\qquad-\left(b_{i+1/2}^{(n)}+\delta b_{i+1/2}^{(n)}\right)\left(\phi_{i+1}^{(n)}+\Delta\phi_{i+1}^{(n)}\right)=d_i^{(n)}+\delta d_i^{(n)}+q_{ext,i}\Delta x_i+\hat{\mathcal{B}}^{j-1}\,, \quad (3.165)
\end{aligned}
$$

We assume that variations in coefficients $a_{i-1/2}$, $b_{i-1/2}$, d_i are very small and neglect $\delta a_{i-1/2}^{(n)}$, $\delta b_{i-1/2}^{(n)}$, and $\delta d_i^{(n)}$ to obtain

$$
\begin{aligned}
&-a_{i-1/2}^{(n)}\left(\phi_{i-1}^{(n)}+\Delta\phi_{i-1}^{(n)}\right)+\left(b_{i-1/2}^{(n)}+a_{i+1/2}^{(n)}+z_i^{(n)}+\delta z_i^{(n)}\right)\left(\phi_i^{(n)}+\Delta\phi_i^{(n)}\right)\\
&\qquad-b_{i+1/2}^{(n)}\left(\phi_{i+1}^{(n)}+\Delta\phi_{i+1}^{(n)}\right)=d_i^{(n)}+q_{ext,i}\Delta x_i+\hat{\mathcal{B}}^{j-1}\,. \quad (3.166)
\end{aligned}
$$

Note that this assumption gives rise to an approximation of the Jacobian. Neglecting the terms of order two and higher, we derive the linearized equations of the following form:

$$
\begin{aligned}
&-a_{i-1/2}^{(n)}\Delta\phi_{i-1}^{(n)}+\left(b_{i-1/2}^{(n)}+a_{i+1/2}^{(n)}+z_i^{(n)}\right)\Delta\phi_i^{(n)}\\
&\qquad-b_{i+1/2}^{(n)}\Delta\phi_{i+1}^{(n)}+\phi_i^{(n)}\left(\frac{dz}{dT}\right)_i^{(n)}\Delta T_i^{(n)}=\mathcal{R}_{GLOQD,i}^{(n)}\,. \quad (3.167)
\end{aligned}
$$

where

$$
\begin{aligned}
\mathcal{R}_{GLOQD,i}^{(n)}&=a_{i-1/2}^{(n)}\phi_{i-1}^{(n)}-\left(b_{i-1/2}^{(n)}+a_{i+1/2}^{(n)}+z_i^{(n)}\right)\phi_i^{(n)}+b_{i+1/2}^{(n)}\phi_{i+1}^{(n)}+d_i^{(n)}\\
&\qquad+q_{ext,i}\Delta x_i+\hat{\mathcal{B}}^{j-1}\,, \quad (3.168)
\end{aligned}
$$

$$
\left(\frac{dz}{dT}\right)_i^{(n)}=\left(\left(\frac{d\overline{\Sigma}_{a,i}}{dT}\right)_i^{(n)}-\left(\frac{d}{dT}\left[\overline{(1-\beta)\nu\Sigma_f}\right]\right)_i^{(n)}-\Delta t^j\left(\frac{d}{dT}\left[\left\langle\tilde{\beta}\nu\Sigma_f\right\rangle\right]\right)_i^{(n)}\right)\Delta x_i\,. \quad (3.169)
$$

The system of linearized equations (3.158) and (3.168) is solved for $\Delta T_i^{(n)}$ and $\Delta\phi_i^{(n)}$.

Chapter 4

Numerical Results

In the previous chapters, the details of the methodology were described. In this section, we proceed to show the performance of the methodology and present numerical results of model transient problems. The first test is a single fuel pin problem with reflective boundary conditions, two group neutron cross sections, and six groups for the delayed neutron precursor concentrations. The second test is a transient problem in a quarter core model of a BWR assembly.

In order to model the evolution of a transient process of any one of these systems, the corresponding k-eigenvalue problem is solved to obtain the initial configuration [36]. The initial flux distributions are normalized such that the average power density

$$\overline{P} = \frac{1}{L_{core}} = \int_{L_{core}} \int_{E} w_f(x)\Sigma_f(x,E)\phi(x,E)dE\,dx = P_0, \tag{4.1}$$

for an initial power $P_0\left(Wcm^{-2}\right)$. The initial precursor concentrations and thermal flux distribution are evaluated by solving the steady-state equations using the power-normalized neutron flux values. A transient is then induced in the system by changing the absorption cross sections at certain region(s) within the problem domain. This process simulates the removal of control material in these regions.

In each of these tests, the performance of the method is measured by studying the number of iterations that are required at each level for some chosen instants of time. Results will be presented for the number of iterations that are required for various time step sizes and various stages of the transient. Results of the convergence order obtained with temporal refinements will also be shown. The performance of the multilevel method using method of short characteristics and α- approximation for time-discretization of transport will be analyzed. The results of these numerical experiments are compared with the results from the fixed-point iteration method to

show the properties of the multilevel methodology.

The multilevel methodology has three different iteration cycles (nested iterations) at which the problem is solved in at each time step. Convergence of the high-order and low-order multi-group QD solutions is determined by means of the following convergence criteria:

$$||1 - \frac{\phi^{(k-1)}}{\phi^{(k)}}||_\infty < \epsilon^k$$

where $k = s, n$. The values of the parameter ϵ^k used to determine convergence for the different levels are,

- For the high-order transport equation, $\epsilon^s = 10^{-6}$
- For the multigroup low-order QD equations, $\epsilon^n = 10^{-7}$

The Newton's iterations are converged using the following condition for convergence:

$$||\phi^k - \phi^{(k-1)}||_\infty < \left(1.0 + ||\phi^{(k)}||_\infty\right) \epsilon^k \tag{4.2}$$

where $\epsilon^l = 10^{-4}$. Eq. (4.2) ensures that the magnitudes of the fluxes do not affect convergence determination because of cancellation errors due to finite arithmetic.

4.1 Test 1: Transient in A Fuel Pin

A fuel pin is an elementary unit of any reactor core. A typical fuel pin consists of fissile material at the core surrounded by gap and cladding material. In this test, the pin-cell comprises of fissile material surrounded by a moderating material at either sides. The details of this configuration are shown in Figure 4.1. The boundary conditions for the neutron flux are set to be reflective at both ends. The fuel material in the pin is subject to Doppler broadening which is an important effect of physics of interaction. In the fuel, the Doppler effect is modelled with the following relation [50, 32],

$$\Sigma_{a,1}(T,t) = \Sigma_{a,1}(T_0,t)\left[1 + \gamma\sqrt{T(x,t)+273} - \sqrt{T_0+273}\right]$$

where, γ is the Doppler constant for fuel material and is evaluated to be 7.471×10^{-3} for the pin (see Appendix A). $T(x,t)$ is measured in degrees Celcius (^oC). T_0 is the reference temperature evaluated at $t = 0$ s. A transient is introduced in the system by decreasing the thermal absorption cross-section of the fuel over a very short period of time. This models, to some extent, a fast removal of the control material from the reactor and causes the power of

the reactor to increase. The thermal absorption cross-section is evaluated using the following relation:

$$\Sigma_{a,2}(T,t) = \Sigma_{a,2}(T_0,0) \times \begin{cases} \left(1 - 0.02\frac{t}{t_{final}}\right), & \text{if } t \leq t_{final}, \\ 0.08, & \text{if } t > t_{final}. \end{cases}$$

Here, t_{final} represents the point in time when removal of the control material is stopped. In this test, we choose that time to be 10^{-2} seconds. The choice of this time is made to model a rapid insertion of positive reactivity.

The temperature distribution is another important part in this problem. In order to formulate the heat conduction problem the boundary conditions have to be specified as well. In this test, the temperatures at the boundaries are set to be fixed at 500^0C. This value is chosen to reflect the approximate boundary temperature of the moderator in real core operations. The heat transfer coefficient (κ) of the moderator is taken to be that of water, and it is set to be a constant through the whole process. The heat transfer coefficient of the fuel is determined using the thermal conductivity integral for $U0_2$ [31]. It is modeled as a function of temperature as follows:

$$\kappa_f(T) = \frac{38.24}{402.4 + T} + 6.126 \times 10^{-13}(T + 273)^3 \frac{W}{cmK}. \tag{4.3}$$

4.1.1 Evolution of Solutions

Figures 4.3 and 4.4 show the evolution of the average power and temperature in the fuel pin. As the control material is removed from the fuel region of the pin, the neutron flux and consequently the average power increase exponentially in the pin. The rapid increase in the neutron flux also results in the rapid buildup of the delayed neutron precursor concentrations in the fuel. This buildup is sustained until the power peak is reached. As the neutron flux decreases after the peak, the average concentration of the precursors stays almost steady. This is because the average characteristic life span of the precursors is much longer than the time scales characterizing the rapid change in neutron population in the pin. After some tens of seconds following the power peak, a decline in the magnitude of precursor concentrations is observed. This is caused by the precursors decaying to release neutrons back into the system. This results in a slight increase of the total neutron flux in the system. After about 200 seconds from the beginning of the transient, the power, delayed precursor concentrations, and the temperature stabilize.

Figure 4.2 shows the scaled magnitudes of the average power, temperature and precursor concentration in the pin. The peak average temperature is about 1.5 times initial steady-state temperature. From Figure 4.4, it is seen that the average temperature increases rapidly in

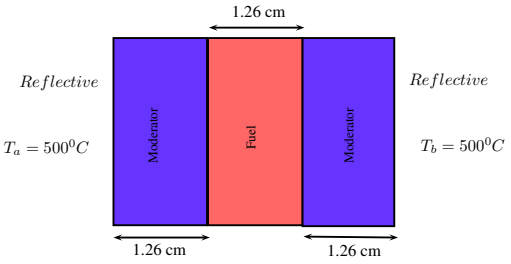

Figure 4.1: Model UO_2 fuel pin cell in Test 1

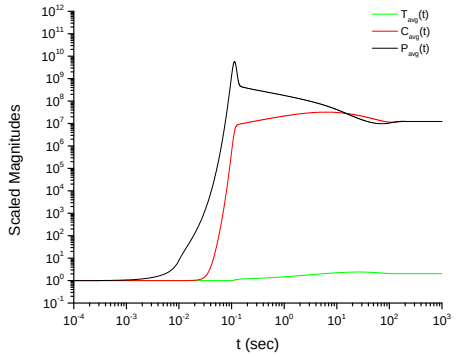

Figure 4.2: Test 1: Scaled average power, total precursor concentration, and temperature as functions of time.

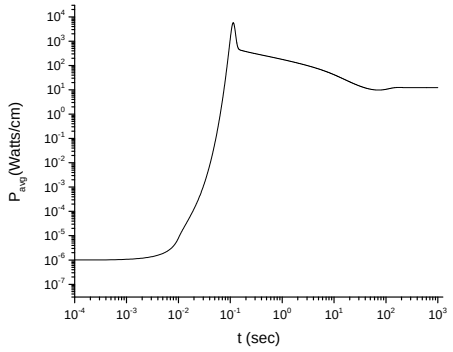

Figure 4.3: Test 1: Evolution of P_{avg}.

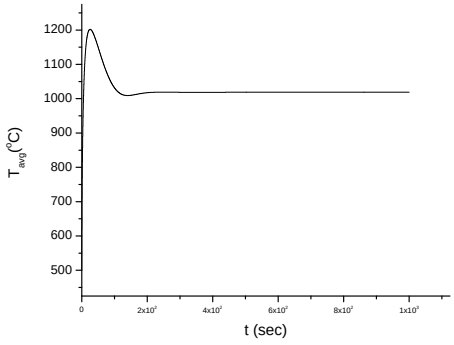

Figure 4.4: Test 1: Evolution of T_{avg}.

the first few seconds followed by a rapid decline to give it a pulse shape. The increase in temperature is driven by the exponential growth of power in the first stage of the transient. As the temperature rises, the absorption cross-section in the first group also increases. This is the effect of Doppler broadening outlined in Eq. (4.1). When the temperature of the fuel is high enough, the fuel becomes subcritical and the total neutron flux will decrease. This occurs at around 0.1 seconds in the pin under the given circumstances. The average temperature in the pin is 528^oC at this instant. Detailed look at the spatial distribution of the temperature in the pin reveals that the average temperature of the *fuel* is close to being 560^oC at that instant of time. At its maximum, the average temperature in the fuel pin is about 1200^oC. The maximum average temperature in the fuel region is around 1300^oC, with the centerline temperature of 1500^oC at this instant. The average temperature in the pin steadies out about 200 seconds after the initiation of the transient. The average steady-state temperature of the pin is approximately

1000^oC.

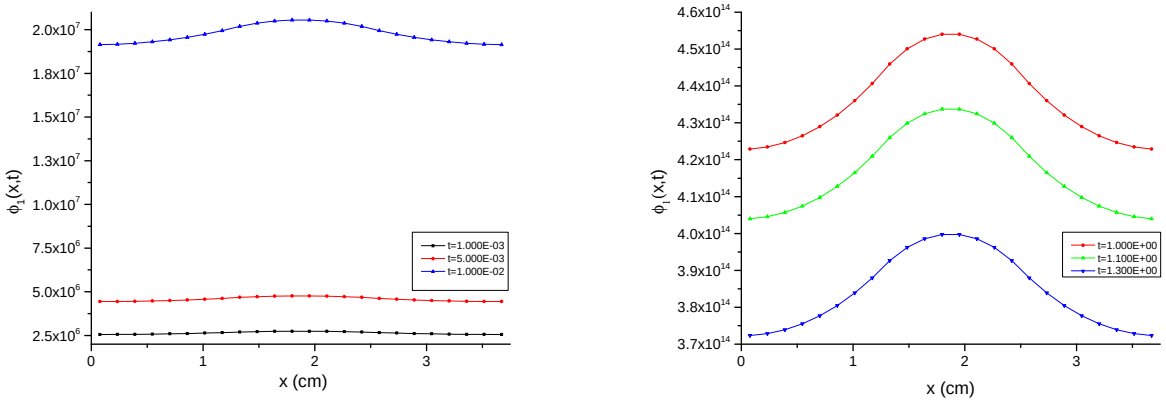

Figure 4.5: Test 1: Fast scalar flux as a function of space and time.

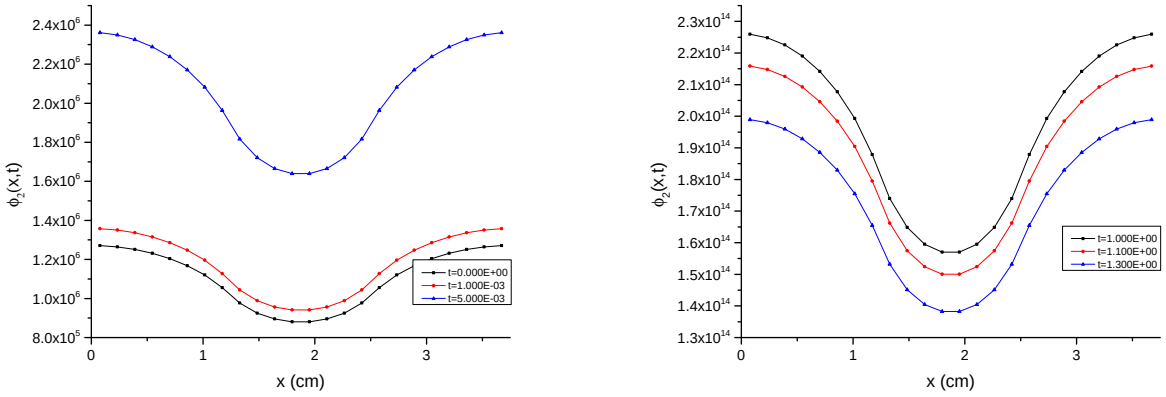

Figure 4.6: Test 1: Thermal scalar flux as a function of space and time.

Figure 4.5 and Figure 4.6 show the spatial distribution of the group fluxes in the fuel pin at various moments of time. As the control material is removed, the magnitudes of the fluxes increase while the shapes of the fluxes stay relatively similar. The fast (first) group flux is raised in the fuel region because of fission neutrons in the fuel. The thermal flux level is slightly raised in the moderator region. This is expected because fast neutrons are slowed down in the

moderator. As the temperature rises in the fuel, the fast group absorption cross section increases due to Doppler effect. This causes the total power and group fluxes to decrease in the pin.

Figure 4.7 shows the group QD factors in the pin at various instants of time. In 1-D slab geometry, the QD factor E_g is the average value of μ^2 over the angular domain $(-1 \leq \mu \leq 1)$ with the angular flux as an averaging function. The diffusion theory assumes that the angular flux is a linear function of the angular variable. In this case, $E^g = \frac{1}{3}$ and $\frac{\partial E^g}{\partial x} = 0$. The degree of transport effects is characterized by the deviation of the QD factor E_g from its diffusion value, i.e., $\frac{1}{3}$, and by the magnitude of its spatial derivative. In the domain of the fuel pin, the transport effects are expected to be most pronounced at the edges, the fuel-moderator interfaces, and in the fuel. These effects are reflected in the plots of the group QD factors. The QD factors are most different from the diffusion value at the edges and the center of the pin, while in the fuel-moderator interfaces the spatial derivative is of the largest magnitude within the entire domain.

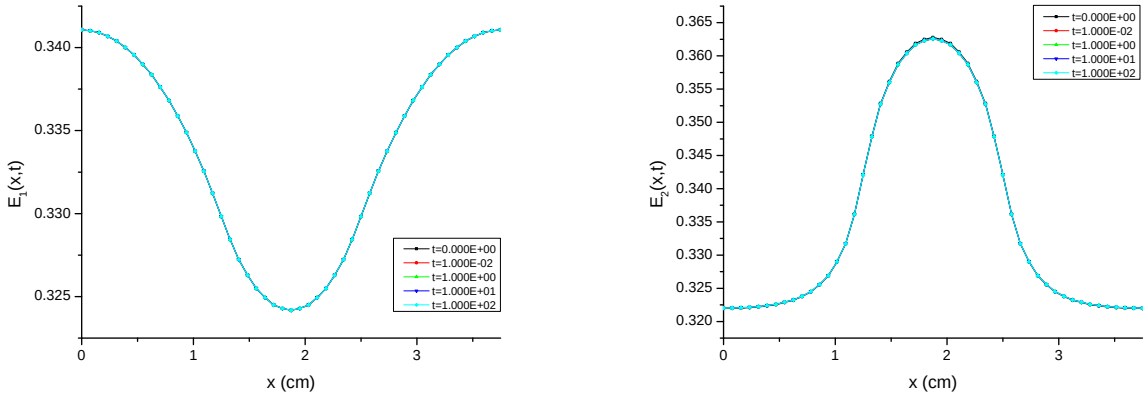

Figure 4.7: Test 1: Quasidiffusion factors (E_g) as functions of space and time.

In the QD method, the QD factors define the closure between the high-order (transport) problem and the low-order QD equations. It is seen that the values of QD factors do not change significantly over the course of time for the given problem. In the data whose plots are given in Figure 4.7, the group QD factors change by less than a percent through the entire period with reference to the values at $t = 0$. The first group QD factors change by a maximum of about 0.003% over the entire course of the evolution with reference to values at $t = 0$. The second group QD factors change by a maximum of about 0.055% over the course of the evolution with reference to values at $t = 0$. Recall that the group QD factors are evaluated as averages of μ^2

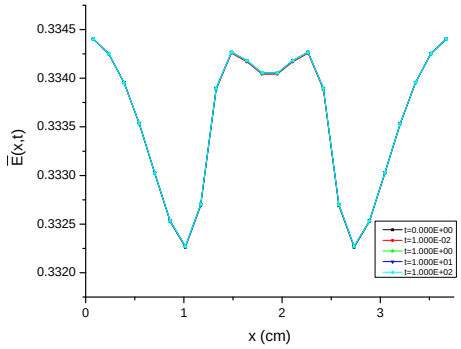

Figure 4.8: Test 1: $\overline{E}$(x,t).

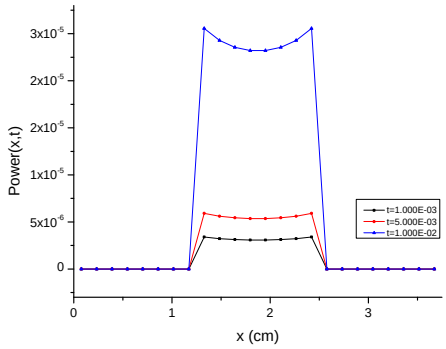

Figure 4.9: Test 1: P(x,t).

with $\psi^g(x, \mu, t)$ as the averaging spectrum. From this result we infer that in this test, although the magnitudes of the angular flux may grow and fall significantly in time, the angular flux does not change much with respect to angle in the pin.

Figures 4.9 and 4.10 show the spatial distribution of the power and temperature in the fuel pin at various instants of time, respectively. All fission events in Test 1 occur only in the thermal group. As a result, the spatial shape of the power follows the spatial shape of the thermal scalar flux in the fuel region of the pin. The spatial shape of the temperature in the fuel pin is slightly more intricate. The initial temperature distribution is found by solving the steady-state heat transfer equation with the steady-state flux (Eq. (2.5)). The temperatures at the boundaries are fixed to be 500^oC through the entire process. We start off with a reactor operating at very low power ($10^{-6}W/cm^2$). As the control material is removed and neutron fluxes increase in the system, the temperature initially acquires the spatial shape of the power distribution in the fuel region of the pin. The spatial shape of the temperature distribution is slightly concave which also characterizes the spatial shape of the power distribution in the pin. Over the course of the evolution, the spatial shape of the temperature distribution in the *fuel* resembles more like that of a parabolic function. The spatial shape of the temperature is linear in the moderator. This happens because the moderator does not have any local heat sources in its domain. The heat produced in the fuel is conducted to the edges of the pin.

4.1.2 Iteration Tables

Table 4.1 lists the numbers of iterations required for solving the problem by means of the MP method. The iteration counts are reported for various instants of time representing states when the total flux in the system changes at different rates. Recall that $\alpha^j(x) = \frac{Log\left(\phi(x)^j\right) - Log\left(\phi(x)^{j-1}\right)}{\Delta t^j}$ approximates the rate of change of the flux at the given instant of time and position. Table 4.2

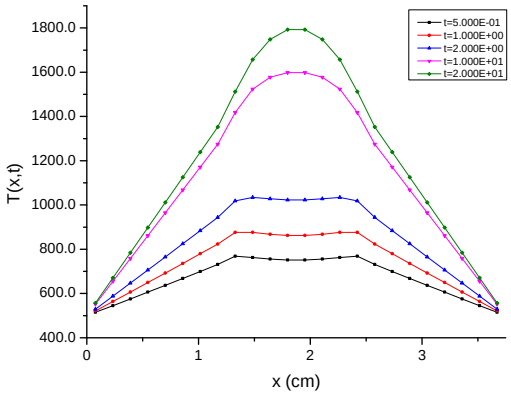

Figure 4.10: Test 1: Temperature as a function of space and time in the fuel pin.

shows the maximum of these values over the spatial domain (α_{max}) for some moments of time. This table shows the comparative rates of change of flux in the system for the given time instants. They were generated using $\Delta t = 2 \times 10^{-4}$ s.

We notice that the numbers of transport iterations depend on the rate of change of physics in the system and the size of time-steps used. The total flux in the system changes rapidly in the first few fractions of a second. These instants of time are marked by relatively high number of transport iterations. The high numbers of transport iterations required is a result of significant changes in the fuel cross-sections at these moments. This is caused by the insertion of positive reactivity and the nonlinear dependence of the absorption cross-sections on temperature. When the insertion of reactivity is stopped (for $t > 10^{-2}$ s), it is observed that fewer transport iterations are required at these stages of the transient.

The number of transport iterations is affected by the size of the time step because the time step is related to the resulting change in the solution during a unit advancement in time. The smaller the size of the step, the fewer the iterations required. Likewise, more transport iterations are required for larger time step sizes since more changes in the system have to be resolved then. The numbers of multigroup QD iterations required per transport solve remain fairly constant with different Δt. In this problem, about 3-4 multigroup QD iterations are required. They are also similar for various instants of time in this test. It takes about 1 to 2 Newton's iterations per multigroup QD iteration to solve this problem. Next, the problem is solved using the α-approximation scheme for the time-dependent transport equation. We refer to this as the MP$^\alpha$ method.

From Table 4.3, it is seen that the MP$^\alpha$ method requires fewer numbers of transport iterations for most instants of time than the MP method. For $t \leq 10^{-2}$ s, this method requires

Table 4.1: Test 1: Numbers of iterations for MP Method.

Δt	t	$N_{transp.}$	N_{mgqd}	N_{newton}	$\frac{N_{mgqd}}{N_{transp}}$	$\frac{N_{newton}}{N_{transp}}$	$\frac{N_{newton}}{N_{mgqd}}$
2.00E-04	1.00E-03	5	19	23	3.80	4.60	1.21
	5.00E-03	5	19	21	3.80	4.20	1.11
	1.00E-02	7	27	32	3.86	4.57	1.19
	2.00E-02	5	18	20	3.60	4.00	1.11
	5.00E-02	1	7	9	7.00	9.00	1.29
	1.00E-01	1	8	10	8.00	10.00	1.25
	1.00E+00	1	5	6	5.00	6.00	1.20
	1.00E+01	1	4	4	4.00	4.00	1.00
1.00E-04	1.00E-03	3	13	15	4.33	5.00	1.15
	5.00E-03	3	13	15	4.33	5.00	1.15
	1.00E-02	5	18	20	3.60	4.00	1.11
	2.00E-02	3	10	12	3.33	4.00	1.20
	5.00E-02	1	6	8	6.00	8.00	1.33
	1.00E-01	1	6	8	6.00	8.00	1.33
	1.00E+00	1	5	5	5.00	5.00	1.00
	1.00E+01	1	4	4	4.00	4.00	1.00
5.00E-05	1.00E-03	3	9	10	3.00	3.33	1.11
	5.00E-03	3	10	11	3.33	3.67	1.10
	1.00E-02	3	11	13	3.67	4.33	1.18
	2.00E-02	1	6	8	6.00	8.00	1.33
	5.00E-02	1	6	8	6.00	8.00	1.33
	1.00E-01	1	6	7	6.00	7.00	1.17
	1.00E+00	1	4	4	4.00	4.00	1.00
	1.00E+01	1	4	4	4.00	4.00	1.00

Table 4.2: Test 1: $(\alpha)_{max}$ using $\Delta t = 2 \times 10^{-4} s$

t_0	$(\alpha)_{max}$
1×10^{-3}	9.286917E+01
5×10^{-3}	1.781087E+02
1×10^{-2}	4.744266E+02
2×10^{-2}	2.202258E+02
5×10^{-2}	2.046172E+02
1×10^{-1}	1.739615E+02
$1 \times 10^{+0}$	4.771138E-01
$1 \times 10^{+1}$	9.116764E-02

Table 4.3: Test 1: Numbers of iterations for MP$^{\alpha}$ Method.

Δt	t	$N_{transp.}$	N_{mgqd}	N_{newton}	$\frac{N_{mgqd}}{N_{transp}}$	$\frac{N_{newton}}{N_{transp}}$	$\frac{N_{newton}}{N_{mgqd}}$
2.00E-04	1.00E-03	2	10	12	5.00	6.00	1.20
	5.00E-03	2	10	12	5.00	6.00	1.20
	1.00E-02	2	11	14	5.50	7.00	1.27
	2.00E-02	1	7	9	7.00	9.00	1.29
	5.00E-02	1	7	9	7.00	9.00	1.29
	1.00E-01	1	7	9	7.00	9.00	1.29
	1.00E+00	1	5	6	5.00	6.00	1.20
	1.00E+01	1	4	4	4.00	4.00	1.00
1.00E-04	1.00E-03	2	9	11	4.50	5.50	1.22
	5.00E-03	2	9	11	4.50	5.50	1.22
	1.00E-02	2	10	12	5.00	6.00	1.20
	2.00E-02	1	6	8	6.00	8.00	1.33
	5.00E-02	1	6	8	6.00	8.00	1.33
	1.00E-01	1	6	8	6.00	8.00	1.33
	1.00E+00	1	5	5	5.00	5.00	1.00
	1.00E+01	1	4	4	4.00	4.00	1.00
5.00E-05	1.00E-03	2	8	9	4.00	4.50	1.12
	5.00E-03	2	9	10	4.50	5.00	1.11
	1.00E-02	2	9	11	4.50	5.50	1.22
	2.00E-02	1	6	8	6.00	8.00	1.33
	5.00E-02	1	6	8	6.00	8.00	1.33
	1.00E-01	1	6	7	6.00	7.00	1.17
	1.00E+00	1	4	4	4.00	4.00	1.00
	1.00E+01	1	4	4	4.00	4.00	1.00

only two transport iterations. For $t > 10^{-2}$ s, this method requires only one transport iteration for all sizes of time-steps used. The numbers of multigroup iterations required per transport iteration for this method is slightly larger than those for the MP method. It is about 5 multigroup iterations per transport iteration. For moments of time when the system is comparatively much relaxed (i.e. $t = 1.0$ s and $t = 10.0$ s) the numbers of transport, multigroup and newton's iterations required are identical for both these methods.

Next, we analyze the quality of the solutions obtained using α-approximation by comparing the results with those computed by means of the original system of equations that uses time-dependent high-order transport. For that matter, we evaluate the relative differences in the average power and temperature obtained using these methods at each moment of time and plot them.

Figure 4.11 shows the relative differences in the solutions obtained by the two methods. The

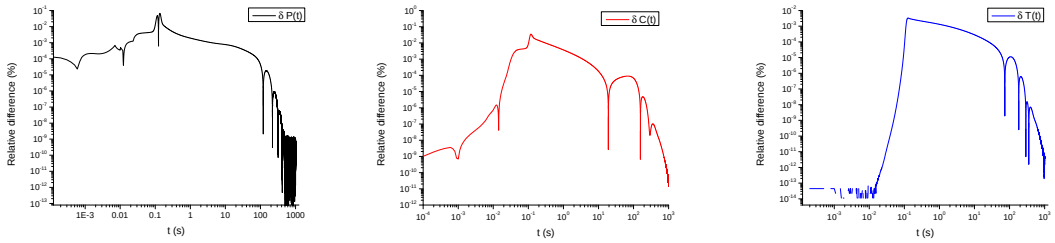

Figure 4.11: Test 1: Relative differences in solutions.

relative differences for the power and the precursor concentration stay under 0.1 % through the entire period of evolution. The relative differences in the temperature stay under 0.2 % through the entire process. These differences are at their maximums at around $0.1s$ in time, which also corresponds to the moment of peak values for the power and the precursor concentration.

4.1.3 Convergence in Time

Tables 4.4 - 4.7 show the estimated rate ($\delta f(\Delta t)$) of convergence of the solutions at two instants of time using the MP and MP$^\alpha$ methods. The values are evaluated using the following expression:

$$\delta f(\Delta t) = \frac{\| f(4\Delta t) - f(2\Delta t) \|_\infty}{\| f(2\Delta t) - f(\Delta t) \|_\infty}, \tag{4.4}$$

where f stands for the solutions: ϕ, T, and C. The spatial mesh is kept unchanged in these sets of experiments.

Table 4.4: Test 1: Rate of Temporal Convergence for MP method in L_∞ norm at $t = 0.1s$.

Δt	$\delta\phi(\Delta t)$	$\delta T(\Delta t)$	$\delta C(\Delta t)$
$1.\times10^{-4}$	1.90	1.78	1.80
$5.\times10^{-5}$	1.96	1.89	1.90
2.5×10^{-5}	1.98	1.94	1.95
1.25×10^{-5}	1.99	1.97	1.97

Table 4.5: Test 1: Rate of Temporal Convergence for MP method in L_∞ norm at $t = 1\ s$.

Δt	$\delta\phi(\Delta t)$	$\delta T(\Delta t)$	$\delta C(\Delta t)$
$1.\times10^{-4}$	1.82	1.76	1.77
$5.\times10^{-5}$	1.91	1.88	1.88
2.5×10^{-5}	1.96	1.94	1.94
1.25×10^{-5}	1.98	1.97	1.97

The rates of convergence are presented for both the MP and MP$^\alpha$ schemes. From these results, we see that as the size of the time-step is refined by a factor of two, the error is also reduced approximately to a half. As smaller time steps are considered, the factor by which the

Table 4.6: Test 1: Rate of Temporal Convergence for MP$^\alpha$ method in L_∞ norm at $t = 0.1\ s$.

Δt	$\delta\phi(\Delta t)$	$\delta T(\Delta t)$	$\delta C(\Delta t)$
$1.\times10^{-4}$	1.90	1.78	1.80
$5.\times10^{-5}$	1.96	1.89	1.90
2.5×10^{-5}	1.98	1.94	1.95
1.25×10^{-5}	1.99	1.97	1.97

Table 4.7: Test 1: Rate of Temporal Convergence for MP$^\alpha$ method in L_∞ norm at $t = 1s$.

Δt	$\delta\phi(\Delta t)$	$\delta T(\Delta t)$	$\delta C(\Delta t)$
$1.\times10^{-4}$	1.82	1.76	1.77
$5.\times10^{-5}$	1.91	1.88	1.88
2.5×10^{-5}	1.96	1.94	1.94
1.25×10^{-5}	1.98	1.97	1.97

error decreases becomes closer to being 2. This shows us that both the methods give first-order convergence in time.

Figure 4.12 shows the rates at which the errors in the solutions decrease with refinement of the time-steps. As can be seen from the plots, the rates of reduction in the errors of the solutions for the MP$^\alpha$ scheme are very close to the rates of reduction in the errors of the solutions for the MP scheme.

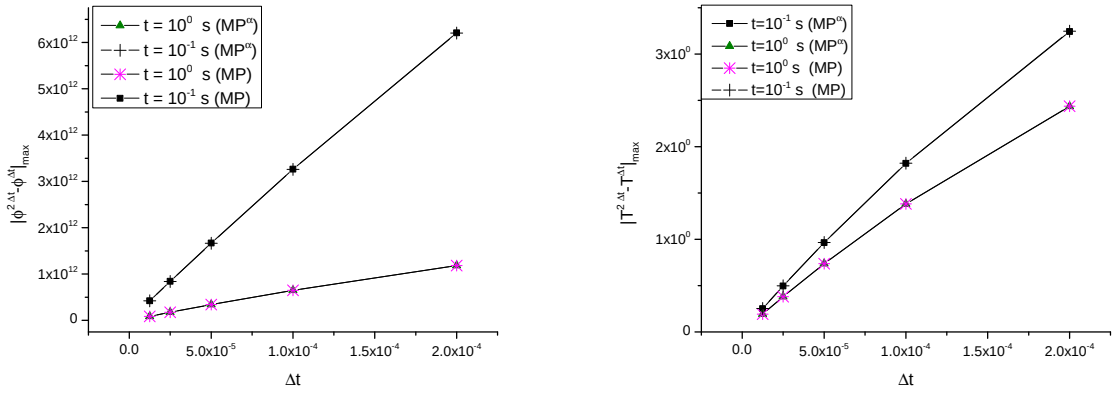

Figure 4.12: Test 1: Rate of decrease of error with refinement of time-step. size

4.1.4 Results with the Fixed Point Iteration Method

In this section, we present the tables of iterations required in case of the FPI method. The results are presented for the short-characteristics discretization (FPI) and the α-approximation (FPI$^\alpha$) of the time-dependent transport equation in Table 4.8 and Table 4.9, respectively. The results show that the MP method requires fewer transport (#S) iterations than the FPI method in

Table 4.8: Test 1: Iterations for FPI Method.

Δt	t	#S	#L	#T	$\frac{\#L}{S}$
2.00E-04	1.00E-03	6	21	2	3.50
	5.00E-03	6	21	2	3.50
	1.00E-02	8	29	2	3.62
	2.00E-02	6	19	2	3.17
	5.00E-02	2	8	2	4.00
	1.00E-01	8	25	3	3.12
	1.00E+00	8	21	3	2.62
	1.00E+01	4	11	3	2.75
1.00E-04	1.00E-03	4	15	2	3.75
	5.00E-03	4	15	2	3.75
	1.00E-02	6	19	2	3.17
	2.00E-02	4	11	2	2.75
	5.00E-02	2	7	2	3.50
	1.00E-01	6	18	3	3.00
	1.00E+00	4	12	3	3.00
	1.00E+01	2	6	2	3.00

Table 4.9: Test 1: Iterations for FPI$^{\alpha}$ Method.

Δt	t	#S	#L	#T	$\frac{\#L}{S}$
2.00E-04	1.00E-03	3	12	2	4.00
	5.00E-03	3	12	2	4.00
	1.00E-02	3	13	2	4.33
	2.00E-02	2	8	2	4.00
	5.00E-02	2	8	2	4.00
	1.00E-01	10	31	3	3.10
	1.00E+00	6	16	3	2.67
	1.00E+01	4	10	3	2.50
1.00E-04	1.00E-03	3	11	2	3.67
	5.00E-03	3	11	2	3.67
	1.00E-02	3	12	2	4.00
	2.00E-02	2	7	2	3.50
	5.00E-02	2	7	2	3.50
	1.00E-01	6	19	3	3.17
	1.00E+00	4	11	3	2.75
	1.00E+01	2	6	2	3.00

each and every instance. The advantage is more distinct when more fixed-point iterations (#T) are required. For instance, using $\Delta t = 10^{-4}$ s, the MP method requires only a single transport iteration at t=1.0 s. The FPI method requires 4 iterations of the transport and 3 fixed-point

iterations at this moment. For the same moment in time, 8 iterations of the transport and 3 fixed-point iterations are required using $\Delta t = 2.10^{-4}$ s. The MP method still requires only a single transport iteration.

Table 4.9 presents iterations required for the MP$^{\alpha}$ and the FPI$^{\alpha}$ method. The results for efficiency are consistent with that for the comparisons made between the MP and the FPI methods. The MP$^{\alpha}$ methods require fewer iterations of the transport problem than with the FPI$^{\alpha}$ method for each instance. The reduction is especially significant for t=0.1 s and t=1.0 s when more fixed-point iterations are required to solve the problem. While only a single transport iteration is required using the MP$^{\alpha}$ method, as many as 10 transport iterations are required using the FPI$^{\alpha}$ method.

4.2 Test 2: Transient in a Model BWR Reactor System

The following test is based on the BWR benchmark problem from the Argonne Benchmark Problem book [51]. This test models a transient in a reactor system. Figure 4.13 shows dimensions of the regions that make up the problem domain in this test. Each region is marked with the material type that fills the region. Detailed cross-section data and other parameters of this test are presented in Appendix A.2.

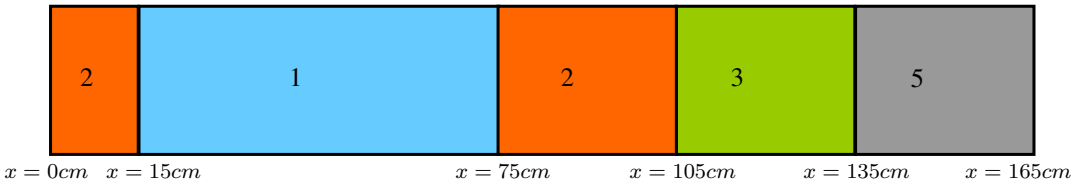

Figure 4.13: Material configuration in Test 2.

The problem is defined with two-group neutron cross sections and two-group delayed neutron data. The heat buildup is adiabatic and has the following form:

$$\frac{\partial T(x,t)}{\partial t} = \alpha(\Sigma_{f,1}\phi_1(x,t) + \Sigma_{f,2}\phi_2(x,t)). \tag{4.5}$$

The boundary conditions for temperature are given by the following:

$$\frac{\partial T(x,t)}{\partial x}|_{x=0} = 0, \tag{4.6}$$

$$\frac{\partial T(x,t)}{\partial x}|_{x=L} = 0. \tag{4.7}$$

The Doppler effect is modeled in the first group as follows:

$$\Sigma_{a,1}(t) = \Sigma_{a,1}(0)\left[1 + \gamma\sqrt{T(x,t)+273} - \sqrt{T_0+273}\right]. \tag{4.8}$$

The initial temperature distribution is set to be 27^oC in the entire problem domain. A transient is induced in the problem by linearly decreasing the thermal absorption cross-section in material 3 over a period of 2 seconds.

$$\Sigma_{a,2}(t) = \Sigma_{a,2}(t_0)\begin{cases}(1 - 0.0606184t) & t \leq 2,\\ 0.8787631 & t > 2.\end{cases} \tag{4.9}$$

By doing this, we simulate the removal of control material from the domain.

4.2.1 Evolution of Solutions

Figure 4.14 demonstrates the evolution of average power in the system during the course of the evolution of the system following the start of the removal of control material. The evolution of the average temperature in the system is shown in Figure 4.15. Figure 4.16 shows the scaled magnitudes of the average power, temperature, and precursor concentration in the domain as a function of time. The power in the system increases rapidly until the first second into the transient process. The temperature and precursor concentrations also increase rapidly upto that moment. Between 1 and 2 s, the temperature is high enough such that the Doppler broadening of the thermal absorption cross-section causes the fuel to become subcritical, and the power drops precipitously. It is seen in Figure 4.16 that the average temperature and precursor concentrations in the problem steady out following the drop in power. However, as more reactivity is being inserted, the power increases in the system. The removal of the control material is stopped at t=2 s. The power drops rapdily following this moment in time.

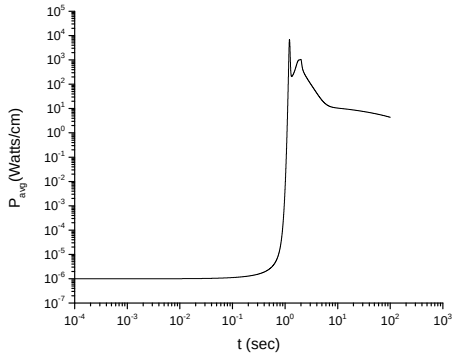

Figure 4.14: Test 2: Evolution of average power.

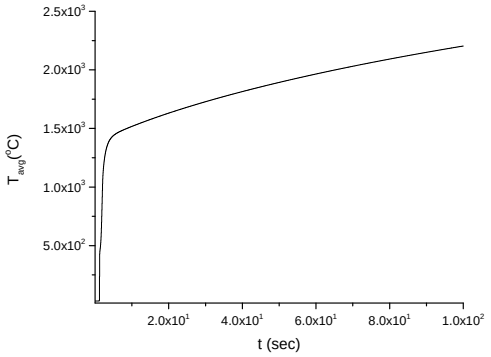

Figure 4.15: Test 2: Evolution of average temperature.

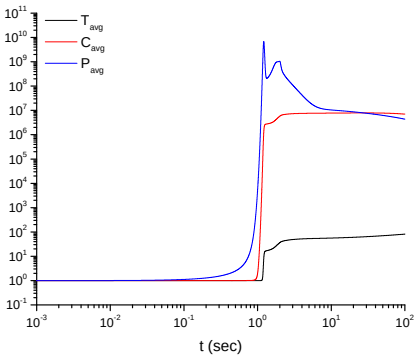

Figure 4.16: Test 2: Scaled average power, temperature, and total precursor concentrations.

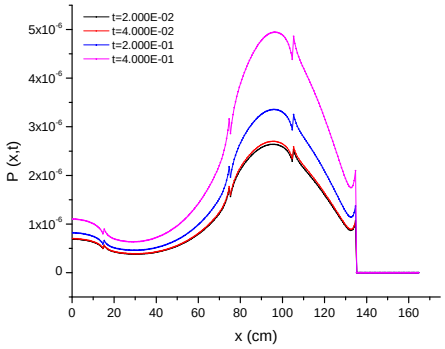

Figure 4.17: Test 2: Power as a function of space and time.

While the power decreases steeply, the concentration of the precursors remains a constant. As it was discussed also in Test 1, this is because the precursors decay slower over time than the rates at which the neutron population change in the domain. As the power drops steeply after the second peak, we notice that at around t = 8 s, the power profile becomes relatively stable. This is because of the decay events of the precursors resulting in delayed neutrons that add to the neutron population in the system.

The average temperature keeps increasing steadily in this test unlike in the previous test. This is because in this problem heat is not lost through conduction, a consequence of its being an adiabatic system. As a consequence, the absorption cross-section modeled by doppler broadening continues to increase at a small rate. This results in neutron population loss, and so we see that the power is at a state of decline even at 100 seconds after the transient was initiated.

Figures 4.18 - 4.27 show how various parameters of the problem evolve as a function of space and time. The control material is removed from material 3. We notice that the magnitudes of the group fluxes in this region change more than in other parts of the domain. We see in Figure 4.20 that the temperature distribution also increase the most in and around the region occupied by material 3. The spatial shape of the temperature show discontinuities at material interfaces. The reason behind this is that no heat is conducted between materials (a consequence of adiabtic heat buildup), and thus the temperatures at either sides of an interface remain different.

The thermal flux has a peak in the reflector region since the moderator in the reflector region slows down fast neutrons (see Figure 4.23). We also see that the fast group flux is depressed in this region. The plots of the fast group flux as a function of space are presented in Figure 4.22. In Figure 4.18, we see that the total neutron flux is higher in material 2 (fuel without control material) than in material 1 (fuel with control material). Figures 4.24 and 4.25 show the plots of the fast and slow group currents as a function of space respectively. Figure 4.21 show the plot of the total current as a function of space for this test.

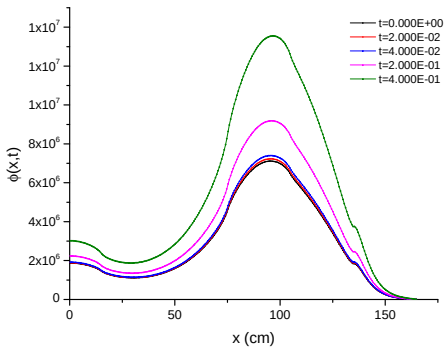

Figure 4.18: Test 2: Total scalar flux as a function of space and time.

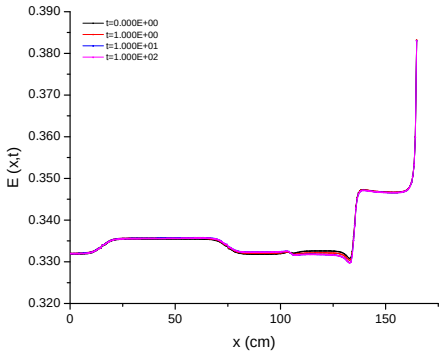

Figure 4.19: Test 2: Spectrum-averaged QD factors as a function of space and time.

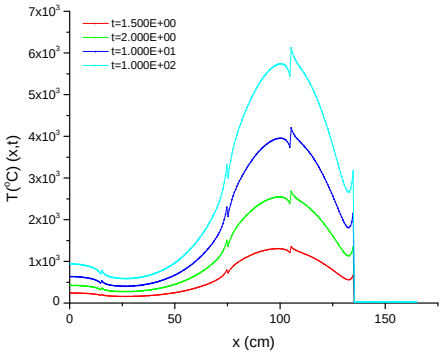

Figure 4.20: Test 2: Temperature as a function of space and time.

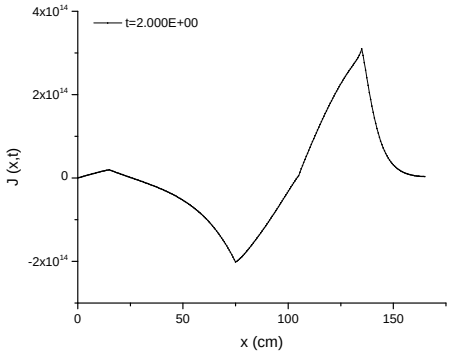

Figure 4.21: Test 2: J (total current) as a function of space for t=2s.

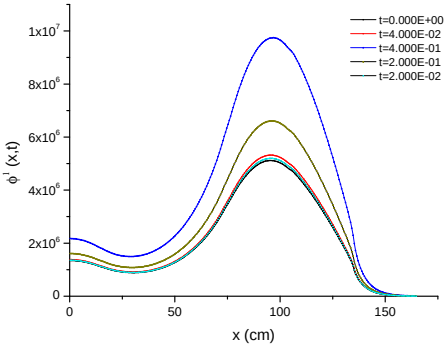

Figure 4.22: Test 2: Fast (Group-1) flux as a function of space and time.

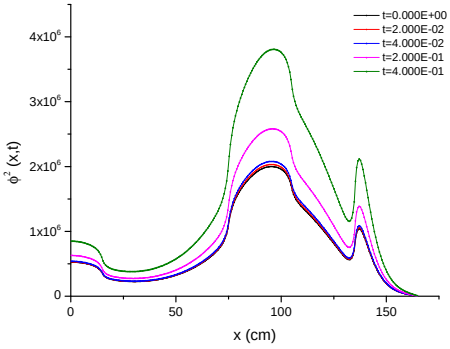

Figure 4.23: Test 2: Thermal (Group-2) flux as a function of space and time.

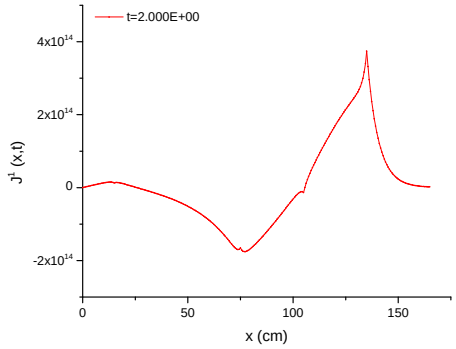

Figure 4.24: Test 2: Group-1 current ($J_1(x,t)$) as a function of space for two instants of time.

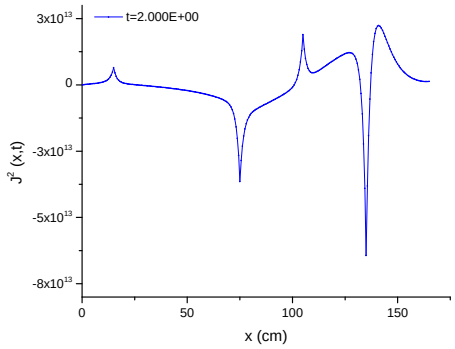

Figure 4.25: Test 2: Group-2 current ($J_2(x,t)$) as a function of space for two instants of time.

Figures 4.26 and 4.27 demonstrate the group quasidiffusion factors on the domain for various moments of time. It is seen that the QD factors differ from the diffusion value of $\frac{1}{3}$ in the reflector as well as at the vacuum boundary. At the material interfaces, the group QD factors change sharply that indicate transport effects. Over the course of the evolution, detailed analysis shows that the first group QD factors change by a maximum of 0.46%, and the second group QD factors change by a maximum of 0.13%. These maximum differences are seen in the interfacial regions of material 3 and material 5.

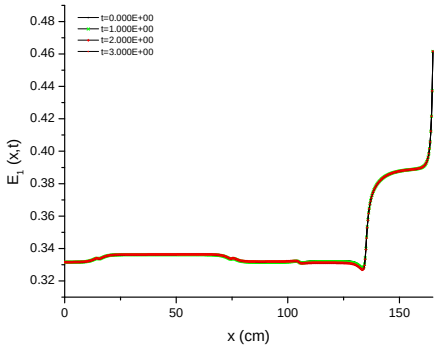

Figure 4.26: Test 2: Fast (Group-1) group quasidiffusion factors as a function of space and time.

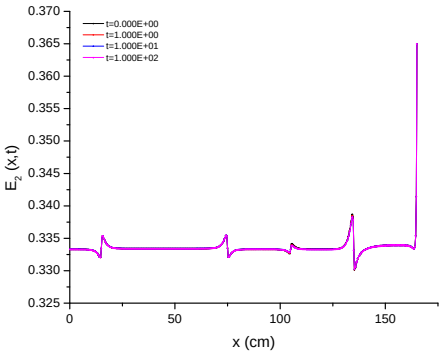

Figure 4.27: Test 2: Thermal (Group-2) group quasidiffusion factors as a function of space and time.

4.2.2 Iteration Tables

Table 4.10 lists the numbers of iterations required to solve this test using the MP method. The numbers of iterations are listed for 8 independent instants of time when the system undergoes change at various rates. At $t = 0.8\ s$ and $t = 1.0\ s$, the average power in the system increases rapidly. Between $t = 1.0\ s$ and $t = 2.0\ s$, the average power displays rapid increase and decrease over quite short periods of time. The first peak is attained at $t = 1.2\ s$. The power attains a second local maximum at $t = 2.0\ s$. At instants $t = 5.0\ s$ and $t = 10.0\ s$, the average power, precursor concentrations and temperature in the system are at relaxation.

For all time-steps studied, the highest numbers of transport iterations are required for $t = 1.2\ s$ when the system is at its most rapid state of change. The least numbers of transport iterations are seen for $t = 10.0\ s$ when the system is at relaxation. This behavior is consistent with the results of Test 1. Additionally, with the refinement of time-step sizes, the number of transport iterations required at each instant of time is reduced.

The average numbers of multigroup QD iterations required per transport iteration vary with time. It is seen that approximately 6 multigroup QD iterations per transport sweep is required for moment until $t = 1.2\ s$. These values jump to approximately 20 and 15 for $t = 1.8\ s$ and $t = 2.0\ s$, respectively. The average numbers of multigroup QD iterations fall to values between 10 and 6 after $t = 2.0\ s$.

The average numbers of Newton's iterations required per transport sweep also vary with time. Upwards of 20 and 10 average numbers of Newton's solve per transport sweep are seen for $t = 1.8\ s$ and $t = 2.0\ s$, respectively. Next, we look at the numbers of iterations required for this test using the MP^α method.

Table 4.11 lists the numbers of iterations required to solve this test using the MP^α method. This method shows similar behavior in terms of the correlation between the numbers of transport iterations required and the rate of change of physics in the system at a given instant of time. Also, as time-steps are refined, the required iteration numbers decrease. Fewer numbers of transport iterations are required using the MP^α method than the MP method. However, slightly larger numbers of multigroup QD iterations per transport sweep and average numbers of Newton's iterations per multigroup QD solve are seen for this method. Next, we present analysis on the quality of the solutions obtained by these methods.

Figure 4.28 shows the relative differences in the solutions obtained by means of the α-approximation compared to the solution of the complete system of equations that includes time-dependent high-order transport equation. The solutions are compared using the same spatial mesh and size of the time-step. The particular value of time-step used for this comparison was $dt = 1.10^{-4}\ s$. As it was seen for Test 1, the largest differences are observed at moments of time when the rate of change is relatively rapid. In this test, the physics in the system changes

Table 4.10: Test 2: Numbers of iterations for MP method.

Δt	t	$N_{transp.}$	N_{mgqd}	N_{newton}	$\frac{N_{mgqd}}{N_{transp}}$	$\frac{N_{newton}}{N_{transp}}$	$\frac{N_{newton}}{N_{mgqd}}$
8.00E-03	8.00E-01	6	34	38	5.67	6.33	1.12
	1.00E+00	7	47	54	6.71	7.71	1.15
	1.20E+00	7	45	55	6.43	7.86	1.22
	1.80E+00	3	81	93	27.00	31.00	1.15
	2.00E+00	3	35	40	11.67	13.33	1.14
	3.00E+00	3	14	17	4.67	5.67	1.21
	5.00E+00	1	9	11	9.00	11.00	1.22
	1.00E+01	1	6	7	6.00	7.00	1.17
4.00E-03	8.00E-01	5	27	31	5.40	6.20	1.15
	1.00E+00	6	34	39	5.67	6.50	1.15
	1.20E+00	7	44	53	6.29	7.57	1.20
	1.80E+00	3	66	74	22.00	24.67	1.12
	2.00E+00	2	28	32	14.00	16.00	1.14
	3.00E+00	1	10	13	10.00	13.00	1.30
	5.00E+00	1	8	10	8.00	10.00	1.25
	1.00E+01	1	6	7	6.00	7.00	1.17
2.00E-03	8.00E-01	4	21	24	5.25	6.00	1.14
	1.00E+00	5	28	32	5.60	6.40	1.14
	1.20E+00	6	34	38	5.67	6.33	1.12
	1.80E+00	3	47	51	15.67	17.00	1.09
	2.00E+00	2	24	27	12.00	13.50	1.12
	3.00E+00	1	10	12	10.00	12.00	1.20
	5.00E+00	1	8	10	8.00	10.00	1.25
	1.00E+01	1	6	6	6.00	6.00	1.00
1.00E-03	8.00E-01	3	15	18	5.00	6.00	1.20
	1.00E+00	3	19	23	6.33	7.67	1.21
	1.20E+00	5	27	31	5.40	6.20	1.15
	1.80E+00	2	34	37	17.00	18.50	1.09
	2.00E+00	2	20	23	10.00	11.50	1.15
	3.00E+00	1	8	10	8.00	10.00	1.25
	5.00E+00	1	7	8	7.00	8.00	1.14
	1.00E+01	1	6	6	6.00	6.00	1.00

most rapidly over the time interval: $1\ s < t < 2\ s$. The maximum relative difference in the average power is about 0.05% and this value is attained at $t = 1.2\ s$. At other moments of time, the relative differences in the average power stay under 10^{-4} %. The same trend is observed for both the relative differences in average precursor concentration and the average temperature. For both these solutions, the largest differeces are observed between $t = 1\ s$ and $t = 2\ s$ when

Table 4.11: Test 2: Numbers of iterations for MP$^{\alpha}$ method.

Δt	t	$N_{transp.}$	N_{mgqd}	N_{newton}	$\frac{N_{mgqd}}{N_{transp}}$	$\frac{N_{newton}}{N_{transp}}$	$\frac{N_{newton}}{N_{mgqd}}$
8.00E-03	8.00E-01	3	22	26	7.33	8.67	1.18
	1.00E+00	3	28	33	9.33	11.00	1.18
	1.20E+00	3	28	36	9.33	12.00	1.29
	1.80E+00	4	86	98	21.50	24.50	1.14
	2.00E+00	4	38	43	9.50	10.75	1.13
	3.00E+00	1	11	14	11.00	14.00	1.27
	5.00E+00	1	9	11	9.00	11.00	1.22
	1.00E+01	1	6	7	6.00	7.00	1.17
4.00E-03	8.00E-01	3	19	23	6.33	7.67	1.21
	1.00E+00	3	23	28	7.67	9.33	1.22
	1.20E+00	3	23	30	7.67	10.00	1.30
	1.80E+00	3	67	75	22.33	25.00	1.12
	2.00E+00	3	31	35	10.33	11.67	1.13
	3.00E+00	1	10	13	10.00	13.00	1.30
	5.00E+00	1	8	10	8.00	10.00	1.25
	1.00E+01	1	6	7	6.00	7.00	1.17
2.00E-03	8.00E-01	2	16	19	8.00	9.50	1.19
	1.00E+00	2	19	23	9.50	11.50	1.21
	1.20E+00	3	18	21	6.00	7.00	1.17
	1.80E+00	2	47	51	23.50	25.50	1.09
	2.00E+00	2	25	28	12.50	14.00	1.12
	3.00E+00	1	10	12	10.00	12.00	1.20
	5.00E+00	1	8	10	8.00	10.00	1.25
	1.00E+01	1	6	6	6.00	6.00	1.00
1.00E-03	8.00E-01	2	13	16	6.50	8.00	1.23
	1.00E+00	2	16	20	8.00	10.00	1.25
	1.20E+00	3	16	20	5.33	6.67	1.25
	1.80E+00	2	35	38	17.50	19.00	1.09
	2.00E+00	2	20	23	10.00	11.50	1.15
	3.00E+00	1	8	10	8.00	10.00	1.25
	5.00E+00	1	7	8	7.00	8.00	1.14
	1.00E+01	1	6	6	6.00	6.00	1.00

the relative differences are about 0.05%. For most other periods during the evolution, the relative differences in the solutions are less than 10^{-4} %.

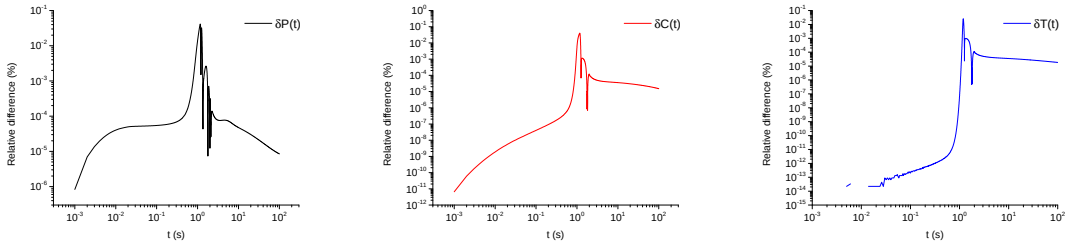

Figure 4.28: Test 2: Relative differences in average power, precursor concentration and temperature.

4.2.3 Convergence in Time

Tables 4.12 - 4.13 show the estimated rates of temporal convergence using the MP method for $t = 1\ s$ and $t = 2\ s$, respectively. Tables 4.14 - 4.15 show the estimated rates of temporal convergence using the MP$^{\alpha}$ method for the same instants of time, respectively. It can be seen from the tables that both the methods converge identically for each instant of time. Also, the convergence is of order 1.

Table 4.12: Test 2: Rate of Temporal Convergence for MP method in L_∞ norm at t=1 s.

Δt	$\delta\phi(\Delta t)$	$\delta T(\Delta t)$	$\delta C(\Delta t)$
$1.\times10^{-4}$	2.05	2.05	2.05
$5.\times10^{-5}$	2.02	2.02	2.02
2.5×10^{-5}	2.01	2.01	2.01
1.25×10^{-5}	2.01	2.01	2.01

Table 4.13: Test 2: Rate of Temporal Convergence for MP method in L_∞ norm at t=2 s.

Δt	$\delta\phi(\Delta t)$	$\delta T(\Delta t)$	$\delta C(\Delta t)$
$1.\times10^{-4}$	1.78	2.02	1.92
$5.\times10^{-5}$	1.89	2.02	1.96
2.5×10^{-5}	1.95	2.01	1.98
1.25×10^{-5}	1.97	2.00	1.99

Table 4.14: Test 2: Rate of Temporal Convergence for MP$^{\alpha}$ method in L_∞ norm at t=1 s.

Δt	$\delta\phi(\Delta t)$	$\delta T(\Delta t)$	$\delta C(\Delta t)$
$1.\times10^{-4}$	2.05	2.05	2.05
$5.\times10^{-5}$	2.02	2.02	2.02
2.5×10^{-5}	2.01	2.01	2.01
1.25×10^{-5}	2.01	2.01	2.01

Table 4.15: Test 2: Rate of Temporal Convergence for MP$^{\alpha}$ method in L_∞ norm at t=2 s.

Δt	$\delta\phi(\Delta t)$	$\delta T(\Delta t)$	$\delta C(\Delta t)$
$1.\times10^{-4}$	1.78	2.02	1.92
$5.\times10^{-5}$	1.89	2.02	1.96
2.5×10^{-5}	1.95	2.01	1.98
1.25×10^{-5}	1.97	2.00	1.99

Figures 4.29 - 4.31 show the rate of decrease of errors in the total flux, temperature and precursor concentration with refinement of Δt. We observe that the errors decrease when time-step is refined for each method.

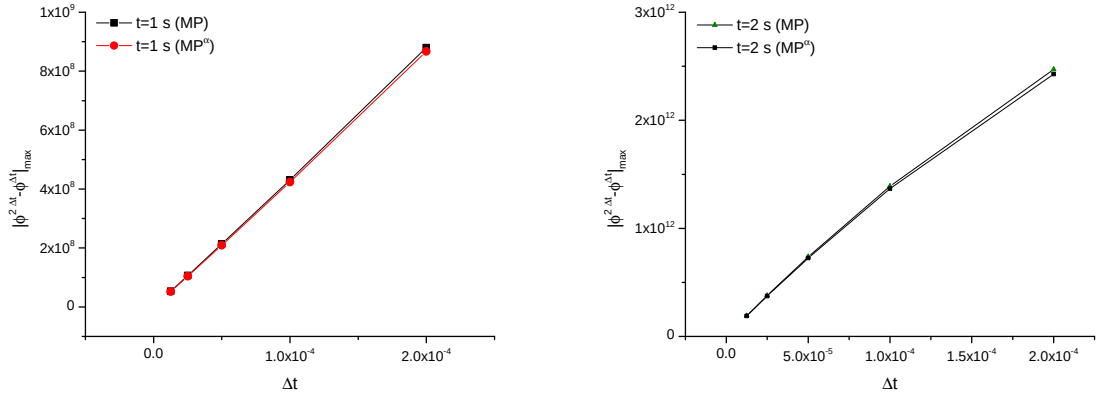

Figure 4.29: Test 2: Rate of decrease of errors in total flux (ϕ) with refinement of time-step sizes for $t = 1\ s$ and $t = 2\ s$ respectively.

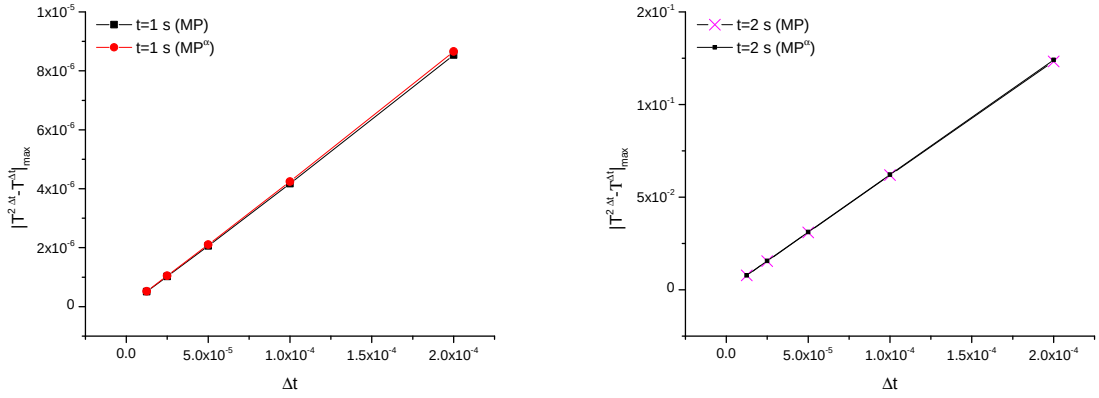

Figure 4.30: Test 2: Rate of decrease of errors in temperature (T) with refinement of time-step sizes for $t = 1\ s$ and $t = 2\ s$ respectively.

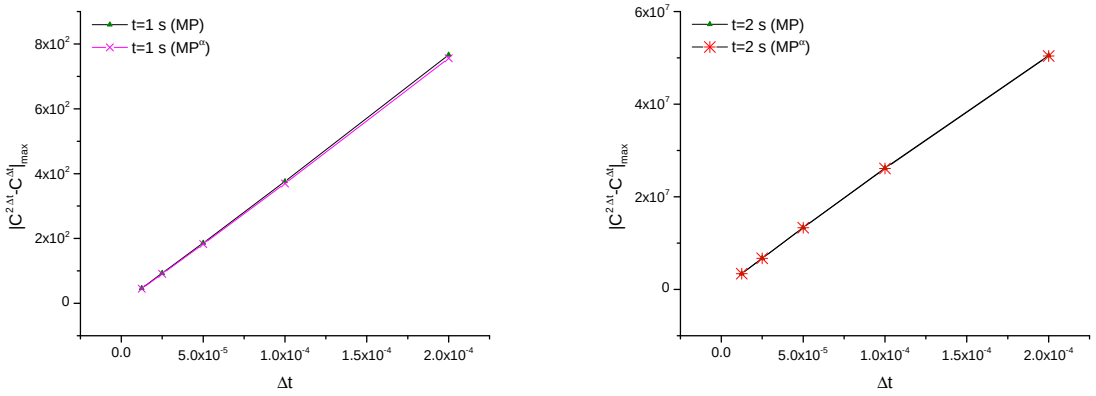

Figure 4.31: Test 2: Rate of decrease of errors in total precursor concentration (C) with refinement of time-step sizes for $t = 2$ s.

4.2.4 Results with the Fixed Point Iteration Method.

Table 4.16 show the iterations required at various levels using the FPI method. The results clearly show that the MP method requires much fewer numbers of transport (#S) iterations. The differences are more pronounced at moments when more fixed-point iterations (#T) are required. For instance, at $t = 1.2$ s, 6 fixed-point iterations are required using the FPI method and Δt=8.10^{-3} s. In the meantime, a total of 27 transport iterations are required at this moment. The MP method requires only 7 transport iterations to solve the problem at the given instant using the same time-step. We notice a reduction in the numbers of transport iterations by a factor of about 4 using the MP method.

Similarly, for $t = 1.8$ s, 21 iterations of the transport equation are required using the FPI method and Δt=8.10^{-3} s. The MP method requires 3 transport iterations at this instant of time. This represents a reduction in the numbers of transport iterations by a factor of 7.

Table 4.17 shows the iterations required using the FPI$^{\alpha}$ method. Similar correlations that were drawn for the MP and FPI methods are seen. Significantly fewer numbers of transport iterations are required using the MP$^{\alpha}$ method than the FPI$^{\alpha}$ method. The difference is more remarkable during moments of time when more fixed-point iterations are required to solve the problem. Note that there is no variation in the numbers fixed-point iterations required between the FPI and the FPI$^{\alpha}$ methods. This is as expected because these two methods vary only in how the transport problem is solved, and that does not affect the convergence of temperature at any instant of time.

Table 4.16: Test 2: Iterations for FPI Method.

Δt	t	#S	#L	#T	$\frac{\#L}{S}$
8.00E-03	8.00E-01	7	44	2	6.29
	1.00E+00	10	62	3	6.20
	1.20E+00	27	153	6	5.67
	1.80E+00	21	212	5	10.10
	2.00E+00	21	141	5	6.71
	3.00E+00	14	62	4	4.43
	5.00E+00	8	40	3	5.00
	1.00E+01	8	30	3	3.75
4.00E-03	8.00E-01	6	35	2	5.83
	1.00E+00	7	45	2	6.43
	1.20E+00	24	133	5	5.54
	1.80E+00	16	146	4	9.12
	2.00E+00	14	97	4	6.93
	3.00E+00	10	46	3	4.60
	5.00E+00	8	32	3	4.00
	1.00E+01	4	18	3	4.50

Table 4.17: Test 2: Iterations for FPI$^{\alpha}$ Method.

Δt	t	#S	#L	#T	$\frac{\#L}{S}$
8.00E-03	8.00E-01	4	26	2	6.50
	1.00E+00	6	34	3	5.67
	1.20E+00	27	160	6	5.93
	1.80E+00	22	221	5	10.05
	2.00E+00	22	145	5	6.59
	3.00E+00	11	52	4	4.73
	5.00E+00	7	33	3	4.71
	1.00E+01	7	25	3	3.57
4.00E-03	8.00E-01	4	23	2	5.75
	1.00E+00	4	26	2	6.50
	1.20E+00	24	138	5	5.75
	1.80E+00	15	149	4	9.93
	2.00E+00	15	97	4	6.47
	3.00E+00	8	38	3	4.75
	5.00E+00	6	27	3	4.50
	1.00E+01	6	19	3	3.17

Chapter 5

Discussion

This thesis presents the application of the multilevel scheme based on low-order quasidiffusion equations to solve a particular class of multiphysics problems from reactor physics. The system of equations (and the method) can be interpreted as nonlinear multigrid method in phase space. Results arising out of this research suggest that this scheme has the potential to be more efficient than conventional methods for solving problems discussed in this work. In this chapter, we discuss the main resulting conclusions out of this work, as well as potential avenues for future work in both the theoretical and applied numerical aspects of the method.

5.1 Main Conclusions

The multilevel scheme studied in this work provides a new stage in the development of nonlinear multilevel methods for solving reactor physics problems. We developed a method based on multilevel projection (MP) for solving a particular class of coupled system of equations. We compared the performance of the multilevel method with the conventional iteration method based on fixed point iterations (FPI) of the coupled equations. Secondly, we used the α- approximation (MP^α , FPI^α) to solve the time-dependent transport problem. This is an approximate method based on low-order scalar flux. We compared the performance and quality of the solutions obtained with α- approximation to the solutions obtained with short-characteristic discretization of the transport equation. The relative efficiency of each method is determined on the basis of the numbers of transport iterations required to solve the problem at any given moment of time.

For any given method, the numbers of transport iterations required are seen to depend on the rate of change of physics of the system and the size of the time-steps used to solve the problem. This is not entirely unexpected. When the physics change more rapidly in the system, higher numbers of transport iterations are required because there are more changes to resolve at these instants. Likewise, larger time-steps may require larger numbers of transport iterations.

This is also as expected because when the time-steps are larger, the solutions at successive moments of time are further apart.

It was demonstrated that the MP method is more efficient at solving the concerned problems than the FPI method. This conclusion is based on the results from both the test problems. The gain in efficiency with the MP method is more significant at moments of time when the temperature change is rapid. At these instances, the MP method resolve the effects of temperature iterations in the innermost cycle so that the transport problem needs to be evaluated minimal numbers of times. In the FPI approach, the effects of temperature are resolved through iterations of the heat transfer and the transport problem. As a result, more transport iterations are required.

The computational efficiency of the MP method stem from the following features. First, the MLOQD equations are dependent on nonlinear factors (E_g) which are stable quantities that weakly depend on the high-order solution, i.e. angular flux. Secondly, the GLOQD equations serve as a filter in removing error modes from the multigroup spectrum and lead to fast convergence of the multigroup spectrum. The Newton's method also leads to rapidly convergent search of the solutions for the nonlinear coupled system of equations in the innermost cycle of the MP method. All of these features contribute to the increased efficiency of the MP method.

It was observed that the solutions produced by the MP and MP$^\alpha$ method differ by less than 0.05% at all times. The relative differences in the solution are comparatively larger during periods when the system changes rapidly. During most periods of the evolution of the system, the relative differences in the solution stay below 10^{-4}%. It is also observed that both these methods converge with first-order accuracy. Additionally, we observed that the MP$^\alpha$ method required fewer or equal transport iterations than the MP method for solving the transport problem. This is seen despite the fact that the α- approximation method introduces extra nonlinearity in the time-dependent transport problem. Our results show that at least when the presented multilevel method is used to solve the given problems, the extra nonlinearity does not give rise to increased transport iterations of the MP method.

5.2 Future Work

The results obtained in this work establishes a foundation for many directions of further research. Naturally, the next step would be to apply the proposed methodology on multidimensional problems. The solution of multidimensional transport problems are much more complicated and computationally strenuous. The application of the MP method could greatly reduce the computational costs involved by lowering the numbers of transport iterations required for solving multidimensional multiphysics reactor problems.

In the presented work, the nonlinear grey low-order problem for total scalar flux and temper-

ature distribution is solved by Newton's method. Nonlinear methods such as JFNK [13, 52, 53] are very efficient and applicable for solving problems of this kind. These methods could be used to explore the benefits offered by the multilevel scheme when larger time-steps are used. Adapative time-stepping could be used so that at moments of fast transient, important features of the solutions are captured. Additionally, higher-order temporal discretization schemes for time-dependent system of equations can be developed. The α- approximation for time-dependent transport is shown to exhibit first order convergence in time. An interesting question to explore is whether it exhibits second or higher temporal convergence orders.

The multilevel projection method developed in this research has shown to be an effective method for solving multiphysics problems of reactor physics. It shows obvious gain in efficiencies over conventional approach of solving the same class of problems. Based on the results obtained in this research, application of this methodology on more complex problems is strongly encouraged.

REFERENCES

[1] V. Y. Gol'din, "A quasi-diffusion method of solving the kinetic equation," *USSR Computational Mathematics and Mathematical Physics*, vol. 4, no. 6, pp. 136 – 149, 1964.

[2] A. Tamang and D. Y. Anistratov, "A multilevel methodology for coupling neutronics with the heat transfer equation," *Transactions of the American Nuclear Society*, vol. 106, pp. 395–397, 2012.

[3] A. Tamang and D. Y. Anistratov, "A multilevel method for coupling the neutron kinetics and heat transfer equations," in *Proceedings of M&C 2013, International Conference on Mathematics and Computational Methods Applied to Nuclear Science & Engineering*, (Sun Valley, Idaho, USA), pp. 2052–2063, May 2013.

[4] A. Tamang and D. Y. Anistratov, "A multilevel quasidiffusion method for solving space-time multigroup neutron kinetics equations coupled with the heat transfer equation," *Nuclear Science and Engineering*, 2013. submitted for publication.

[5] E. N. Aristova, V. Y. Gol'din, and A. V. Kolpakov, "Multidimensional calculations of radiation transport by nonlinear quasi-diffusion method," in *Proc. of Int. Conf. on Math. and Comp., Reactor Phys. and Environmental Analysis in Nucl. Appl. (M&C 99)*, (Madrid, Spain), pp. 667–676, Sept. 1999.

[6] D. Y. Anistratov and V. Y. Gol'din, "Multilevel quasidiffusion methods for solving multigroup neutron transport k-eigenvalue problems in one-dimensional geometry," *Nuclear Science and Engineering*, vol. 169, no. 2, pp. 111–132, 2011.

[7] E. Lewis and W. Miller, *Computational Methods of Neutron Transport.* American Nuclear Society, 1993.

[8] A. Hebert, *Applied Reactor Physics.* Presses Internationales Polytechnique, 2009.

[9] F. G. Tricomi, *Integral Equations.* Wiley, New York, 1957.

[10] H. J. Kopp, "Synthetic method solution of the transport equation," *Nuclear Science and Engineering*, vol. 17, pp. 65–74, September 1963.

[11] V. Faber and T. A. Mantueffel, *A look at Transport Theory From the Viewpoint of Linear Algebra.* Marcel Dekker, New York, 1989.

[12] Y. Azmy and E. Sartori, *Nuclear Computational Science, A Century in Review.* Springer, 2010.

[13] C. T. Kelley, *Iterative Methods for Linear and Nonlinear Equations.* Society for Industrial and Applied Mathematics, 1995.

[14] M. L. Adams and E. W. Larsen, "Fast iterative methods for discrete-ordinates particle transport calculations," *Progress in Nuclear Energy*, vol. 40, no. 1, pp. 3 – 159, 2002.

[15] K. L. Derstine and E. M. Gelbard, "Use of the preconditioned conjugate gradient method to accelerate S_N iterations," *Transactions in American Nuclear Society*, vol. 50, p. 260, 1985.

[16] P. L. Chambre and B. W. Crawford, "An iterative solution method for the neutron transport equation with anisotropic scattering," *Transactions in American Nuclear Society*, vol. 7, p. 254, 1964.

[17] J. P. Friedman and B. W. Crawford, "A two-dimensional application of an iterative method for solving the neutron transport equation with anisotropic scattering," *Transactions in American Nuclear Society*, vol. 9, p. 254, 1965.

[18] L. A. Hageman and E. M. Gelbard, "The synthetic method as applied to the S_N equations," *Nuclear Science and Engineering*, vol. 37, p. 288, 1969.

[19] W. Reed, "The effectiveness of acceleration techniques for iterative methods in transport theory," *Nuclear Science and Engineering*, vol. 45, p. 245, 1971.

[20] R. E. Alcouffe, "A stable diffusion synthetic accleration method for neutron transport iterations," *Transactions in American Nuclear Society*, vol. 23, p. 203, 1976.

[21] R. E. Alcouffe, "Diffusion synthetic acceleration methods for the diamond-differenced discrete-ordinates equations," *Nuclear Science and Engineering*, vol. 64, p. 344, 1977.

[22] P. N. Brown, "A linear algebraic development of diffusion synthetic acceleration for three-dimensional transport equations," *SIAM J. Numerical Analysis*, vol. 32, p. 179, 1995.

[23] C. T. Kelley, "Multilevel source iteration accelerators for the linear transport equation in slab geometry," *Transport Theory and Statistical Physics*, vol. 24, p. 697, 1995.

[24] B. W. Patton and J. P. Holloway, "Application of Krylov subspace iterative methods to the slab geometry transport equation," in *Advances and applications in radiation protection and shielding*, April 1996.

[25] D. Y. Anistratov and V. Y. Gol'din, "Nonlinear methods for solving particle transport problems," *Transport Theory and Statistical Physics*, vol. 22, no. 2, pp. 42–77, 1993.

[26] D. Y. Anistratov and E. W. Larsen, "α-weighted acceleration methods for the transport equation," *Journal of Computational Physics*, vol. 173, pp. 664–684, 2001.

[27] E. W. Larsen, "Projected discrete ordinates methods for numerical transport problems," *Nuclear Science and Engineering*, vol. 92, p. 179, 1986.

[28] V. Gol'din and B. Chetverushkin, "Methods of solving one-dimensional problems of radiation gas dynamics," *USSR Computational Mathematics and Mathematical Physics*, vol. 12, no. 4, pp. 177 – 189, 1972.

[29] D. Y. Anistratov and V. Y. Goldin, "Numerical solution of the time-dependent transport equation coupled with the burnup and reactor kinetics equations," in *International Symposium on Numerical Transport Theory*, (Moscow, Russia), pp. 33–36, Nuclear Society, May 1992.

[30] J. J. Duderstadt and L. J. Hamilton, *Nuclear Reactor Analysis*. New York: Wiley, 1976.

[31] N. E. Todreas and M. S. Kazimi, *Nuclear Systems I*. 1990.

[32] W. M. Stacey, *Nuclear Reactor Physics*. 2001.

[33] V. S. Ryaben'kii and S. V. Tsynkov, *A Theoretical Introduction to Numerical Analysis*. Chapman & Hall CRC, 2007.

[34] V. Y. Gol'din, D. A. Gol'dina, A. V. Kolpakov, and A. A. Shilkov, "Mathematical modelling of gas dynamic processes with high radiation energy densities," *Problems of Atomic Science and Engineering: Methods and Codes for Numerical Solution of Mathematical Physics Problems*, vol. 2, p. 59, 1986.

[35] V. Y. Gol'din, "On mathematical modeling of problems of non-equilibrium transfer in physical systems," *Modern Problems of Mathematical Physics and Computational Mathematics*, pp. 113–127, 1982.

[36] D. Y. Anistratov and V. Y. Gol'din, "Solution of the multigroup transport equation by the quasi-diffusion method," *Preprint of the Keldysh Institute for Applied Mathematics*, no. 128, 1986.

[37] V. Y. Gol'din, "Characteristic difference scheme for non-stationary kinetic equation," *Soviet Mathematics - Doklady*, vol. 1, p. 902, 1960.

[38] V. Y. Gol'din, N. N. Kalitkin, and T. V. Shishova, "Nonlinear difference schemes for hyperbolic equations," *USSR Computational Mathematics and Mathematical Physics*, vol. 5, p. 229, 1968.

[39] K. Takeuchi, "A numerical method for solving the neutron transport equation in finite cylindrical geometry," *J. Nucl. Sci.*, vol. 6, p. 446, 1969.

[40] D. Mihalas, L. H. Auer, and B. Mihalas, "Two-dimensional radiative transfer. i. planar geometry," *The Astrophysics Journal*, vol. 220, pp. 1001–1023, 1978.

[41] P. Kunasz and L. Auer, "Short characteristic integration of radiative transfer problems: Formal solution in two-dimensional slabs," *J. Quant. Spectrosc. Radiat. Transfer*, vol. 39, no. 1, pp. 67–69, 1988.

[42] S. W. Davis, J. M. Stone, and Y.-F. Jiang, "A radiation transfer solver for athena using short characteristics," *Astrophys.J.Suppl.*, vol. 199, p. 9, 2012.

[43] A. D. Polyanin, *Handbook of Linear Partial Differential Equations for Engineers and Scientists*. Chapman & Hall/CRC press, 2002.

[44] G. D. Smith, *Numerical Solution of Partial Differential Equations*. Oxford University Press, 1975.

[45] J. R. Askew, "A characteristic formulation of the neutron transport equation in complicated geometries," Tech. Rep. AEEW-M 1108, 1972.

[46] J. Rhodes, K. Smith, and D. Lee, "Casmo-5 development and applications," (Vancouver, BC, Canada), PHYSOR, September 10-14 2006.

[47] E. N. Aristova, "Simulation of radiation transport in a channel based on the quasi-diffusion method," *Transport Theory and Statistical Physics*, vol. 37, no. 5-7, pp. 483–503, 2008.

[48] V. Y. Gol'din, V. A. Degtyarev, and A. V. Kolpakov, "Approximate methods for accounting for time-dependent effects in the quasi-diffusion equations," in *Preprint of the Keldysh Institute of Applied Mathematics*, no. 122, USSR Academy of Sciences, 1983.

[49] K. D. Lathrop, "Spatial differencing of the transport equation: Positivity vs. accuracy," *J. Comput. Phys.*, vol. 4, no. 4, pp. 475–498, 1969.

[50] J. H. Lamarsh and A. J. Baratta, *Introduction to Nuclear Engineering.* Prentice-Hall, Inc., 2001.

[51] American Nuclear Society Computational Benchmark Problems Committee, *Argonne Code Center Benchmark Problem Book. Suppl. 2*, vol. 7416, pp. 552–589. Argonne National Laboratory, Dec. 1972.

[52] D. Keyes, L. C. Mclnnes, C. Woodward, W. Gropp, E. Myra, and M. Pernice, "Multiphysics simulations: challenges and opportunities," Tech. Rep. ANL/MCS-TM-321 Rev. 1.1, Argonne National Laboratory (ANL), November 2012.

[53] D. Gaston, C. Newman, G. Hansen, and D. Lebrun-Grandi, "Moose: A parallel computational framework for coupled systems of nonlinear equations," *Nuclear Engineering and Design*, vol. 239, no. 10, pp. 1768 – 1778, 2009.

APPENDIX

Appendix A

Cross-sections and Materials Data

A.1 Test 1

Test 1 is a two group problem. The group velocities are: $v_1 = 4.683 \times 10^6$ cm/s and $v_2 = 5.636 \times 10^6$ cm/s. The material cross-sections are listed in the tables below.

Table A.1: Cross-sections data for fuel.

g	1	2
$\Sigma_{t,g}$	0.2	1.0
$\Sigma_{s,0,1\to g}$	0.0185	0.015
$\Sigma_{s,0,2\to g}$	0.0	0.8
$\Sigma_{f,g}$	0.0	0.1
$\nu_{f,g}$	0.0	2.0
$\chi_{f,g}$	1.0	0.0

Table A.2: Cross-sections data for moderator.

g	1	2
$\Sigma_{t,g}$	0.2	1.1
$\Sigma_{s,0,1\to g}$	0.017	0.03
$\Sigma_{s,0,2\to g}$	0.0	1.1
$\Sigma_{f,g}$	0.0	0.0
$\nu_{f,g}$	0.0	0.0
$\chi_{f,g}$	0.0	0.0

Table A.3: Data for the delayed neutron precursor equations.

d	$\lambda_d(s^{-1})$	β_d
1	0.0124	0.0002145
2	0.0305	0.0014235
3	0.1110	0.0012740
4	0.3010	0.0025675
5	1.1300	0.0007475
6	3.0000	0.0002730

All neutrons born as a result of the decay of the precursors are assumed to be in the first group. Hence, $\chi_1^{delayed} = 1.0$ and $\chi_2^{delayed} = 0.0$. In Table A.3, λ_d represents the decay constant of the precursors of group d. β_d represents the fraction of all fission events that result in the production of precursors of the group 'd'.

A.2 Test-2

Test 2 is a two group problem. The mean number of neutrons per fission, ν_f=2.43. The group velocities are: $v_1 = 3.10^7\ cm\ s^{-1}$ and $v_2 = 3.10^5\ cm\ s^{-1}$. Also, $\chi_1^{delayed} = 1.0$ and $\chi_2^{delayed} = 0.0$. The data for feedback model is as follows:

$\alpha = 3.83 \times 10^{-11}\ ^oK\ cm^3$: conversion factor,
$\gamma = 2.034 \times 10^{-3}\ ^oK^{1/2}$: feedback constant,
$\epsilon = 3.204 \times 10^{-11}\ W\ (fission^{-1})$: energy conversion factor.

The group cross-sections for each material type are given in Table A.4. These values have the units in cm^{-1}.

Table A.4: Initial Two-Group Constants

Material index	Material description	Group i	Σ_t	Σ_a	$\nu\Sigma_f$	$\Sigma_{s,0,i\to j}$
1	Fuel 1	1	0.7968	0.008252	0.004602	0.0
	with rod	2	4.7393	0.1003	0.1091	0.02533
2	Fuel 1 with-	1	0.7886	0.007181	0.004609	0.0
	out rod	2	5.2576	0.07047	0.08675	0.02767
3	Fuel 2	1	0.7943	0.008002	0.004663	0.0
	with rod	2	4.7824	0.08344	0.1021	0.02617
4	Fuel 2 with-	1	0.7943	0.008002	0.004663	0.0
	out rod	2	4.7824	0.0073324	0.1021	0.02617
5	Moderator	1	0.7955	0.0006034	0.0	0.0
		2	6.2814	0.01911	0.0	0.04754

Table A.5: Delayed Neutron Data for Test-2

Group (d)	λ_d	β_d
1	0.00654	0.0054
2	1.35	0.001087